LA-UR-21-25278

Approved for public release; distribution is unlimited.

Title: SOME PHYSICS FUNDAMENTALS OF HIGH ENERGY DENSITY WELDING

Author(s):
Hochanadel, Patrick Wayne
Burgardt, Paul
Elmer, John W.
Kautz, Douglas Dean (Doug)

Intended for: Report

Issued: 2021-06-03

Disclaimer:
Los Alamos National Laboratory, an affirmative action/equal opportunity employer, is operated by Triad National Security, LLC for the National Nuclear Security Administration of U.S. Department of Energy under contract 89233218CNA000001. By approving this article, the publisher recognizes that the U.S. Government retains nonexclusive, royalty-free license to publish or reproduce the published form of this contribution, or to allow others to do so, for U.S. Government purposes. Los Alamos National Laboratory requests that the publisher identify this article as work performed under the auspices of the U.S. Department of Energy. Los Alamos National Laboratory strongly supports academic freedom and a researcher's right to publish; as an institution, however, the Laboratory does not endorse the viewpoint of a publication or guarantee its technical correctness.

SOME PHYSICS FUNDAMENTALS
Of
HIGH ENERGY DENSITY WELDING

Prepared By: Dr. Paul Burgardt
Welding and Joining Dept.
Los Alamos National Laboratory (Retired)

With important input from:
J.W. Elmer, LLNL
P.A. Hochanadel, LANL
D.D. Kautz, SRP(cont)

February 16, 2021

PART I: A BRIEF DISCUSSION OF THE FUNDAMENTALS OF HIGH ENERGY DENSITY WELDING

The purpose of this section of this document is to provide a brief summary of the physics aspects of high energy density welding (HEDW). One reason for this is to help elucidate some of the differences between EBW and LBW. A fundamental understanding of these differences can help guide an appropriate choice of process for a particular application.

A. Weld Mode

Normal fusion welding can be accomplished in two distinct penetration "modes". Figure 1 illustrates the two basic modes of weld penetration. Typical arc welds, such as GTAW, occur when arc energy is deposited on the material top surface and the melt zone achieves a size where the power carried away by thermal conduction balances the input power (basically true at the slow travel speeds typical of arc welds). In that case, the weld is reasonably symmetric and has a weld aspect ratio, weld depth versus weld top-surface width of about, d/w ≈ 1/2. HEDW is clearly different with d/w >> 1. The weld dimensions always represent a balance between input power and thermal conduction and the power consumed in the heat of melting of the material in a traveling weld. However, it is clear that HEDW occurs with a much different penetration mechanism. It is interesting to note that the two weld modes are sometimes called 3-D versus 2-D heat flow. Figure 2 illustrates the point being made. In the usual conduction mode welds the input power is carried away fairly uniformly in all directions; hence the term 3-D heat flow. Deep penetration welds are often used to produce full or near to full penetration of the material; in that case the heat flow only occurs in the lateral direction and is therefore called 2-D heat flow. Note that even in partial penetration welds, heat flow is nearly 2-D immediately around the weld because of the fairly parallel sides of the fusion zone. The considerably greater thermal conduction away from the heat source that occurs in 3-D versus 2-D heat flow is one reason why deep penetration welds require considerably less power input.

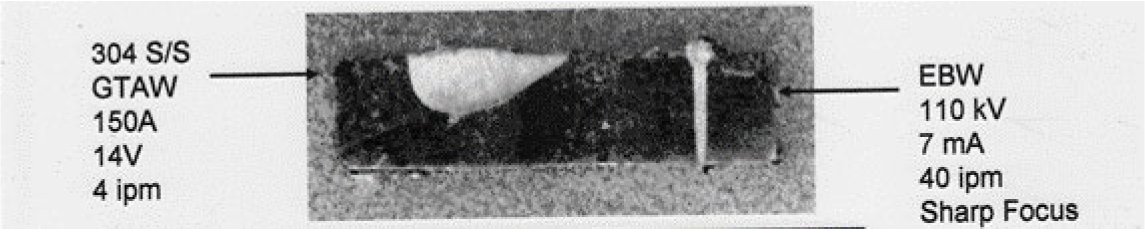

Figure 1: Typical welds made on stainless steel illustrating the differences between "conduction mode" and "deep penetration mode" welds. The EBW process resulted in greater weld penetration while depositing roughly 25 times less heat per unit length of weld. Note: unless otherwise cited, all weld data are from: P. Burgardt, Los Alamos National Laboratory (Ret.).

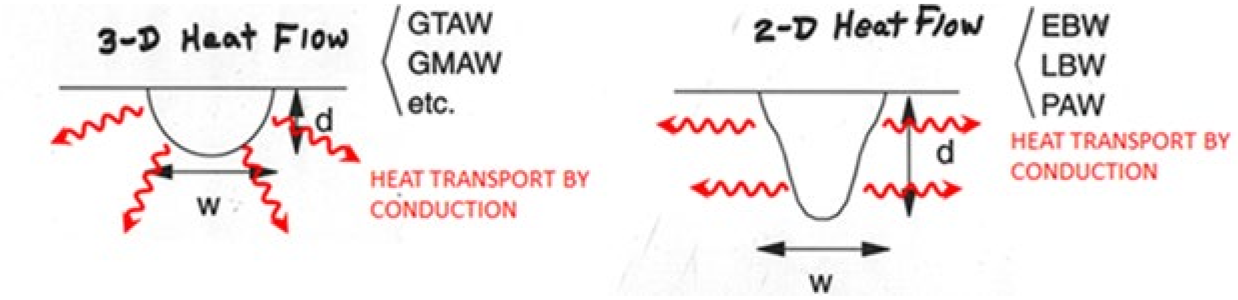

Figure 2: Schematic diagram illustrating the difference between shallow and deep penetration welds.

Figure 1 illustrates the great advantages of deep penetration welding. One major advantage is that a desired weld penetration depth is achieved with much less overall power input. The overall less heating of material results in much less potential modification of base metal properties (grain size changes, material composition changes and etc.) and heating of surrounding materials. Further, the much smaller overall weld dimensions and the parallel sided weld shape result in less part shrinkage and distortion, which is of critical concern for most potential weld applications.

A detailed dissertation on deep penetration mode welding is clearly beyond the scope of this discussion. However, some details of why this happens is important to the comparison between LBW and EBW. Therefore, a few concepts relevant to deep penetration welding will be presented.

Normal welding occurs when the metal has been heated by the power source to a temperature T > Tm, where Tm is the metal melting point. In arc welds, for example, increasing power usually results in an accompanying increase in heat source diameter resulting in a larger weld pool but no unusual change in weld shape. However, beam welding is different because the heat source diameter can be adjusted to stay small even at high power (ie. the beam is focused to a small spot size). In that case, the welded material surface temperature can increase to considerably above Tm. As the surface temperature approaches the boiling point, Tb, metal evaporation starts and the resulting vapor pressure will start to deform the top surface and change the shape of the resulting weld. With further increases in beam power the molten metal is pushed out from under the beam resulting in a cavity drilled down into the metal. This cavity is usually called a keyhole. Keyhole formation is what leads to deep penetration welds. Any weld example with d/w > 1 is likely exhibiting some amount of keyhole formation. Notice that this only happens when considerable power is deposited inside of a small spot size, ie. a focused beam. The deep penetration weld shown in Figure 1 is a result of a keyhole drilled down into the liquid metal whose depth is almost equal to the resulting fusion zone depth. Additionally, the overall width of the fusion zone is roughly equal to the keyhole width (true for typical high travel speed welds) and, therefore, is about equal to the diameter of the beam.

Figure 3 illustrates the sequence of events leading to keyhole formation. Figure 4 reiterates the point that keyhole formation starts when the surface vapor pressure exceeds the ability of the liquid metal surface tension to prevent significant surface deformation. Again, that means that the heat source power density, power per unit area, is large enough that the surface temperature approaches the material boiling point. As an aside it is worth noting that the material surface temperature doesn’t necessarily rise to Tb. Figure 4 shows a simple calculation of the vapor pressure versus surface tension values for pure Fe. In that case, keyhole formation starts with a vapor pressure of a bit less than 100 torr. That corresponds to a surface temperature of about 0.9 Tb (in degrees K). It is interesting to note that direct measurements of keyhole temperature basically agree with this lower required temperature, see: D.A. Schauer, W.H. Giedt and S.M. Shintaku, “Electron beam welding cavity temperature distribution in pure metals and alloys”, Welding Journal, pp,127s-133s (1978). It is important to note that if the keyhole wall temperature becomes too high, the vapor pressure will push the liquid metal out of the keyhole so vigorously that cutting or drilling can occur. In any case, the crucial point is that deep penetration welding results when the beam power density is large enough to heat the metal to where its vapor pressure becomes significant.

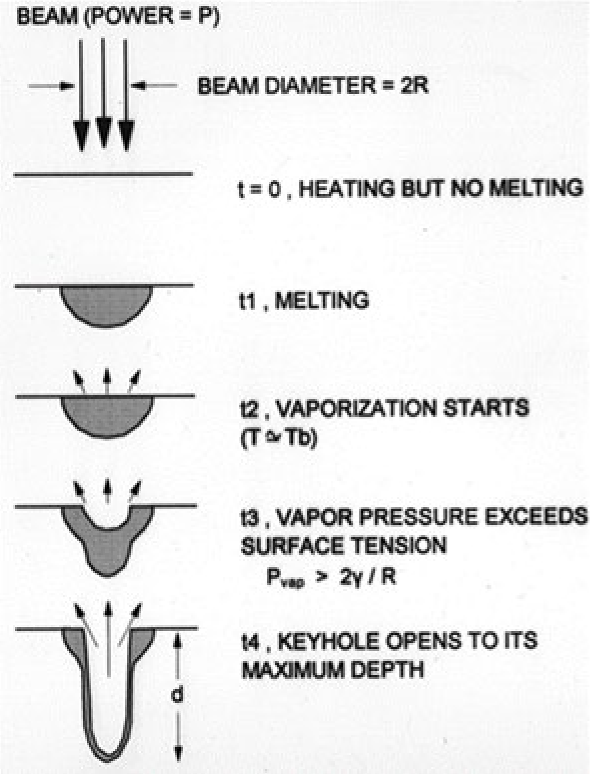
BEAM (POWER = P)
BEAM DIAMETER = 2R
t = 0 , HEATING BUT NO MELTING
t1 , MELTING
t2 , VAPORIZATION STARTS
(T ≃ Tb)
t3 , VAPOR PRESSURE EXCEEDS
SURFACE TENSION
P_{vap} > 2γ / R
t4 , KEYHOLE OPENS TO ITS
MAXIMUM DEPTH
d

Figure 3: Schematic diagram illustrating the sequence of events that lead to deep penetration welds.

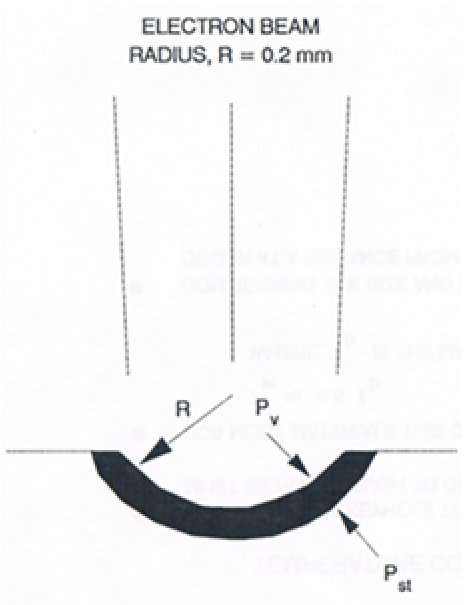
ELECTRON BEAM
RADIUS, R = 0.2 mm
R
P_v
P_{st}

AT THE ONSET OF KEYHOLE FORMATION
VAPOR PRESSURE MUST EXCEED SURFACE
TENSION, OR:

$$P_V \geq \frac{2G}{R}$$

EX: IRON AT ELEVATED TEMPERATURE
Surface tension coefficient, G = 1.2 N/m

Therefore, $P_V \geq 90$ torr

Note: significantly less than the boiling point
where $P_V = 760$ torr (at atmospheric pressure)

Figure 4: Schematic diagram of the weld top surface at the onset of keyhole formation. This is included to accentuate the point that keyhole formation requires a surface temperature high enough to overcome surface tension forces.

One reason for discussing the keyhole in some detail is that it helps explain another important attribute of deep penetration welds. To start this discussion note that the material displaced from the keyhole must go somewhere. The basic idea is that liquid is melted from the front surface of the keyhole in a travelling weld. That liquid flows around the walls of the keyhole due a combination of vapor pressure and surface tension driven flow. Note that calculations and measurements of flow around the keyhole walls suggest high flow velocities of perhaps 5m/s accompanied by swirling behavior in the metal behind the keyhole; see for example: F. Tenner, et al, "Experimental Approach for quantification of fluid dynamics in laser metal welding", J. Laser Appl., 27, pp. 1 (2015). This is important because the considerable stirring of the molten metal around a well-developed keyhole can be important for breaking up surface oxides on the mating joint faces within the extent of keyhole penetration. Another often useful result of the vigorous stirring is that it will help break up grain growth at the trailing edge of the weld. The result of the metal flow out of the keyhole is a "lump" of liquid trailing behind the keyhole which eventually flows back into the keyhole as that material cools and the local vapor pressure drops rapidly. The rapid movement of material in and out of the keyhole can lead to instabilities in the filling of the keyhole behind the beam, which can lead to unwanted void formation in the resulting weld. It is clear that the details of keyhole liquid motion are related to the details of beam power distribution (beam diameter and cross-sectional shape).

B. Weld Penetration and Energy Density

Let us continue the discussion of high energy density welding with the ultimate goal being a comparison of EB and LB. A good starting point is to take a basic look at the thermodynamics of welding. The ability of the beam to heat the metal and produce a weld is related to the beam power density and the time over which the beam interacts with any bit of metal surface. The power density is defined as:

$$P' = \frac{4\ P}{\pi\ D^2} \quad (\mathrm{W/mm^2}) \qquad (1)$$

Where P is total beam power and D is the "effective" diameter of the beam. A simple way to quantify the amount of beam energy deposited in the metal and that can result in metal heating is by how long it takes for the beam to pass across any portion of the surface. This is called the interaction time, which is:

$$t' = \frac{D}{v} \quad (\mathrm{sec}) \qquad (2)$$

Where: D is beam diameter, and v is the weld travel speed. In this formulation of the problem, the ability of the beam to heat the metal is the product of P' and t'. This leads to beam energy density, E':

$$E' = P'\ t' = \frac{P}{v\ D} \quad (\mathrm{J/mm^2}) \qquad (3)$$

Note that a factor of (π/4) has been ignored just to simplify the formula. Welding occurs when E' is large enough that it exceeds the total heat of melting for a volume of metal. Deep penetration occurs when the resulting temperature increase approaches the metal boiling point. Equation 3 makes the point that the fundamentals of HEDW are related to power and travel speed and on the extent to which the beam can be focused.

Equation 3 can be reformulated to produce a description of weld dimensions by making the simplifying assumption that the weld fusion zone, has width D and that a rectangular cross-section melt zone of depth, d, is moving through the metal. In that overly simplified picture the fusion zone would have a depth, d, that is just: $d = E'/H$, where H is the heat of melting of the metal. Of course, especially at low travel speed, much of the beam power is lost to thermal conduction. Thus, a more complex equation for weld dimensions is required. A more realistic description of the energy balance in a weld is suggested by 2-D heat flow calculations. In that case the energy balance between the input power and the combination of thermal conduction and metal heat of melting might be described by:

$$\mathrm{d} = \mathrm{C}\,\frac{(\eta\, P)}{(v\, D)^{\gamma}} \qquad (4)$$

where: d is the weld depth of penetration; C is a constant determined by the thermal properties of the material being welded (its melting point, thermal conductivity and heat capacity); P is beam power; v is part travel speed relative to the beam; D is the "effective" diameter of the beam (that will be defined later in this paper); η is the process efficiency (this will be discussed considerably later in this section); γ is a power law coefficient. This simple equation has some theoretical justification and Equation 4 describes much actual weld data quite well. However, for the purposes of this document, assume that it is just an empirical description of typical HEDW welds that does include the major weld variables in a sensible way. Notice that Equation 4 is basically just d = E'/H when the heat capacity of the material dominates the process. In other words, materials with small thermal diffusivity are well-described with γ =1 and materials with high thermal diffusivity are described with a smaller value of γ. Metal thermal diffusivity is: $\alpha = K/\rho C$ = the ratio of thermal conductivity to heat capacity. As will be shown later: γ is about 0.4 - 0.5 for materials like pure aluminum and copper; for typical structural materials the value of γ is generally 0.5 – 0.7 . It is important to note that γ = 0.5 is the expected value derived from fundamental thermodynamic considerations. See: D.B. Hann, J. Iammi and J. Folkes, "A simple methodology for predicting laser weld properties from material and laser parameters", J. Phys. D: Appl. Physics, 44, 445401 (2011). Equation 4 is presented largely to introduce the fact that EBW and LBW can be different primarily through the factors of beam coupling efficiency, η, and beam size/shape, D. Those potential differences will be discussed in some detail subsequently.

C. Focused Beam Size/Shape

One potential significant difference between EB and LB is the beam "effective" diameter and the beam cross-sectional shape. Before discussing the EB versus LB differences it is important to note that an agreed upon definition of beam diameter is necessary. The proper way to consider beam diameter is a calculation of the beam power density second-moment. This is defined in: ISO Standard 11146-1. It has long been recognized that electron beams are nearly Gaussian in shape over much of the parameter range. For a Gaussian beam, the second-moment diameter is the width of the beam where it falls to $1/e^2$ of its central value. For a Gaussian beam with width parameter, σ, the second-moment diameter is $D = 2\sqrt{2}\sigma$. Note that in this case the Gaussian is defined as: $I = I_o \exp(-r^2/\sigma^2)$. Laser beams often have a different shape. Most modern LBW machines utilize a fiber delivered beam. In that case, the beam typically has a "top hat" shape, which is just a focused image of the output end of the typical multi-mode delivery fiber. In that case the second-moment diameter is just the diameter of that circle of fairly uniform beam power density. Two examples of measured typical EB and LB beam shapes at sharp focus are shown in Figure 5. In this paper data for measurements of beam diameter and shape will be presented. The data for electron beam diameter were obtained using a device and software initially described in: J.W. Elmer and A.T. Teruya, "An Enhanced Faraday Cup for Rapid Determination of Power Density Distribution in Electron Beams", Welding Journal 80(12), p.288s (2001). The laser beam diameter data are from a commercial device: Primes GmbH - Focus Monitor.

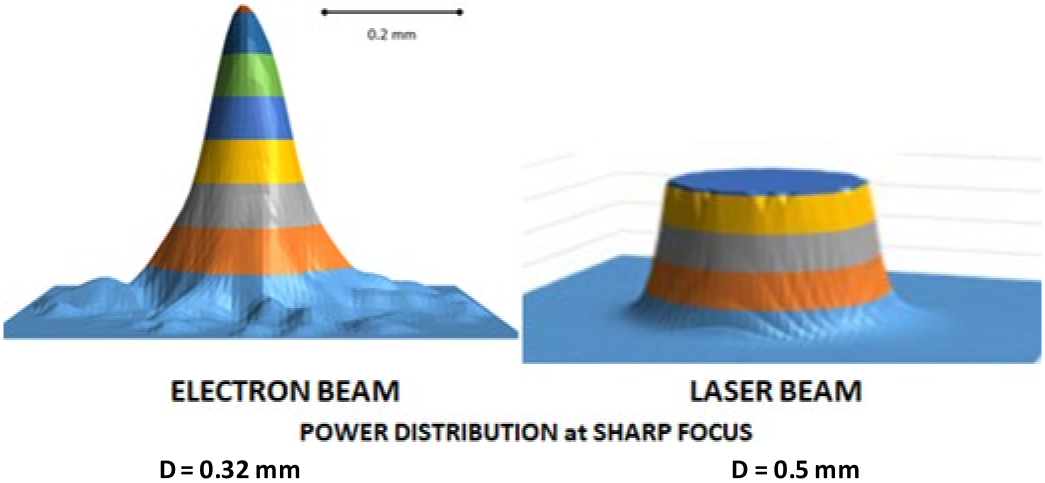

Figure 5: Measured beam profiles for typical electron and laser beams at sharp focus.
[EB: 110 kV; 8.5 mA; W.D. = 240 mm] [LB: 1000 W; 300u fiber; f.l. focus/coll. lens. = 200/120].

It would be reasonable to ask if defining beam diameter as the second moment of the power distribution is realistic or merely arbitrary. Figure 6 is presented to illustrate that the resulting weld width, measured at a place indicative of keyhole width, does agree nicely with the measured beam diameter values. There is a constant offset between weld width and D meaning that the limits of the melt zone extend a bit beyond the keyhole as is necessarily the case. It is important to note that the offset between W and D is small at high travel speed and increases a bit at slow travel speed. However, the overall agreement of W and D illustrates the basic validity of the second moment diameter.

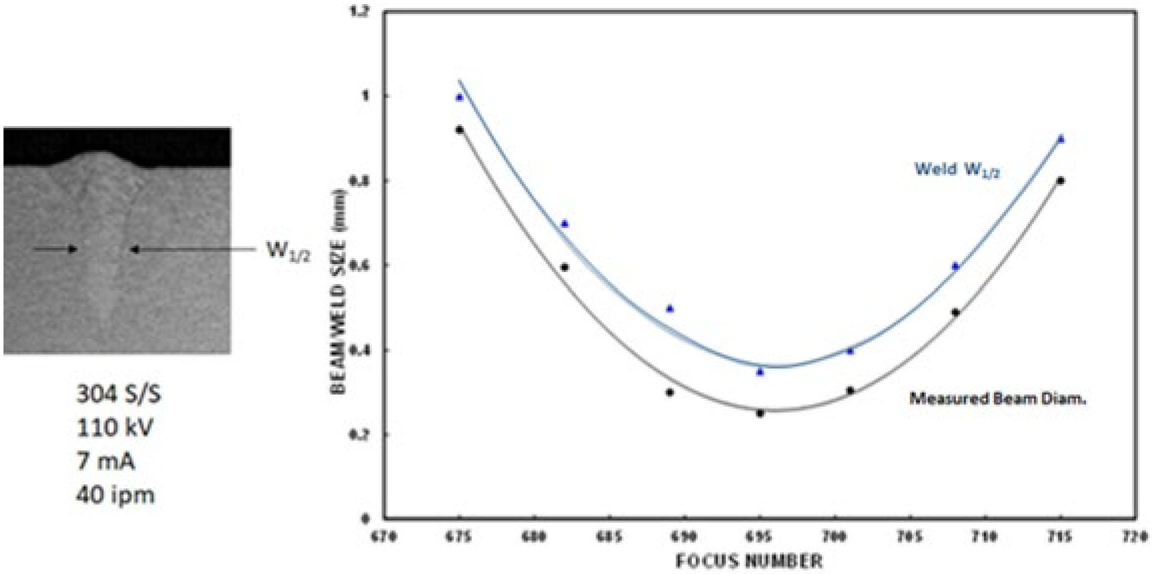

Figure 6: Measured width of EB welds in the keyhole regime versus beam diameter, defined as the second moment of the beam power distribution. This figure is illustrating that the definition of D does adequately describe the resulting weld shape.

It should be noted that the laser beam shape shown in Figure 5 is typical of a fiber delivered beam. However, that top hat shape isn't necessarily descriptive of all laser welding machines. It is possible for the beam to be directly delivered to the weld station from a single-mode resonant cavity laser. For a description of beam mode structure see: “Chap. 22, Laser Beam Welding”, AWS Welding Handbook, Vol. 2. Also, it is possible for the laser beam to be delivered to the weld by a single mode optical fiber (a very small core diameter). In these latter two cases, the laser beam profile would be Gaussian and much more similar to the typical electron beam and the beam diameter can actually be smaller than typically achieved in electron beam machines. Nevertheless, a top hat distribution of beam power is quite common and the subsequent discussion will mostly assume that beam distribution.

The fact that the beam diameters and shapes can be considerably different does affect the resulting welds. An example of this is shown in Figure 7 where EB and LB welds were made on the same Type 304 stainless steel material. The LB weld is noticeable shallower consistent with its larger beam diameter. It should also be noted that the laser weld is even wider and shallower than might be expected because of other effects caused by interaction of the laser beam with gas molecules and metal vapor above the weld; that will be discussed subsequently. Additionally, the LB weld has a bit of a rectangular shape indicative of the importance of the shape of the power distribution. This certainly suggests that the EB weld would be more flexible for applications where deep penetration welds are desired.

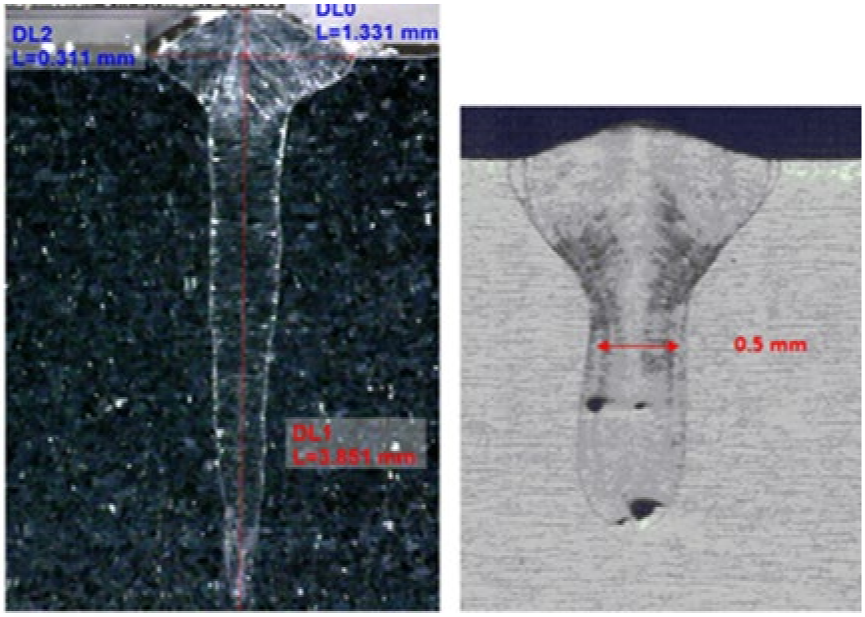

EB Weld **LB Weld**

Figure 7: Welds made in stainless steel using the measured beam profiles shown in Figure 5. Both welds were made with 1000W of beam power; sharp focus; 60 ipm travel speed. Weld data is from: “Considerations for Transitioning EB Welds to Equivalent LB Welds”, A. Black, A. Duffield, P. Burgardt and B. Preston, AWS Professional Program (2018) and accompanying internal LANL report.

The obvious advantage of EBW, as illustrated in Figure 7, should be considered with some caution for two basic reasons. First, the laser beam can have a shape and overall spot size comparable or even smaller than the electron beam, as was mentioned above. This small laser beam spot size is often a result of a short focal length output lens which does result in much more rapid clouding of the lens assembly by metal vapor but, presumably, that drawback could be acceptable. The second reason why EB and LB are more directly comparable is that actual production welds are often made with beams that are not at sharp focus.

One reason for using somewhat defocused beams is to facilitate adequate joint penetration where some joint runout and beam misalignment to the joint is possible. A sharp focus beam would always be advantageous relative to factors like part distortion. However consider the EB weld in Figure 7. If the combined joint runout plus a bit of misalignment of the beam to the joint added up to be more than perhaps 0.2 mm, the potential for missed joint is high. Thus, a defocus beam is a typical approach to making good welds. Another reason why minimum diameter beams are not always advantageous is related to the basic keyhole behavior discussed briefly in Part A of this paper. A satisfactory weld will only result if the liquid displaced from the keyhole flows smoothly back into the keyhole at the trailing edge of the keyhole. When the keyhole is exceptionally deep and narrow that filling process tends to become unstable. In Figure 7 two possible ramifications of keyhole stability are illustrated. Looking closely one can see some evidence of variable penetration at the root of the EB weld. The accompanying LB weld shows trapped gas in the weld. Figure 8 shows two other examples of "cold shut" type voids in the weld root that can occur in deep penetration welds in metals and alloys that are particularly sensitive to instabilities in keyhole filling. Note: these root voids are often called cold shut type voids because they do seem to occur because the liquid metal solidified before it could fully fill the keyhole; that is similar to cold shuts that occur in casting when a narrow feature in a mold is being filled and the mold is not adequately pre-heated.

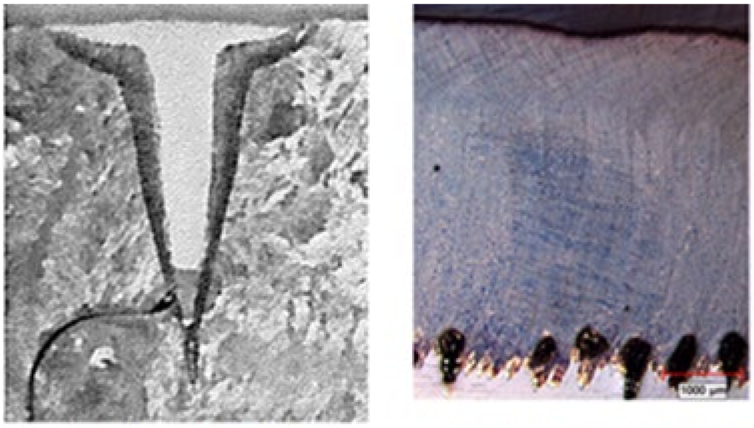

HVEB – Uranium
(early Y-12 publ.)

HVEB – Type 21-6-9 S/S
Longitudinal Met Section

Figure 8: Two examples of the cold-shut type voids often seen in deep penetration welds produced by High Voltage EB machines when welding in vacuum.

The simplest solution to missed joint and to voids in deep penetration welds is often to widen the weld a bit. This is actually successful in most materials but more extreme process variations may be necessary in harder to weld materials. In any case, moving the process away from beam sharp focus is a common way to ensure good weld quality. This can be accomplished most simply by some level of beam defocus. Other alternatives include some manner of beam deflection.

Before discussing this matter further it is important to note that not all voids seen in beam welds are directly related to keyhole instability problems. The spherical voids seen in the LBW in Figure 7 are probably gas voids and are not directly connected to keyhole stability issues. However, it is often the case that widening the weld a bit will help minimize these voids. The basic concept being that a bit longer time required for the weld metal to solidify will give those gas voids time to float out of the molten metal. However, an additional possible cause for weld voids may not be helped by these keyhole widening strategies. An example is where the voids are a result of decomposition of inclusions, such as large oxide particles, in the base metal. In that case widening the weld (thereby encountering more inclusions) may well be counter-productive. An appropriate void mitigation strategy requires detailed knowledge of the origin of the voids.

A detail mentioned above should be stressed a bit. For some applications and in some particularly difficult materials, the proper way to make the weld and control weld quality is some manner of beam deflection. That could be circle deflection but might include more exotic techniques such as rapid beam deflection that partitions beam energy between the leading and trailing edge of the keyhole thereby controlling the cooling of the material at the trailing edge of the keyhole. It is a bit difficult to do this with laser equipment since it would involve some mechanical motion of the optics. Laser beam deflection via a mechanism such as a “wobble head” is available. However, its reliability in a production environment remains to be demonstrated. Very complex beam deflection in EB is simple via appropriate input to the magnetic deflection coils that are already present in the machine. Thus, in cases where maximum machine flexibility is desired, EB machines are the obvious best choice.

Because sharp focus welds are often not desired, the relative merits of LBW and EBW should be assessed for some level of beam defocus. In that case, the overall beam sizes and shapes are much more similar. Figure 9 illustrates the LB and EB beam shapes when the overall beam diameters are matched at an appropriate level of beam defocus. Figure 10 shows the resulting welds from EBW and LBW. As can be seen, the overall weld shape and penetrations are not exactly the same but it is clear that comparable weld quality can be achieved with either process. An interesting factor shown in Figure 10 is the considerable difference in EB and LB power needed to provide the desired weld penetration. That is a result of beam coupling efficiency; that will be discussed in Part D of this paper.

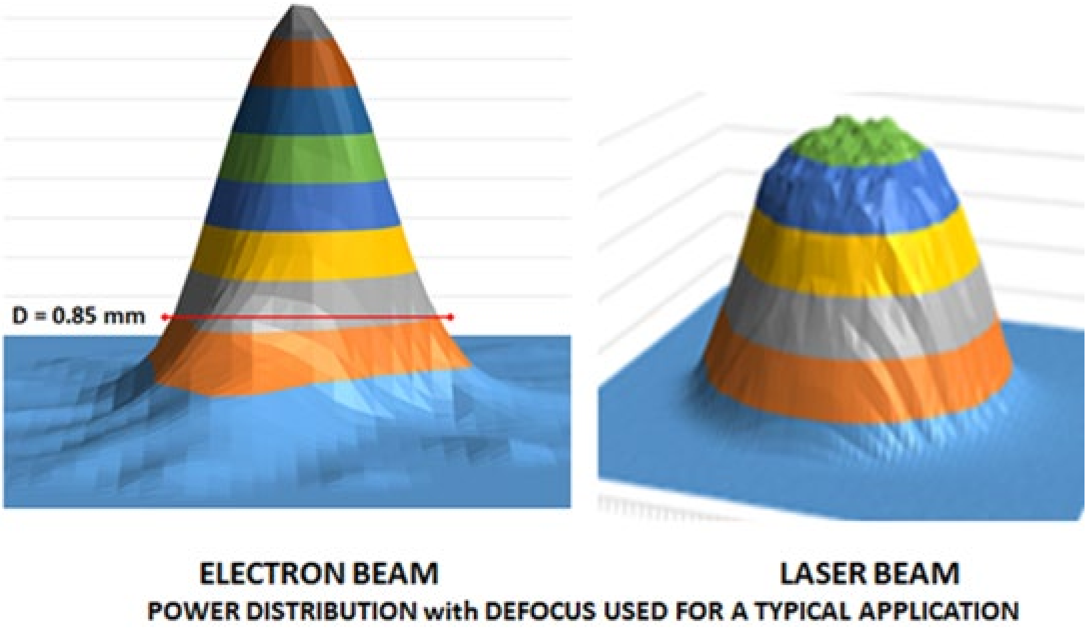

Figure 9: Measured beam power distributions for EB (left) and LB (right) when the overall beam diameters are matched at a value of 0.85 mm.

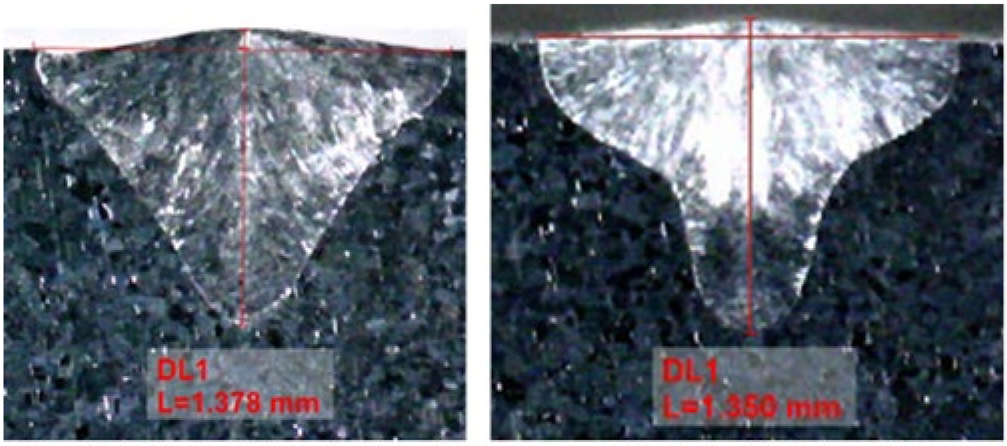

EB: 1000 W, S+23 incr (≈ 20 mm)

LB: 1300 W, S+0.280″

Figure 10: Welds made in stainless steel with EB and LB using the beams illustrated in Figure 9. The values of S+X give an idea of how much defocus was used in each case. v = 25.4mm/s (60 ipm)

D. Beam Coupling Efficiency

From a beam physics perspective, the major difference between EB and LB properties is the fundamental difference between the makeups of the beams, which results in different beam coupling efficiency values, η. In Equation 4 the quantity η was introduced to make the point that only some fraction of the total beam power is deposited in the metal. The electron beam consists of rapidly moving electrons that have mass and that mostly just enter the metal, slow down and deposit their kinetic energy in the metal surface as useful heat. The laser beam is just an intense light beam. For the purposes of this discussion it is simplest to consider that beam as being a high intensity electromagnetic wave impinging on the metal surface. Any time an EM wave encounters an interface (a difference in optical density) it undergoes some amount of reflection as well as transmission through that interface. In the case of welding, only the fraction of light transmitted through the interface (the metal surface) will be available to heat the material. Thus, the fundamental problem for welding is that at least some fraction of the incoming light is simply reflected from the metal surface. This is the basic reason that the beam coupling efficiency, η, can be much different for electron and laser beams. The complex behavior of η in LBW is the major drawback or at least complication to that process.

It should immediately be made clear that the process efficiency in EBW is not 100%. Some fraction of the incoming electrons do simply scatter from metal atoms and rebound from the surface (the result is secondary electrons that can be used for interesting things such as imaging of the part surface). Additionally, some beam power is lost to radiation (thermal and X-ray), perhaps a tiny bit of loss to conduction even in the vacuum levels used in EB and the metal vapor created in the keyhole carries away substantial energy. An additional complication to EB is that the amount of electron scattering from the surface is dependent on the Z-number of the atoms in the substrate (although this effect is minimized in low incidence angle interactions typical of welding). The result of all these factors is that η is a bit different for different materials in EBW. In typical structural materials η ≈ 0.9 and is probably noticeably lower in higher Z materials (U and Pu being examples). However, the crucial point is that η is reasonably constant for a particular material and set of welding variables in the case of EBW.

The complication to LBW is that the process efficiency is distinctly not a constant. It is less than 1 due to the usual radiation and vapor losses but, because of the wave nature of light, the amount of beam reflection can be large. A simple expression for light wave absorptance at a material surface is:

$$A \approx C\frac{1}{\sqrt{\sigma}} \qquad (5)$$

Where: A is the beam absorptance value (the fraction of laser light absorbed into the metal); C is a constant; σ is the material electrical conductivity. Note that Equation 5 works quite well in the far infrared and less well in the near infrared (such as 1.06microns [Nd lasers] or 1.07microns [Yb lasers]) but adequately describes the physics to be discussed subsequently. In the context of this part of the discussion, the process efficiency in LBW is largely limited by its intrinsic absorptance; in other words for LBW, process efficiency is no better than η = A when the beam first strikes the part.

Metals are called metals precisely because their internal electronic structure yields a high value of electrical conductivity. Thus, metals have intrinsically low values of light absorptance. To put this in perspective note that pure metals like copper and aluminum have high values of light reflectance of 97 – 99% even at 1.06 microns. Of course, that is why mirrors can be made from copper. Other metals have lower values of electrical conductivity and will absorb a bit more of the laser light. Alloys have a disordered structure and accompanying lower electrical conductivity. Thus, an alloy like stainless steel will have significantly larger absorptance than most pure fcc metals. At room temperature the absorptance value for stainless steel (at 1.06 microns) is about A = 1–R = η ≈ 25%. Obviously this is a considerably limiting factor to successful LBW. Because of the sensitivity of laser coupling to metal electrical conductivity, alloys with varying composition would cause at least some problems with a stable LBW process. Some supporting data reinforcing the points made here are shown in Figure 11.

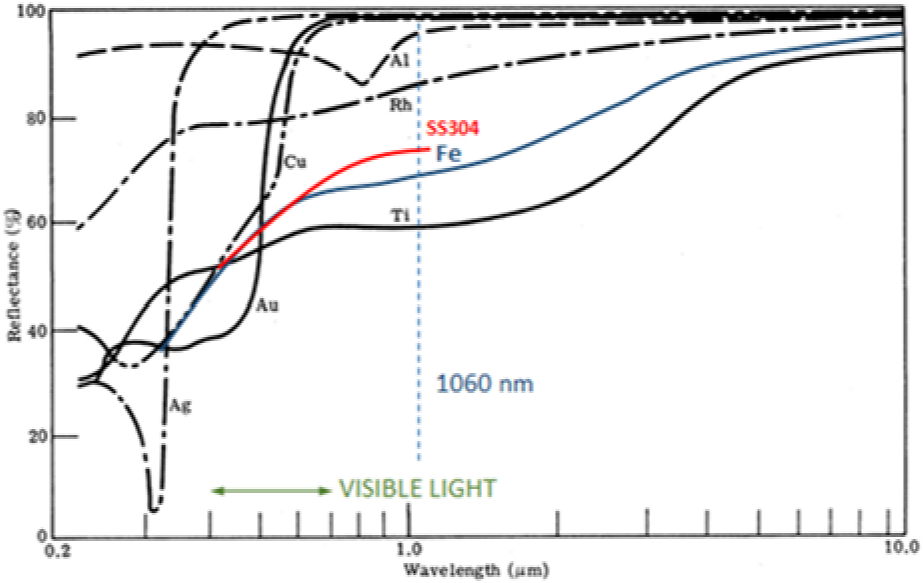

Copied from: Wikipedia - reflectance

Figure 11: Representative data for laser light reflection from various metals. Note that this diagram is a plot of material reflectance (given in %).

As an interesting aside, it can be asked how electrons might fit onto Figure 11. The basic idea is that electrons, being quantum mechanical entities, can be thought of as an EM wave with some wavelength.

Electrons at normal beam energies have a wavelength of < 0.0001 microns (equivalent to very high energy X-rays). That places the electron wavelength far to the left of Figure 11. In that wavelength range all metals have a low value of reflectance, hence the good coupling of electrons to the metal. Most electrons penetrate perhaps 10 microns into the metal and deposit their kinetic energy there.

An important additional point not addressed in Figure 11 is surface condition. Fundamental measurements of metal reflectance are usually made with the cleanest practically achievable surfaces and those data aren't necessarily relevant to welding. Reflectivity does change with factors such as surface roughness and oxide films. This has been seen to be a significant effect for 10.6 micron lasers and less so at 1.06 microns. Nevertheless, factors such as the existence of a surface oxide layer will change the reflectance of the surface. For example in studies of laser marking, the value of R is lowered by at least a factor of two (at 1.06 microns) for a heavily oxidized versus a clean surface in stainless steel and titanium, see: V.P. Veiko, et. al., "Controlled oxide films formation by nanosecond laser pulses for marking", Optics Express, 22(20), pp. 24342-24347 (2014). Reflectivity of the metal surface might be particularly variable in reactive metals. In any case, it is important to note that the success of LBW can depend on the surface quality of the parts to be welded and that is another factor that must be controlled as best as possible in LBW production.

Another interesting aspect of Figure 11 is related to the even bigger problem with LBW encountered in the early days of its development. In those times the welding machines were CO2 lasers with output at 10.6 microns. In that case, the beam reflectance was > 90% for all metals and alloys, making welding very difficult. The modern generation of lasers operating at shorter wavelength are much more satisfactory for LBW.

Equation 5 suggests another interesting complication with LBW. This additional factor arises because the electrical conductivity of metal is a function of its temperature. Specifically, the electrical conductivity of most metals decreases approximately inversely proportional to its temperature. As an example consider values for stainless steel: absorptance increases from about A = 25% at room temperature to about A = 35% as it approaches the melting point. Already one can see the potential for non-linear behavior of welds versus beam energy density, E', even if one were trying to make conduction mode LB welds.

A more important non-linear behavior relative to laser light reflectance occurs once a keyhole starts to form. Any light striking the sides of the keyhole cavity will be mostly reflected downward and have a high probability of undergoing at least one more reflection before leaving the keyhole altogether. That light with two reflections will overall be absorbed at about the 60% level. If any light ray can undergo multiple internal reflections in the keyhole (perhaps more than 5 reflections) that fraction of the beam will be absorbed with an effective absorptance that will be >90%. The result is that the LB process efficiency, η, will go from about 35% as the keyhole starts to form up to perhaps 80% for fairly small further increases in beam power density. Once that transition zone is passed, the coupling efficiency is relatively constant and further beam energy density increases produce predictable results. However, the key problem is that weld behavior is very non-linear in that transition region.

Some weld data directly comparing EB and LB welds in a particular heat of Type 304 S/S are shown in Figure 12. Of particular interest is the rapid transition from melting to deep penetration welding seen in the LBW data occurring for P = 600-750 W. The notes on the figure about the η values reinforce the points made in the preceding paragraph. Clearly, weld penetration control is effectively impossible in the penetration transition regime where process sensitivity to small weld variable variations or metal quality variations is impossibly high. Another interesting example of the extreme sensitivity of LBW to energy density is shown in Figure 13. This was an interesting experiment where a traveling LB weld was made across a stainless steel sample while the beam power was slowly ramped up from zero to 1000 W. Notice in Figure 13 that the beam started to produce some melting at about 90 W. The FZ size continued to increase roughly linearly up to about 355 W but with very small weld penetration throughout. Suddenly at about 360 W the FZ size increased dramatically. The graph in Figure 13 is a result of calculating the FZ cross-sectional area (effectively the melting efficiency of the process) from metallography resulting from serial sectioning through that region. Notice that the melting efficiency increased by 2.4 times over only about a 5 W range as the keyhole started to form. This again illustrates the extreme difficulty of process control in this "transition" regime. Therefore, a critical limitation to LBW is that weld development must result in a choice of beam focus, power and travel speed that meet requirements and avoid the penetration transition regime. For shallow penetration welds it can be difficult to ever achieve a stable process with LBW.

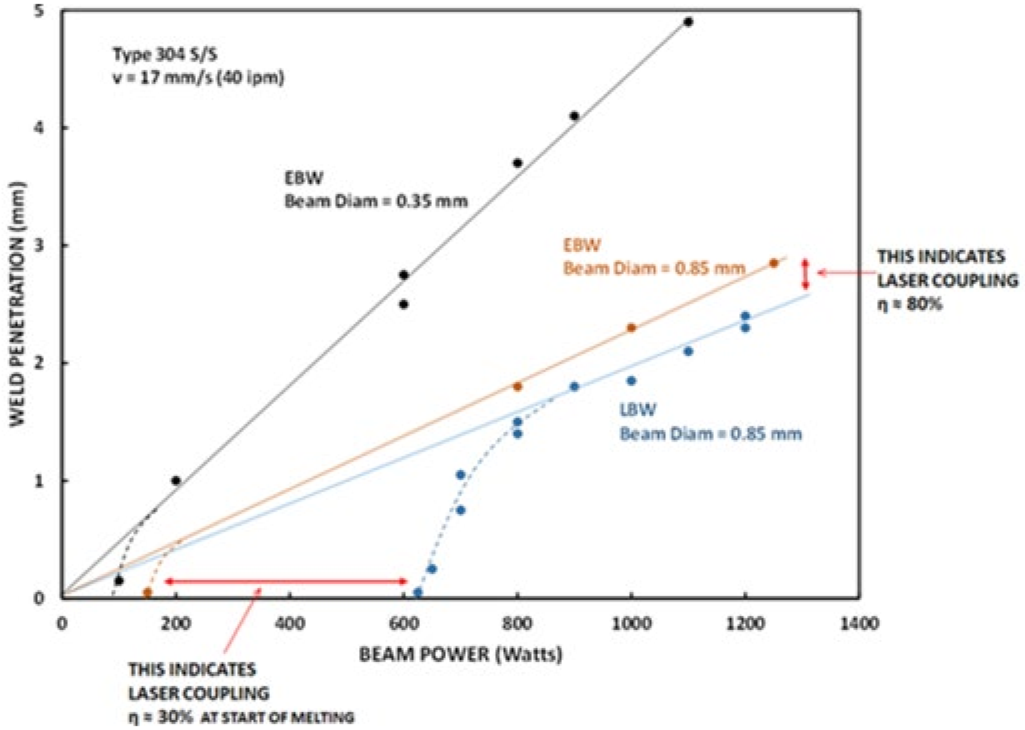

Figure 12: Weld penetration data for EBW and LBW of stainless steel (all at 40ipm travel speed). These data illustrate the complicated penetration behavior of LBW versus beam power.

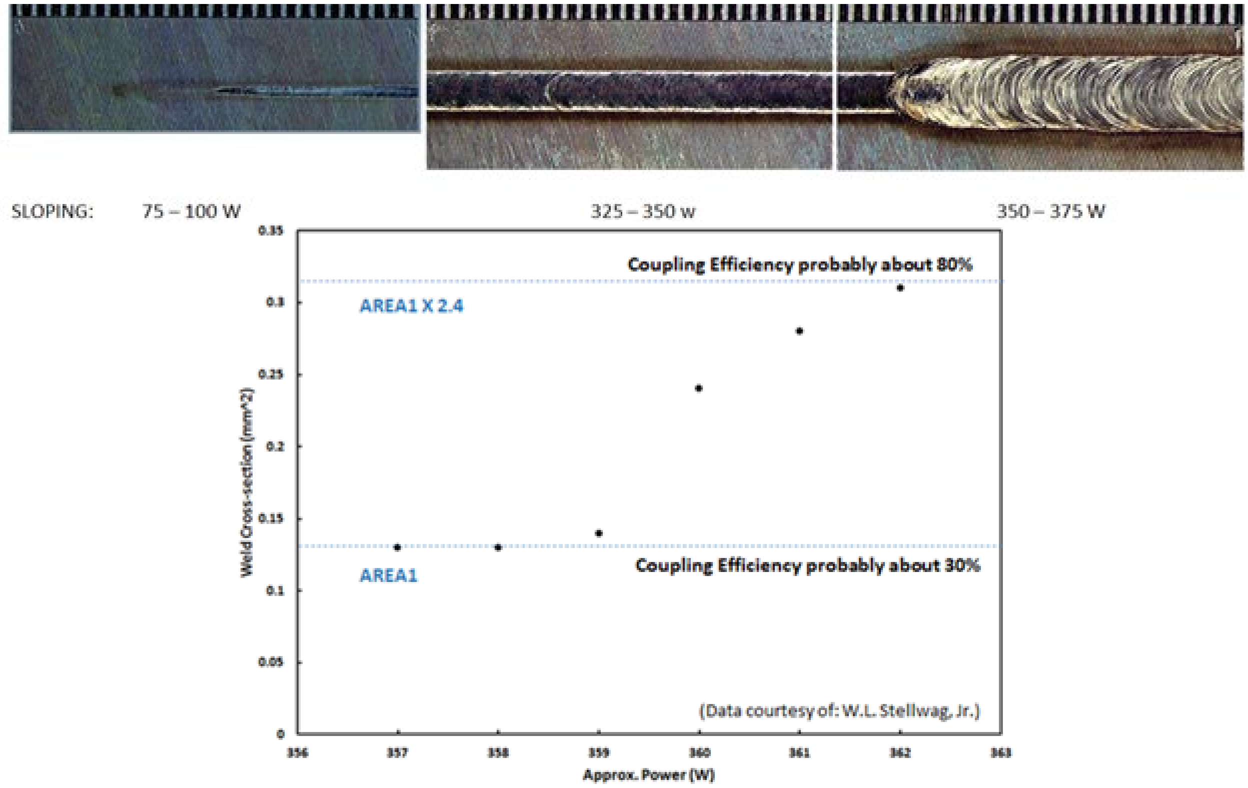

Figure 13: Another example of the large change in laser beam coupling as the keyhole forms. In this example the beam power is slowly being ramped up. Notice the large change in FZ area that happens over a range of only about 5 Watts. From: W.L. Stellwag, Jr., OSU MS Thesis.

Related to the above discussion of beam coupling, pulsed LBW should be mentioned. Many modern LB machines are mostly designed around continuous output (CW) but pulsing is still possible and could be advantageous. The basic idea behind pulsed laser ouput is that a high beam power for some short time would be followed by zero power or a lower power background level. The essential concept is that the high pulse power is large enough and applied for long enough to open the keyhole and produce the desired relatively good beam coupling efficiency. Since it takes a finite time for the keyhole material to cool and refill the keyhole, no beam power (or low backgroud power) can be applied during the time interval while that material cools. By properly adjusting the high (and low background if that is possible) pulse power, durations and pulse frequency good quality welds can be achieved with overall lower power than can be achieved with a CW laser. That can be highly advantageous in heat sensitive materials and assemblies. Pulsed LBW should at least be considered for any production application.

The major complication with LBW is clearly the intrinsic reflectivity of metals. However, referring back to Figure 10 we see an example where, all obvious weld variables being the same and in keyhole mode, that a comparable LB weld is consistent with the LB coupling efficiency being only about 0.7, a bit smaller value than expected. Therefore, it is important to consider other factors that might limit LB process efficiency. It seems most likely that the primary difference between the processes is that the EB welds were made in vacuum and the LB welds were made at atmospheric pressure. Oxidation of the weld metal is prevented in LBW by flooding the weld area with an inert cover gas such as argon. The presence of this gas does introduce potential additional complications. The simplest point is that flowing gases will carry away considerable heat from the weld area; this is especially true for helium gas. This is undoubtedly relevant but it appears that the major factor in further limiting LB coupling efficiency is presence of the “plume”. The plume is a region of brightly glowing material seen above the weld pool and often extending for a significant distance above the weld. It is apparent that the plume is absorbing considerable beam energy and also potentially causing the beam energy density to decrease by diffusing the beam and thereby increasing the spot size, D.

The plume has sometimes been referred to as a plasma. A plasma is generally thought of as having considerable ionization leading to a high electrical conductivity of that gas. That would be significant since the laser light would interact with that conductive region by being reflected, absorbed and refracted. A phenomenon known as plasma breakdown has been observed in high power CO2 laser welds. This is a situation where the gas has gotten hot enough to start some level of ionization which leads to accelerating beam absorption. At that point the plasma temperature rises very rapidly towards a high level of plasma ionization and the beam rapidly becomes totally absorbed by the plasma. In fact, that is the main reason that helium shielding gas was recommended for LBW at least in the infancy of LBW technology; the higher ionization potential of helium yielded much less tendency to plasma breakdown by the long wavelength light produced in CO2 lasers. Thus, it is possible for the plume to have a significant level of ionization. This is a result of a process known as inverse Bremmstrahlung, which increases approximately proportional to wavelenth as λ^2 (this phenomenon is roughly 100 times less important in solid state lasers operating at 1.06 microns). Direct measurements of plasma temperature accompanying the welds illlustrated in Figures 7, 10 and 12 showed that the gas temperature in those LB welds ranged from only 2800 – 3200 K. Other data in the literature shows that the plasma temperature could reach 4000K for higher power LBW with solid state lasers. At those temperatures the degree of ionization of the argon or helium shielding gas is too small (< 5%) to have an appreciable effect on the laser beam. The basic message here is that the phenomenon should probably simply be called a plume because its degree of ionization is probably too low for it to realistically be called a plasma (of course, with the exception of high power CO2 lasers).

Another possible reason for existence of the plume is absorption and scattering of laser light by gas molecules and metal vapor atoms above the weld area. Light is affected by these atoms and molecules in a process known as Rayleigh scattering. Rayleigh scattering is elastic scattering of the photons of light from atoms/molecules. As a result of the long wavelength of laser light (assumed to be 1.06 microns for this discussion), the Rayleigh attenuation and scattering coefficients are calculated to be very small and negligible in the context of welding. However, a special case of Rayleigh scattering is relevant. If the atmosphere above the weld contains particles that are large compared to the wavelength of the laser light, then scattering and absorption of the beam will be larger and entirely relevant to welding. This phenomenon is called Mie scattering. Calculations of Mie scattering, assuming particles of about 50 micron diameter, show some scattering resulting in a modest increase in beam diameter but the big effect is beam attenuation via heating of the particulate. Assuming a realistic particle number density the calculated attenuation coefficient can be as large as 5 m^{-1} (this would mean an attenuation of roughly 25% for a normal height plume).

A number of plume studies have shown that the bright light coming from the plume is mostly produced by metal particulate heated to roughly 3000 K. That particulate is a result of coalescence of the metal vapor from the keyhole into particles roughly 40 microns in diameter. That particulate forms in the case of atmospheric pressure welding and not so much in vacuums. The concept is that in vacuum the metal vapor atoms basically freely leave the weld area to be plated on the walls of the weld chamber. However at atmospheric pressure, the metal atoms rapidly collide with gas molecules and are slowed to the point that the metal atoms interact with each other to form up into the small metal particles. Particle formation seems to occur almost immediately as the atoms leave the keyhole. For a review of this phenomenon consult: D. P. Shcheglov, "Study of Vapor-plasma Plume during High Power Fiber Laser Beam Influence on Metals", BAM dissertation (2012). From the perspective of practical LBW applications the plume is important because that particulate can absorb a significant fraction of the incoming beam power and cause that energy to be dispersed away from the weld zone. These plume effects are largely responsible for the shallower welds with accompanying wider top surface melting as seen in Figures 7 and 10.

It is possible to moderate plume effects by various gas flow arrangements. Figure 14 shows some data from a welding publication showing that the plume can be minimized by a cross-flow of shielding gas. For the purposes of this discussion it should be noted that plume suppression by strong shielding gas cross-flow is possible but may not be practical because rather high flow rates are needed. However, these data do point out that some significant variability in LB welds can result from the details of the shield gas flow rates and the orientations of the gas nozzles. This is another process detail that must be properly controlled in order for LBW to be a viable process.

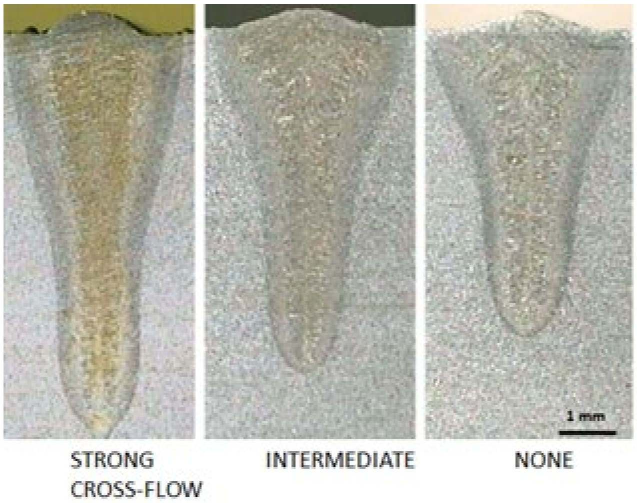

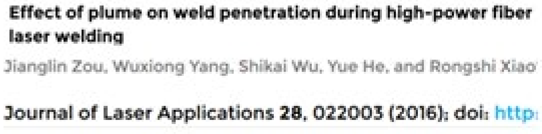
Effect of plume on weld penetration during high-power fiber laser welding

Jianglin Zou, Wuxiong Yang, Shikai Wu, Yue He, and Rongshi Xiao

Journal of Laser Applications 28, 022003 (2016); doi: http

Figure 14: Some LB weld data showing that weld behavior is influenced by the plume. The basic point is that shielding gas cross-flow will disperse the plume and significantly improve weld width and depth.

E. Vacuum versus Non-Vacuum Laser Beam Welding

In the spirit of properly comparing EB and LB processes it should be mentioned that a major improvement in the LB process can accrue from using an equivalent vacuum environment. In the past

LBW-V (vacuum LBW) has not seemed particularly feasible because of the additional equipment complexity that is involved with vacuums. However, it should be noted that welding of reactive materials often occurs inside of an inert box incorporating some manner of gas purifying and gas circulation system. Viewed objectively that means that those LB systems already have many of the same basic components involved in LBW-V. Clearly the relatively simple inert box would have to be strengthened in order to not implode in a vacuum and would require a vacuum feedthrough for the laser fiber. However, these items are mostly just an initial design problem and not a major technical hurdle. Also, there has always been some concern that LBW-V would involve a diffusion pump system, which can be a bit difficult to maintain. Two things should be mentioned in this regard. First, most of the advantages of LBW-V actually occur in a pressure range achievable by normal mechanical vacuum pumps. Second, even if better vacuum levels are desired, new design direct drive mechanical pumps can achieve vacuums comparable to a diffusion pump system without the maintenance problems of a diffusion pump. Thus, the possibility of using LBW-V should at least be considered.

The fundamental question is why would one consider using LBW-V? There are at least three reasons why the additional complexity of a vacuum can be useful. One important reason to weld in vacuum is to prevent oxygen, nitrogen and water interactions with the weld metal. Some reactive metals can react badly to the typical environment provided by shielding gas (gas of UHP purity and inside of a reasonably clean inert box). Welding in vacuum will be a cleaner environment even for fairly modest vacuum levels. A vacuum level of perhaps 0.01 mbar will contain fewer air molecules than can realistically be achieved by any shielding gas arrangement. Another reason for using LBW-V is related to gas pore formation in the weld. Figure 7 is an example of voids in a fairly deep penetration LB weld in stainless steel. There is some discussion in the literature about the exact mechanism for this pore formation. However, it is intuitively obvious that there is a higher likelihood of gas trapping at the trailing edge of the keyhole when the cavity is filled with a mixture of shielding gas and metal vapor at 1 atmosphere of pressure relative to what would happen in a vacuum environment. In any case, LBW-V shows a considerable decrease in the propensity for weld void formation. The third important advantage of LBW-V is that it results in much greater weld penetration for a given power input. Figure 15 shows some LB welds showing the increased weld penetration and improved weld void content that occurs in LBW-V. As an aside, this particular figure was chosen because it shows that at least one vendor (PTR, Precision Technologies, Inc.) has become interested in selling LBW-V equipment, which promises future commercial support for that technology. Other examples of the advantages of LBW-V are presented in:
1) M. Jian, W. Tao and Y. Chen, "Laser Welding under Vacuum: A Review", Appl. Sci., 7, p. 909 (2017);
2) J.W. Elmer, J. Vaja and H.D. Carlton, "The Effect of Reduced Pressure on Laser Keyhole Weld Porosity and Weld Geometry on Commercially Pure Titanium and Nickel", Welding Journal, p. 419s (2016).
Elmer et. al. showed that LBW-V and EB welds are essentially identical when equivalent spot sizes are used, at least in those deep penetration welds. Those authors also found that a vacuum level of 0.1 mbar was adequate to generate good quality LBW-V welds.

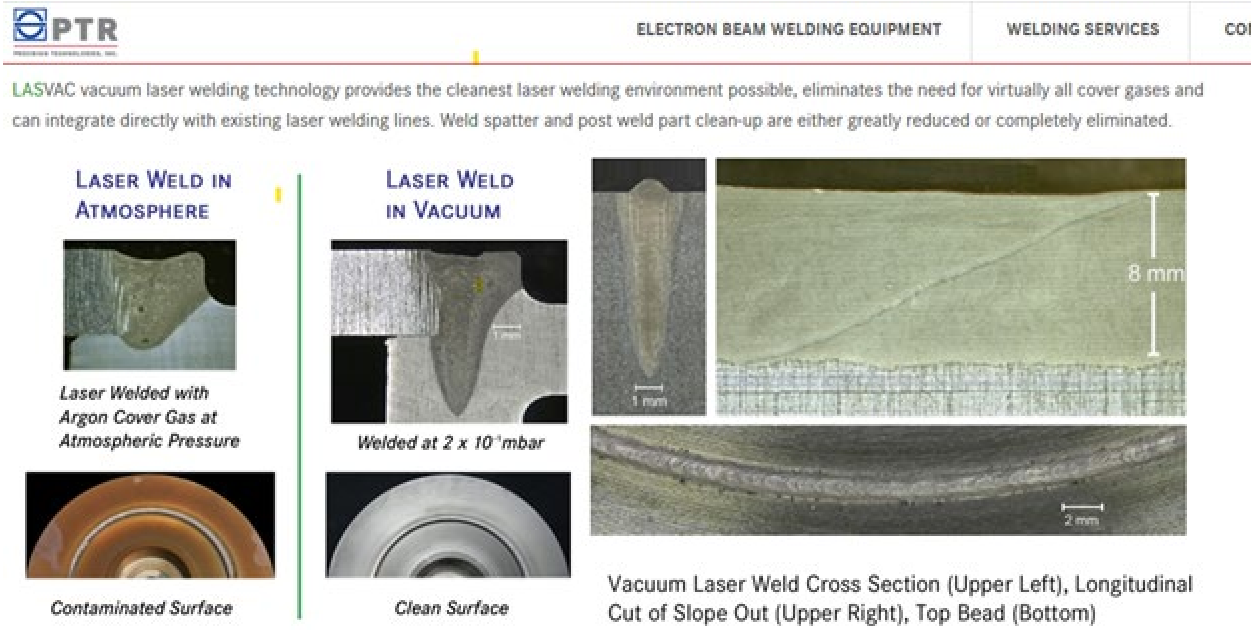
PTR
ELECTRON BEAM WELDING EQUIPMENT
WELDING SERVICES
COI

LASVAC vacuum laser welding technology provides the cleanest laser welding environment possible, eliminates the need for virtually all cover gases and can integrate directly with existing laser welding lines. Weld spatter and post weld part clean-up are either greatly reduced or completely eliminated.

LASER WELD IN ATMOSPHERE
Laser Welded with Argon Cover Gas at Atmospheric Pressure
Contaminated Surface
LASER WELD IN VACUUM
1 mm
Welded at 2 x 10^{-1}mbar
Clean Surface
1 mm
8 mm
2 mm

Vacuum Laser Weld Cross Section (Upper Left), Longitudinal Cut of Slope Out (Upper Right), Top Bead (Bottom)

Figure 15: Examples of the advantages of LBW-V. Note that a vacuum level of only 0.2 mbar produces a factor of 2X greater penetration with a considerable improvement in weld void content and weld cleanliness. (Copied from PTR web-site)

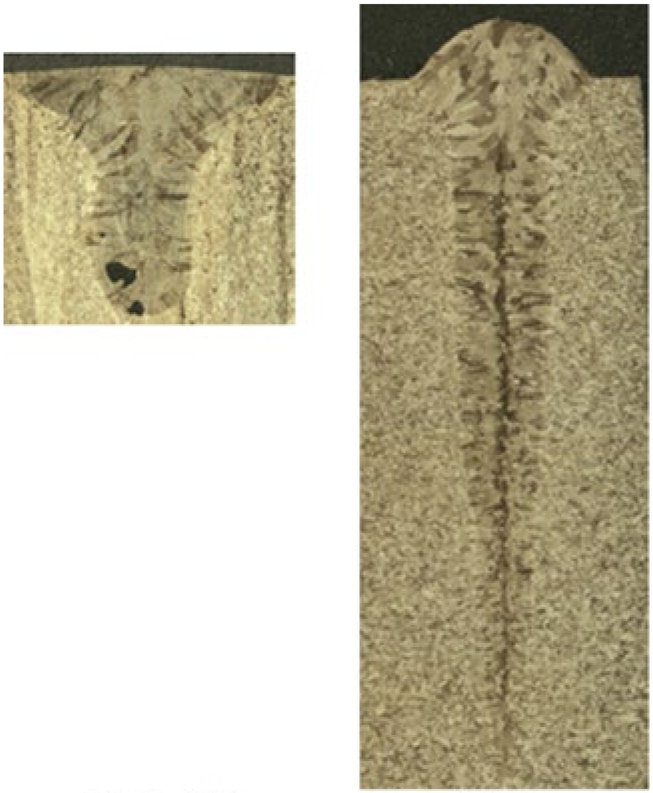

LBW: Ar shielding LBW-V

Figure 16: Conventional and vacuum LB welds in pure Ni made under similar weld conditions. Notice the void content of the conventional LBW versus the LBW-V welds. Note that the vacuum level was about 0.1 mbar. From: Elmer et al, op cit.

A brief discussion of the reasons why LBW-V produces deeper penetration can help in further understanding the potential advantages of that process. At least two mechanisms for greater LBW-V penetration have been discussed in the literature. The first obvious effect is related to the laser plume. Consider Figure 16 for example. In conventional LBW notice the wide and shallow penetration zone at the material top surface (a wide nailhead). Notice that the nailhead is smaller and more similar to equivalent EB welds in LBW-V. This difference is most likely a result of the considerable beam energy absorbed by the plume particulate and then emitted as black-body radiation in all directions. In LBW-V the metal particulate does not form to a significant extent and essentially 100% of the beam power can reach the work. A secondary advantage in this regard is that the welded item will have much less surface discoloration, due to oxidation and particulate deposit, when welding in vacuum. Figure 15 illustrates that point. Further direct data on this concept is presented in: Q. Chen, X. Tang, F. Lu, Y. Luo and H. Cui, “Study on the effect of laser-induced plasma plume on penetration in fiber laser welding under subatmospheric pressure”, Int. J. Adv. Manuf. Tech., 78, pp. 331-339 (2015). The basics of their results are shown in Figure 17. Their data agree that the plume greatly affects weld shape and penetration at pressures above about 100 mbar. In that work, a vacuum level of only 30 mbar (about 22 torr) was adequate to optimize weld penetration. It should be noted that a 30 mbar vacuum may well not be adequate to prevent oxygen and nitrogen effects on the weld metal. The best possible vacuum level is undoubtedly beneficial in LBW-V

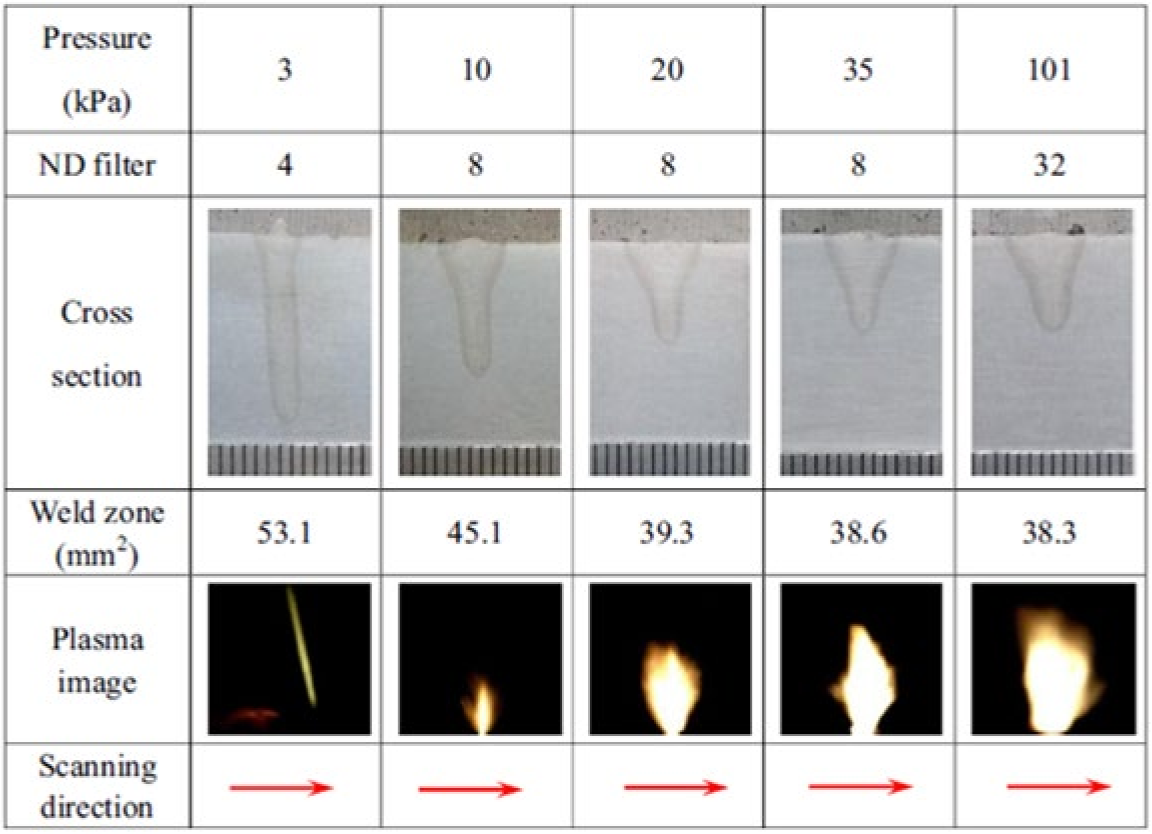

Pressure (kPa)	3	10	20	35	101
ND filter	4	8	8	8	32
Cross section					
Weld zone (mm^2)	53.1	45.1	39.3	38.6	38.3
Plasma image					
Scanning direction	→	→	→	→	→

Figure 17: Images of plume behavior with the resulting LBW-V welds. Notice that the plume is essentially non-existent at 30 mbar pressure and is large and extremely bright at atmospheric pressure (the 101 kPa pictures). From: Chen et. al., op. cit.

A second possible reason for a vacuum versus non-vacuum difference is related to metal vapor pressure versus temperature behavior. The information in this regard is from: S. Pang, K. Hirano, R. Fabbro and T. Jiang, “Explanation of penetration depth variation during laser welding under variable ambient pressure”, J. of Laser Appl., 27, 022007 (2015). The essential concept is that the necessary vapor pressure required to open the keyhole is created by the net flow of metal atoms away from the liquid surface. When an atmosphere of inert gas atoms is at that surface many of the metal atoms collide with the gas atoms and do not leave directly. Those metal atoms then merely recombine with the liquid metal surface resulting in a relatively small overall movement of metal atoms off the surface. Thus, a large enough net vapor pressure to keep the keyhole open does not happen until much higher temperatures than would happen in vacuum. At atmospheric pressure the keyhole wall temperatures must be near to the conventional value of Tb. Further, by suppressing metal evaporation, the ambient atmosphere also tends to make the vapor pressure even more strongly temperature dependent than the usually assumed exponential behavior. This is important because it means that not only is the keyhole overall hotter in atmospheric welding but that the dynamics of the keyhole will be more unstable (hence, one reason for the tendency for greater void formation in atmosphere). In this model, the greater weld penetration in vacuum is mostly a result of the overall lower keyhole temperature with the attendant lower heat loss to thermal conduction in the base metal. The computed values for surface temperature in stainless steel are: T = 3200K at 1 bar pressure versus T = 2200K possible in vacuum. Interestingly, the computed value of T’ = 2200K is consistent with direct measurements of keyhole wall temperature by: D.A. Schauer, W.H. Giedt, and S.M Shintaku,”Electron Beam Welding Cavity Temperature Distributions in Pure Metals and Alloys”, Welding Journal 57(7), p. 127s (1978). Additionally, in a vacuum environment, the lower overall keyhole temperature and the lower slope of the vapor pressure temperature dependence suggest the possibility of improved keyhole stability. Improved keyhole stability would be quite helpful for making beam power absorption more constant. Unfortunately, neither of these reasons for improved penetration in LBW-V would significantly affect the melting-to-keyhole transition region, as illustrated in Figure 11 and that would still be a problem. However, the reasons for greater penetration in LBW-V do mean that those welds might be more stable and overall more controllable than normal LBW even in the rather shallow welds typical of many applications.

PART II: WELDING VARIABLE EFFECTS IN HIGH ENERGY DENSITY WELDING

This portion of this document is intended to provide a basic knowledge of how the various welding variables affect high energy density welds. The goal is to show how the variables such as power, focus and travel speed affect the resulting weld depth of penetration. Do note that most of the data presented in this section will be from studies of welding of stainless steel. Two stainless steels were used including: the commonly available Type 304 and the somewhat more specialized Type 21-6-9 stainless steels (21-6-9 is nominally 21% Cr – 6% Ni – 9% Mn). Stainless steels are commonly available materials that are useful for gaining basic experience with high energy density welding. Much of the data presented in this section are bead-on-plate electron beam welds. EBW is a good starting point for fundamental studies of weld variable effects because of its relatively constant process efficiency. Where possible, equivalent data for LBW are presented. Other materials will weld a bit differently and some concepts relative to those behaviors will be presented in Part III of this document. Note that unless otherwise cited, the weld data for LBW and EBW are courtesy of: P. Burgardt and co-workers, Welding and Joining Section, Los Alamos National Laboratory. Some comparable, but more limited, data for laser beam welding has been extracted from the literature and will be presented later in this section.

To start this discussion let us refer back to the proposed description of weld penetration, Equation 4. Equation 4 is copied below for easier reference.

$$\mathrm{d} = \mathrm{C}\,\frac{(\eta\ P)}{(v\ D)^{\gamma}} \qquad (4b)$$

As suggested by Equation 4, this discussion will include the effects of beam power, travel speed and beam diameter on weld penetration in the stainless steel test material. That initial discussion will be followed by Part III that will discuss how the basic concept that led to Equation 4 is pertinent to other materials with an appropriate adjustment of the constants in order to compensate for the different thermal properties of other materials. Notice that the simple heat flow calculations, that yielded Equation 4, indicate that weld depth of penetration should be proportional to beam power and inversely proportional to travel speed and beam diameter. The purpose of this section is to explore the validity of those conclusions.

Some EBW data illustrating the importance of beam energy density are shown in Figure 18. The important point in Figure 18 is that weld penetration varies with power density (qualitatively similar to energy density) in a fairly complex manner as the weld transitions from conduction mode to deep penetration mode welds. Once the keyhole is clearly formed the weld behavior is more linear and that is especially important in LBW but is true even in EB welding. Because of this complexity, the balance of the discussion herein will largely consider only those welds with a high enough energy density that the keyhole is clearly formed.

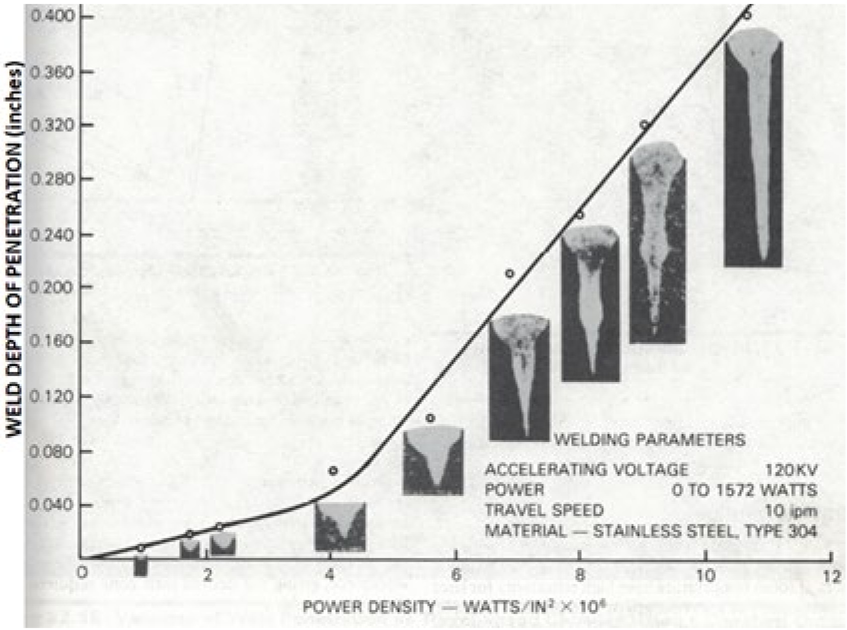

Figure 18: Data showing how weld depth of penetration and weld shape depends on power density in EBW. From: "Laser Beam Welding", Welding Handbook Vol. 2, American Welding Society.

A. Beam Power

The first weld variable to be considered is beam power in the case of EBW. For an electron beam the total available power is the product of the beam current and the accelerating voltage, IV. Of course, the relevant beam power actually must include the process efficiency. To simplify this discussion it is assumed that η is a constant equal to 0.9 and the beam power will be discussed as simply IV. Based on Equation 4 we expect weld penetration to be linearly dependent on beam power. Figure 18 shows EB weld penetration data for stainless steel that illustrates the basic linearity of penetration with beam power (increasing beam current in this example). Thus at least that portion of Equation 2 is proven to be basically valid for EBW.

An important detail of Figure 19 must be discussed. The weld penetration is linearly dependent on power up to about 1500 W of beam power. However, for higher power the results deviate considerably from the simple linear behavior. There are at least two possible reasons for the non-linear behavior. First, at high power there is considerable metal vapor leaving the keyhole. It is likely that some scattering of electrons from that vapor would occur. In fact, one often sees a glowing region above an EB weld that is qualitatively similar to a laser produced plume. That would somewhat decrease the beam power actually arriving at the work and would increase the effective beam diameter a bit and thereby produce a bit less weld penetration. This phenomenon is undoubtedly relevant to EBW for very high beam power and in metals with considerable vaporization of some alloy constituents, but in general, this seems to be a minor effect in EBW. The major cause of the non-linearity is probably the intrinsic behavior of the beam diameter for an electron beam, which does increase noticeably at high beam current. That behavior will be discussed in the following section dealing with beam focus.

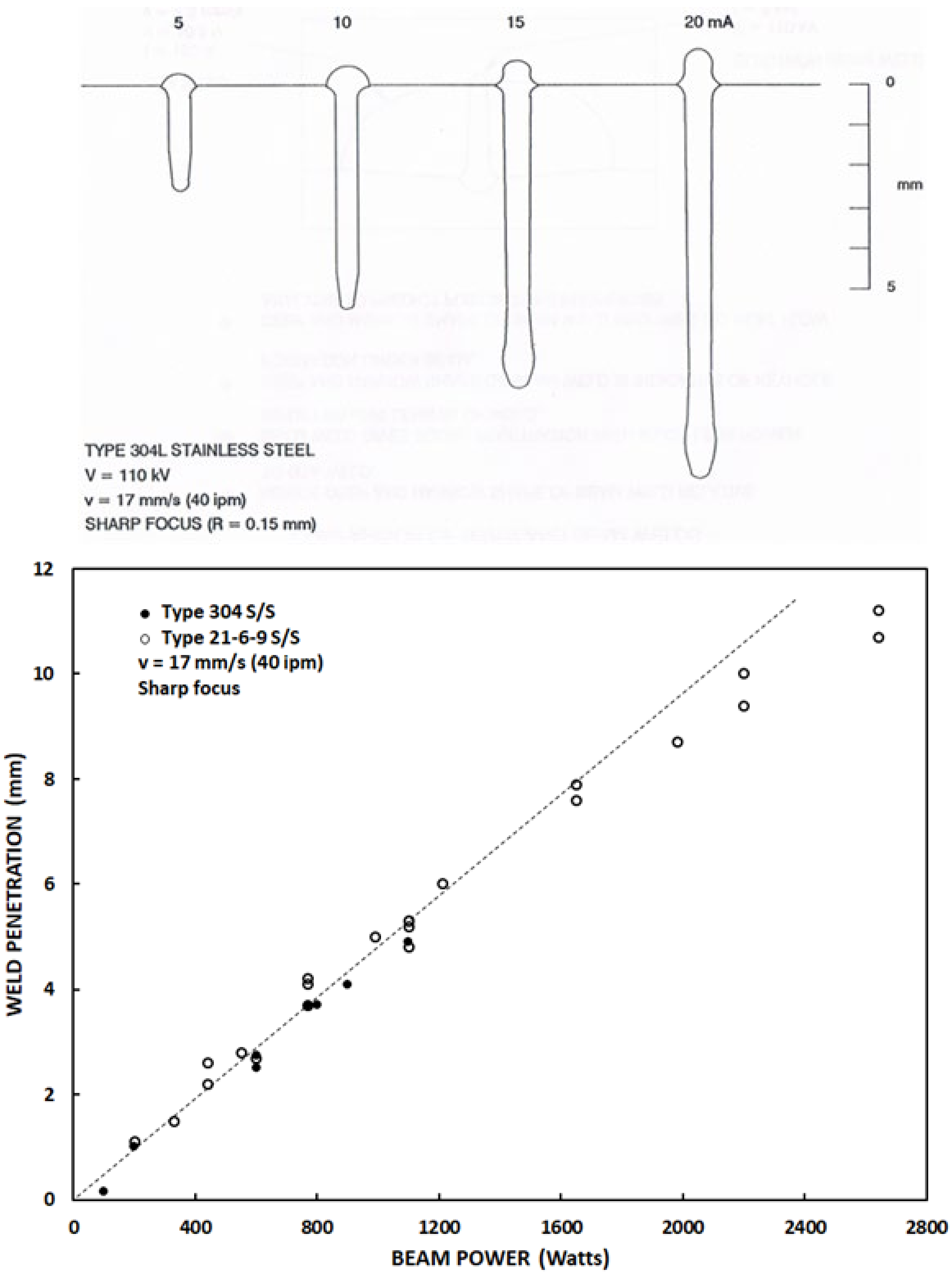

Figure 19: Data showing how weld depth of penetration depends on beam power for typical EB welds in stainless steel.

As would be expected from the fundamentals of heat flow, laser weld data also are largely consistent with a linear dependence of weld penetration on beam power. Some representative data for LB welds made with a Nd:YAG laser are shown in Figure 20. As can be seen for higher power levels, weld penetration does increase linearly with power level. Notice in Figure 20 the rapid shift towards zero melting for power below 900 Watts. This behavior is a further demonstration of the importance of keyhole formation to coupling of laser light to the work. Figure 21 shows data for CO2 laser welds in stainless steel. The dashed straight lines were entered here to accentuate the fact that the results shown in Figure 21 are basically consistent with the expectations that weld penetration should be linear with power in these deep penetration welds. Figure 22 shows some data for fiber laser welds in stainless steel (fiber laser wavelength is typically 1.07 microns). The data in Figure 22 are intended to show the travel speed dependence but do show that for any particular travel speed the penetration does increase proportionally with power. Thus, the theoretical expectations are largely confirmed.

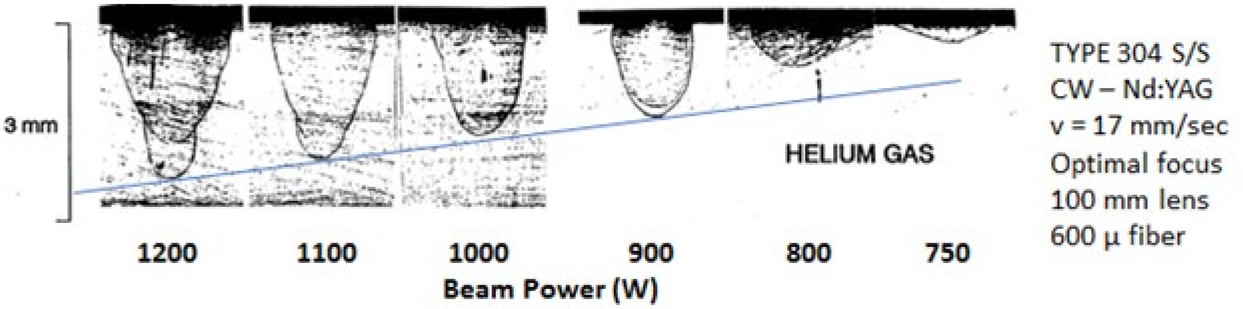

Figure 20: Data showing how weld depth of penetration depends on beam power for laser welds in stainless steel. Note that no melting of metal occurred below 720 W.

The expected simple linear dependence of LBW depth of weld penetration on beam power doesn't necessarily apply for higher power welds in typical atmospheric pressure LBW. It is obvious in Figure 21 that the data deviate considerably from the expected linear behavior at high power. The non-linear behavior is also evident in Figure 22 where the high power level weld penetration values are a bit less per unit power than in the two lower power levels. As mentioned previously, this is probably largely a result of laser beam absorption and scattering by the plume of metal particles emanating from the keyhole. At higher power, the plume effects clearly become more important. Additionally, it should be mentioned that the keyhole shape, especially at the leading edge of the keyhole, may significantly affect the details of laser coupling to the metal. Especially at higher travel speeds and for particularly deep keyholes the leading edge of the keyhole will be substantially tapered from top to bottom reflecting laser light to the back and potentially out of the keyhole altogether. That effect would limit weld penetration. This possibility was mentioned by: Q. Chen, et. al. cited in Part I of this paper and by J.W. Elmer, LLNL, Personal Communication.

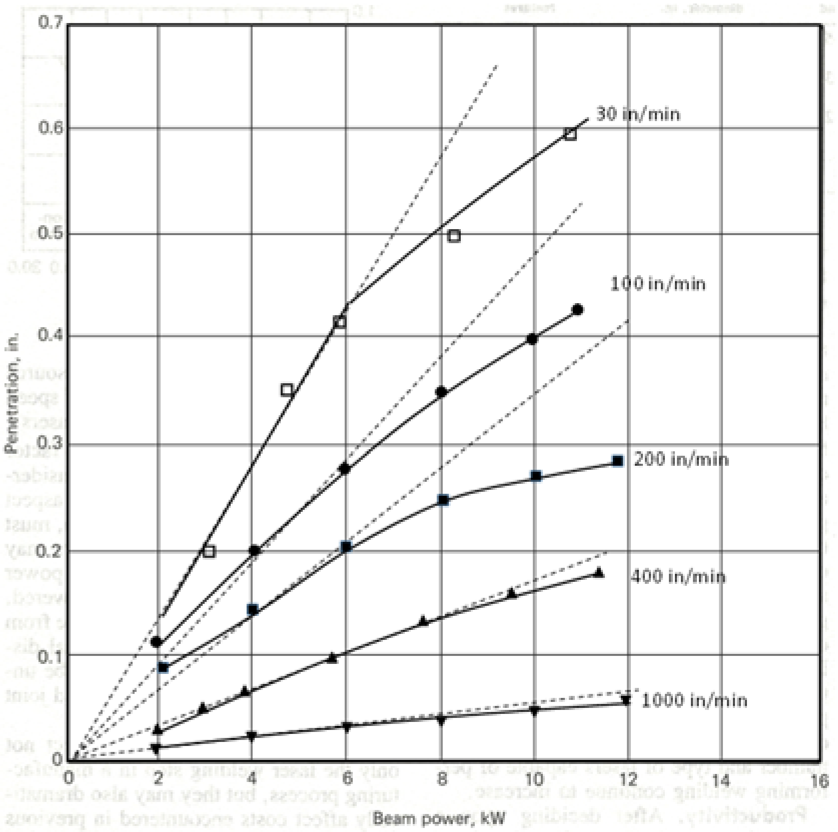

Fig. 10 Effect of beam power on penetration in type 304 stainless steel at various welding speeds

Figure 21: Data showing how weld depth of penetration depends on beam power for CO2 laser welds in stainless steel. From: "Laser Beam Welding", ASM – Metals Handbook, Vol. 6, 9th Edition (1983).

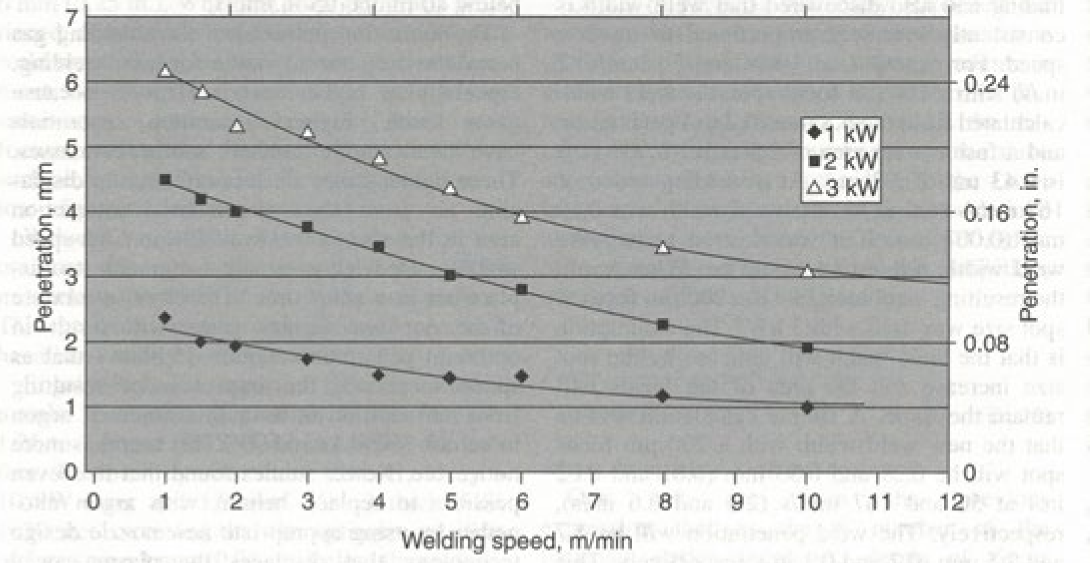

Fig. 12 Fiber laser welding performance for stainless steel. Weld penetration diagram for 200 μm spot size. Courtesy of IPG Photonics

Figure 22: Data showing how weld depth of penetration depends on travel speed for laser welds in stainless steel for three power levels. From: "Laser Beam Welding", ASM Handbook, Vol. 6A, (2011).

B. Travel Speed

In this section the effect of travel speed will be discussed. This would seem like a simple topic since high energy density welds tend to be made at fairly high travel speed. In that case it would seem that most of the beam power would be consumed in supplying the heat of melting of the metal and the weld penetration would simply be inversely proportional to travel speed. That would correspond to a power law coefficient of $\gamma = 1$ in Equation 4. However, the travel speed dependence is a bit more complex and that is specifically why Equation 4 was written to include the potentially more complex behavior via the power law behavior and coefficient γ.

Figure 23 shows data for EB welds in stainless steel for a constant beam power (1100 W) as a function of travel speed. As can be seen the resulting weld depth of penetration does change in the expected manner. A reasonably good fit to the data yields $\gamma = 0.65$. This value for the coefficient is substantially less than one which means that even in stainless steel, with its modest thermal conductivity, the power balance around the weld is largely a result of thermal conduction rather than just the metal heat of melting. From a practical welding perspective, the significance of these results is that overall weld behavior does not change dramatically with travel speed in EBW. Travel speed will likely be chosen as a matter of convenience based on equipment capabilities and possibly for controlling metal cooling rate for metallurgical reasons. A desired weld penetration would be achieved by adjusting beam power and beam focus at a constant and reasonable travel speed.

A comparable data set for LB welds in stainless steel is shown in Figure 24. As can be seen, the LB welds have weld penetration that does decrease with increasing travel speed. The accompanying graph shows that the travel speed dependence is described by: $\gamma = 0.62$. Another travel speed result was obtained from the data in Figure 21 at 6 kW. For that set of CO2 LB welds, the behavior is similar to that seen in the EB welds with the value of γ for Equation 4 being about $\gamma = 0.65$. As expected, these results simply demonstrate that the power balance in the weld is similar for EBW and LBW.

Some additional LBW data dealing with the travel speed dependence are shown in Figures 22b and 26. Once again we see an inverse relationship between weld penetration and travel speed. However, further analysis of those LB weld penetration results revealed an interesting difference between the EBW and LBW data. The dashed lines on Figure 26 and 22b and the accompanying equations are optimized power law dependence fits to the data provided by this author. What is interesting here is the values for γ yielded by the analysis. The three values are: $\gamma = 0.52; 0.37; 0.30$. The substantial difference between these values of γ for LBW and the value typical of EBW ($\gamma = 0.65$) is interesting. This may reveal some interesting physics and is worthy of further discussion.

One possible origin of the differences in γ values seen in the LB welds is that it is an artifact of the mathematical analysis. In the case of a power law fit to data, the resulting γ values tend to be dominated by the low speed data points. The γ values would be considerably skewed if the weld penetration values at slow travel speed were lower than expected. This is a possibility since the amount of metal vapor/particulate in the plume could become greater for slow travel speed welds where the liquid metal spends more time under the beam. The accompanying modifications to beam η and D could account for the different behaviors.

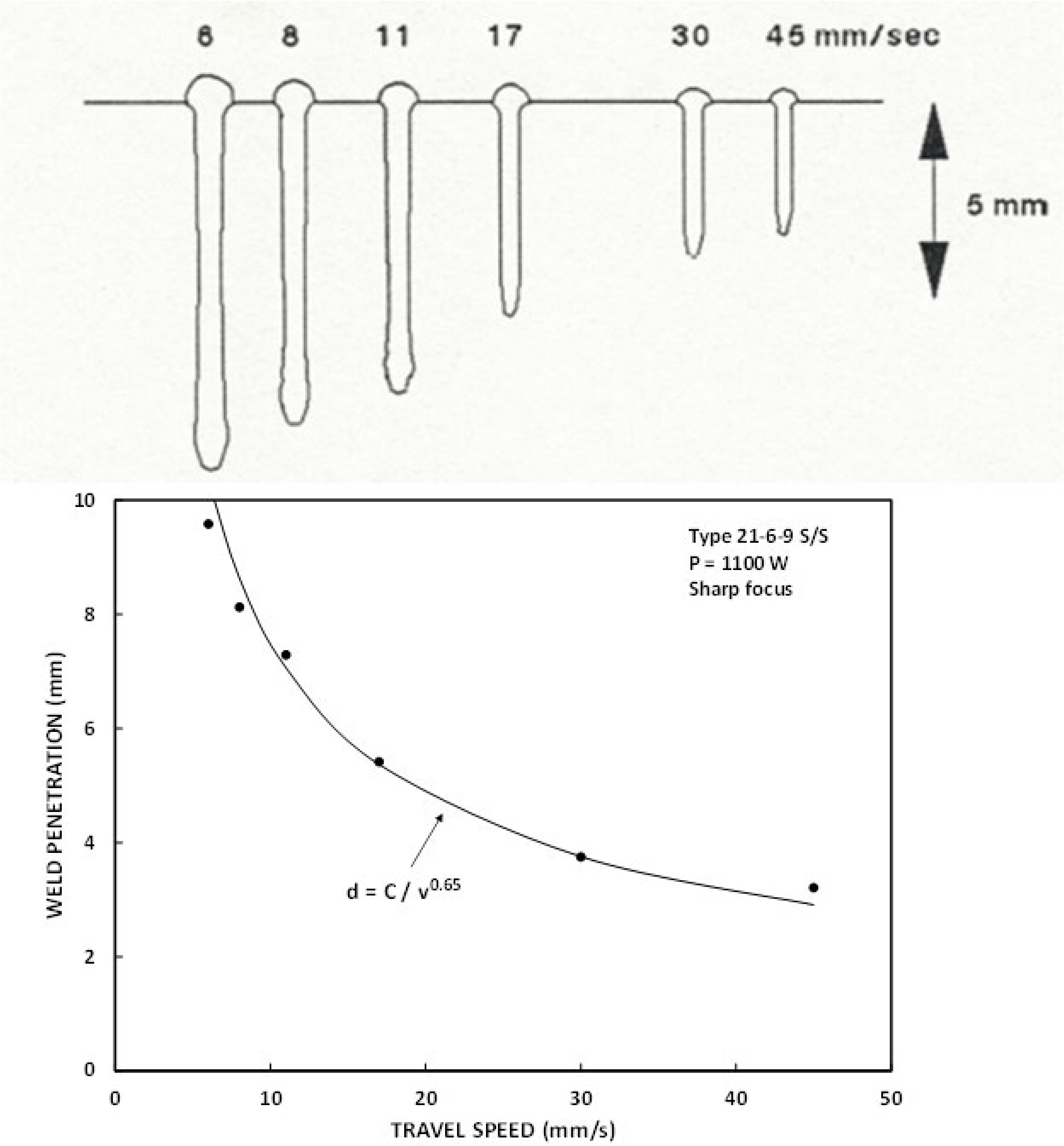

Figure 23: Data showing how weld depth of penetration depends on weld travel speed for EB welds in Type 21-6-9 stainless steel.

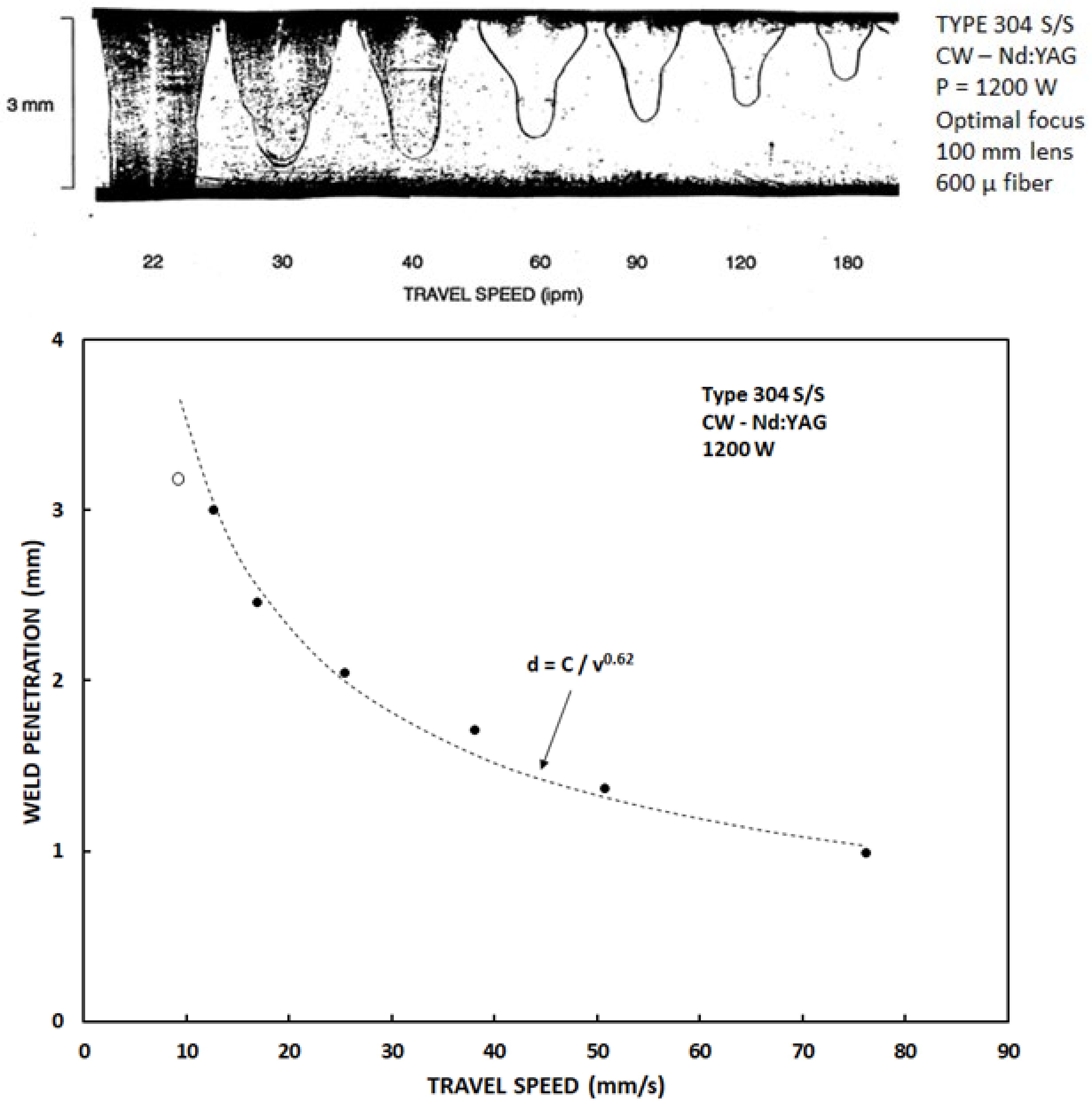

Figure 24: Data showing how weld depth of penetration depends on weld travel speed for LB welds in Type 304 stainless steel. These results are from a CW-Nd:YAG laser using a short focal length lens.

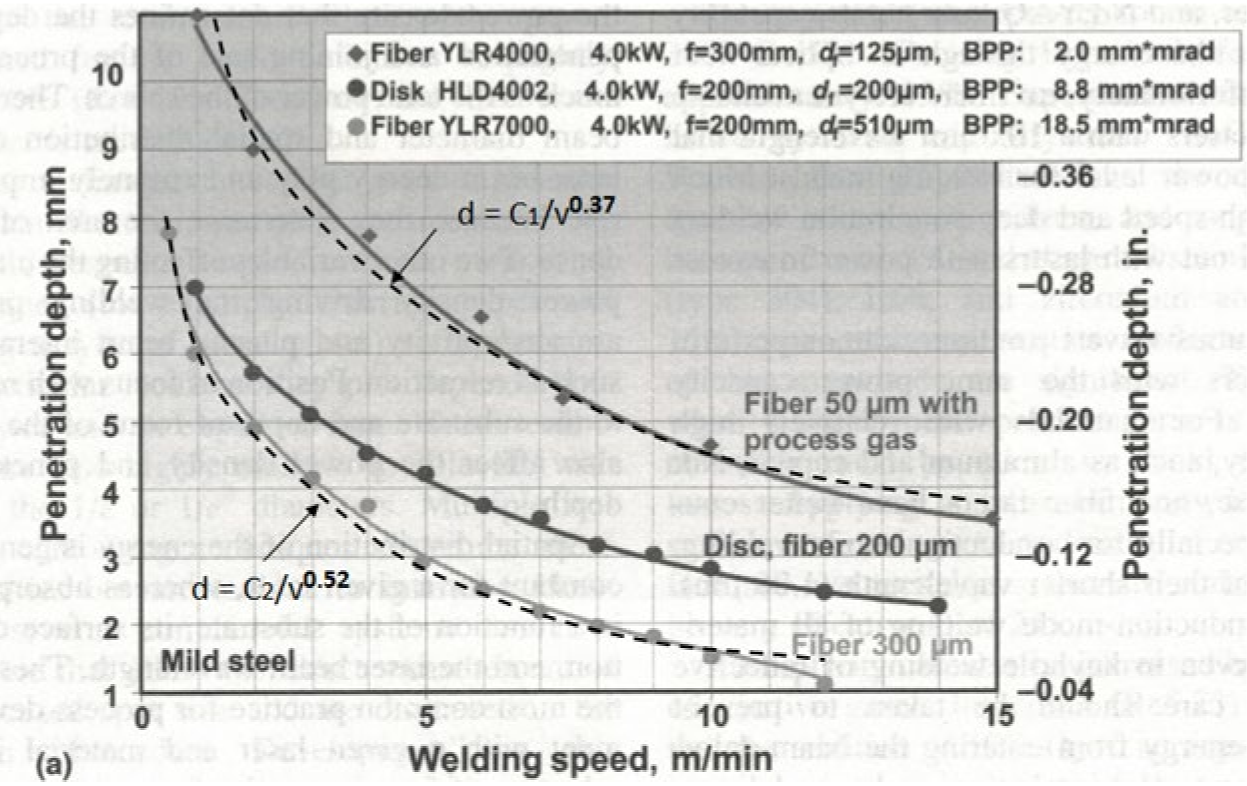

Figure 25: Data showing how weld depth of penetration depends on weld travel speed for LB welds in mild steel. From: "Laser Beam Welding", ASM Handbook, Vol. 6A, (2011).

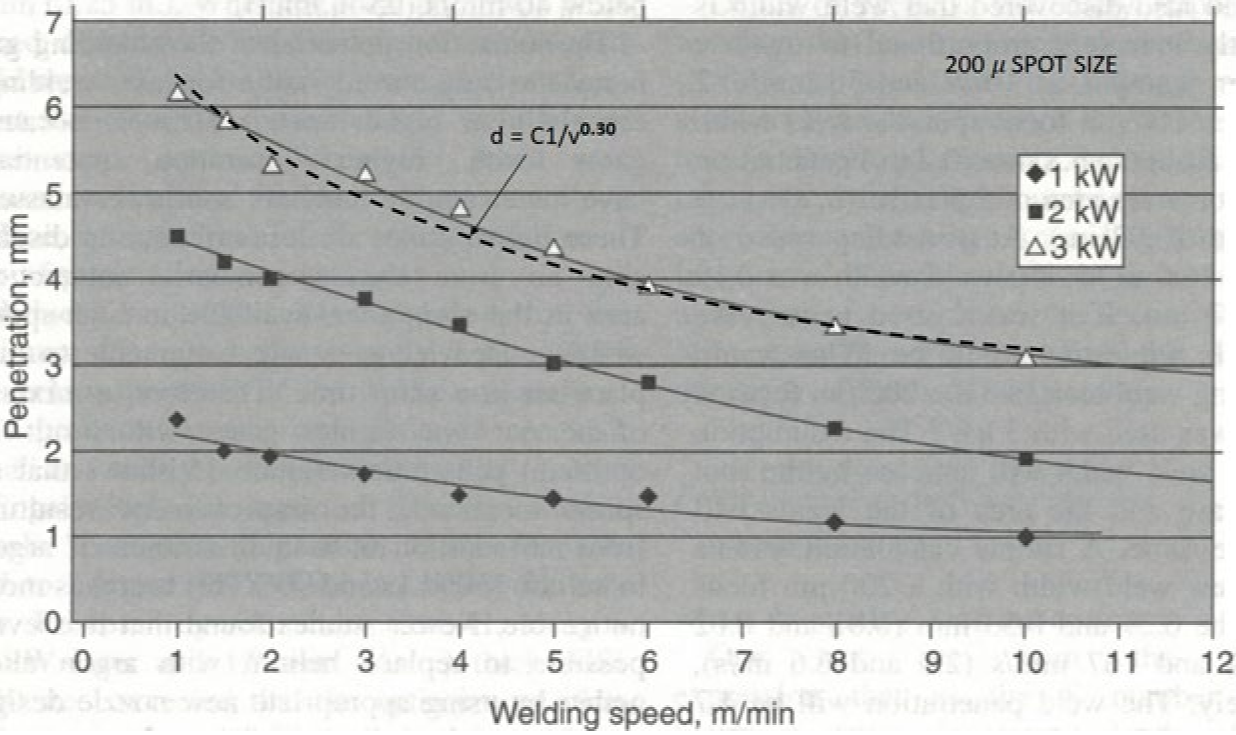

Figure 22b: Data showing how weld depth of penetration depends on travel speed for laser welds in stainless steel for three power levels. From: "Laser Beam Welding", ASM Handbook, Vol. 6A, (2011).

Another possible reason for the big difference in γ values might be the difference in beam diameters associated with those values. The values of 0.30 and 0.37 are associated with beam diameters of 200 and 125 microns respectively. The γ value of 0.52 was from a beam with diameter of 510 microns. Recall that γ = 0.62 described LB data obtained with an unknown but probably fairly large beam diameter (Figure 24). Compare this to the EBW result of γ = 0.65 produced by a beam with a diameter of 350 microns. In broad terms, these results are entirely expected. The small values of γ associated with small beam diameter and the larger values associated with larger beam diameter is simply saying that the power balance around the weld is more dominated by thermal conductivity for small beam diameters. That is obviously correct because the amount of metal melted per unit time for a narrow weld is smaller than that for a wide weld. In other words, a small beam diameter results in less beam power being consumed in the heat of melting of the metal. Also, as will be discussed later, it is also possible that the heat flow around the weld does change character for exceptionally small beam diameter (corresponding to large values of Fourier number, a concept to be discussed later in the beam diameter discussion).

An additional interesting possibility for the possible systematic EBW to LBW difference is suggested in: S. Pang et al, op cit. The basic idea is that the front wall temperature of the keyhole is always at or above Tb when welding in atmosphere. In vacuum the keyhole wall temperature is always much lower. The basic idea is that when welding in atmosphere, the keyhole material is so hot that the power balance around the weld is more dominated by conduction and one would expect a significantly smaller γ than would be the case when welding in vacuum. Pang et al modeled atmospheric pressure and vacuum welds and clearly demonstrated the large difference in γ that would result, with the atmospheric pressure LB welds having a small value of γ. Thus, the small values of γ seen in some of the LBW results may be real and that weld behavior would change noticeably if very small deliver fibers were used in the LB welding equipment. It is again interesting to speculate that this analysis might suggest that vacuum LBW would react to travel speed differently than atmospheric pressure LBW and perhaps much more like EBW.

This is an appropriate point to mention pulsed LBW in regards to its basic weld variable response. Figure 26 shows some typical data that appears in various handbooks. The usefulness of this plot is quite limited because the vertical axis label for penetration is totally enigmatic. However, it is possible to make a few general comments about pulsed LBW. First, notice that pulse frequency and travel speed are often tied together. That is reasonable since pulsed LBW is like any pulsed process in that a traveling weld basically consists of overlapping spot welds. In this case the data would suggest about 4 pulses of power for each mm of travel. A seond point is that the penetration is seen to be proportional to the average input power (adjusted by energy per pulse), at least in broad terms. Because of the strange penetration axis labeling it is not possible to draw any quantitative conclusions but it is clear that the penetration is inversely proportional to travel speed at least in general terms. These behaviors are expected since the energy balance around the weld is the same independent of process. The real advantage of pulsed LBW is that an appropriate choice of pulse energy, duration and repetition frequency can maintain the fusion zone (probably with some keyhole behavior) at an overall lower power than is possible in CW-LBW thus facilitating lower power and limited penetration welds.

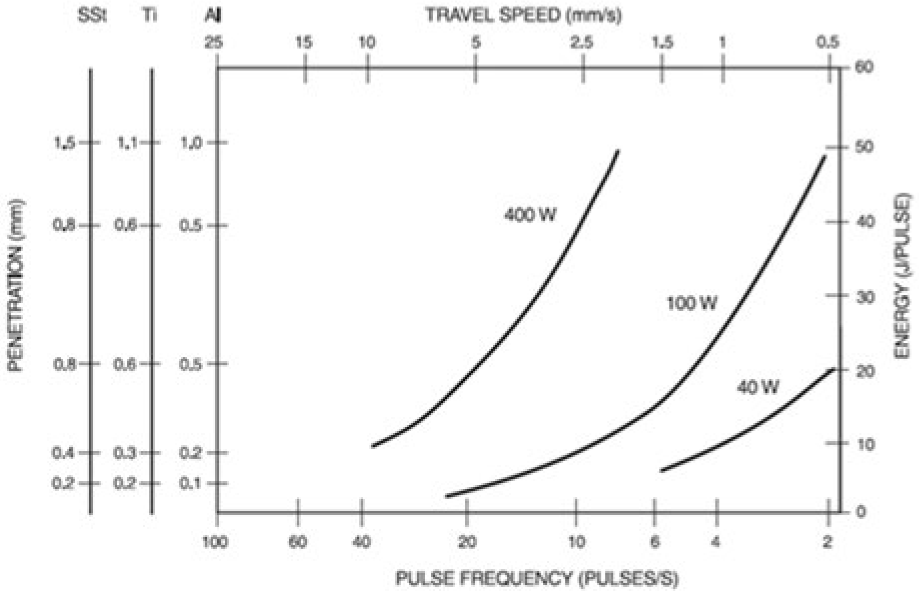

Figure 26: Data showing how weld depth of penetration depends on weld travel speed for pulsed LB welds for three power levels. From: "Recommended Practices for Laser Beam Welding, Cutting and Allied Processes", AWS C7.2M:2010, American Welding Society.

One of the critical parameter choices in pulsed welding is the conditions that will provide a desired level of weld overlap. A beam of fixed diameter, D, moving at speed, v, and with a pulse duration, τ, will deposit energy on an elliptical area whose length is: D + vτ. When the beam is pulsed with frequency, f, the beam moves forward a distance = v/f. Thus, the fractional overlap is given by:

$$\text{Fraction Overlap} = \frac{D+v\tau-(\frac{v}{f})}{D+v\tau} \qquad (6)$$

The appropriate amount of overlap is dependent on application requirements but should probably be at least ½. Once a particular satisfactory overlap is established, the resulting pulsed LB welds react to welding variable changes mostly in keeping with Equation 4. Weld penetration generally increases proportional to average beam power and, as seen in Figure 26 for example, decreases with travel speed. Applications that are typical for pulsed LBW would probably use the best beam diameter possible with the machine optics and not vary the focus but weld penetration would undoubtedly decrease with beam diameter increases in the expected fashion.

One aspect of P-LBW that is a bit different is that the choice of energy per pulse is critical to the result. For a given energy per pulse it has been shown that weld penetration increases for shorter pulse durations as reported by: P.W. Fuerschbach and G.R. Eisler, "Effect of laser spot weld energy and duration on melting and absorptions", Sci. Technol. Welding and Joining, 7, 4, pp. 241-246 (2002). This basically means that weld penetration is related to peak power in the pulse. Figure 27 shows some comparison data between CW-LBW and P-LBW. As can be seen, with a proper choice of pulse parameters, weld penetration is greater with P-LBW and that the coupling efficiency of the beam to the work is greatly improved by optimizing the peak power in the pulse. It is important to note that the transition between conduction-mode and deep penetration-mode welds (the large change in η seen in CW-LBW) is largely eliminated by an appropriate choice of the pulse peak power.

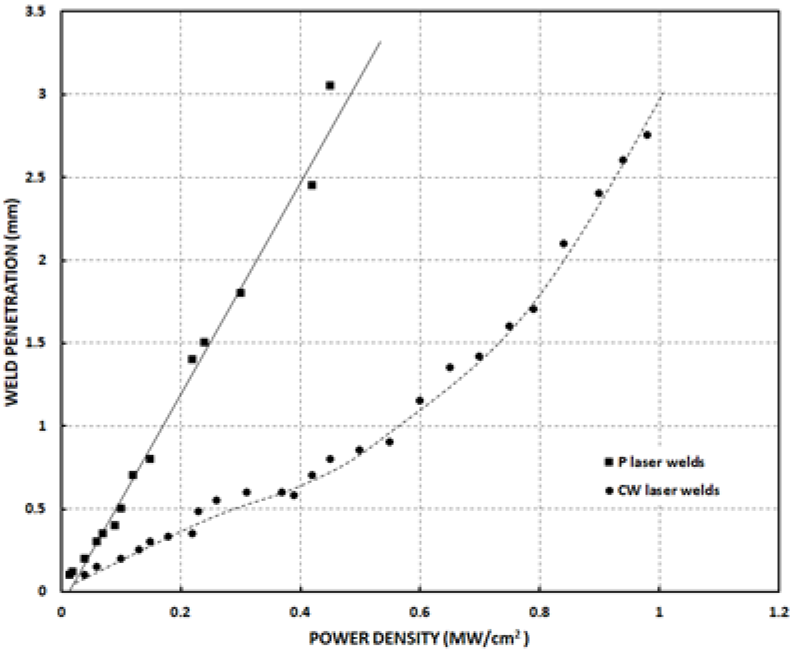

Figure 27: Data showing the considerable improvement in weld penetration possible for pulsed versus CW LB welds. These welds were generated with a beam diameter of D ≈ 0.9mm and D/v = 20 msec and with varying average beam power. Data are from: E. Assuncao and S. Williams, "Comparison of continuous wave and pulsed wave laser welding effects", Opt. Lasers Eng., 51, 9, pp. 674-680 (2013).

C. Beam Diameter

In this section the effects of beam diameter on deep penetration beam welding will be discussed. As will be shown, this is a somewhat complicated subject. As a starting point, Figure 28 shows the basic effect of changes in beam diameter on EB welds in stainless steel. As expected, increasing beam diameter results in greater keyhole width accompanied by decreasing weld penetration. For beam diameters greater than about 4 mm the keyhole is no longer formed and the result is conduction-mode type welds. The accompanying graph shows that the penetration decreases in a fashion that is consistent with Equation 4 and with a power law coefficient of $\gamma = 0.65$. These data are for one particular EB power level but similar behavior happens for all tested power levels. Figure 29 shows a series of EB welds illustrating that overfocus and underfocus produced similar results. For these data, sharp focus is the minimum possible beam diameter as determined at the weld top surface. Overfocus is the term used for when the sharp focus point is above the surface and underfocus is the term used for when the sharp focus point is below the surface. However, as will be discussed subsequently, the similarity of overfocus and underfocus does not hold for deeper penetration welds. LB welds should have a similar dependence on beam diameter with the exception of the behavior at larger beam diameters. Recall that coupling of the laser light to the metal rapidly decreases once a prominent keyhole is no longer formed. Thus, the weld penetration would rapidly go towards zero for large defocus in the case of LBW. That aspect of fairly low power LBW is illustrated in Figure 30. Unfortunately, at the time those LB welds were made there was no tool available for measuring laser beam diameter. Therefore, the dependence of penetration on beam diameter could not be quantified. Nevertheless, it is clear that penetration decreases with increasing beam diameter as expected.

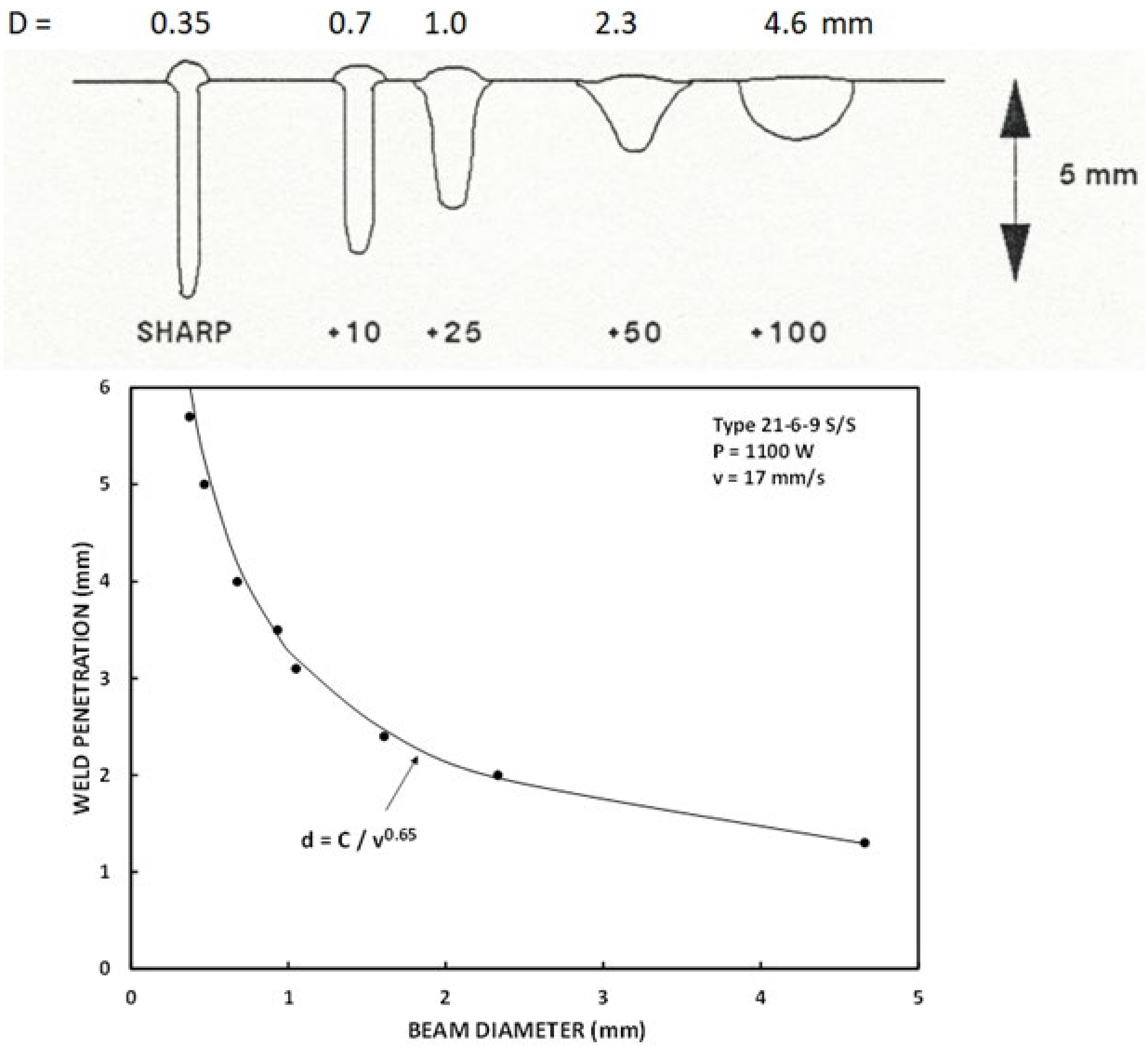

Figure 28: Data showing how weld depth of penetration depends on beam diameter (sharp plus overfocus) for EB welds in Type 21-6-9 stainless steel.

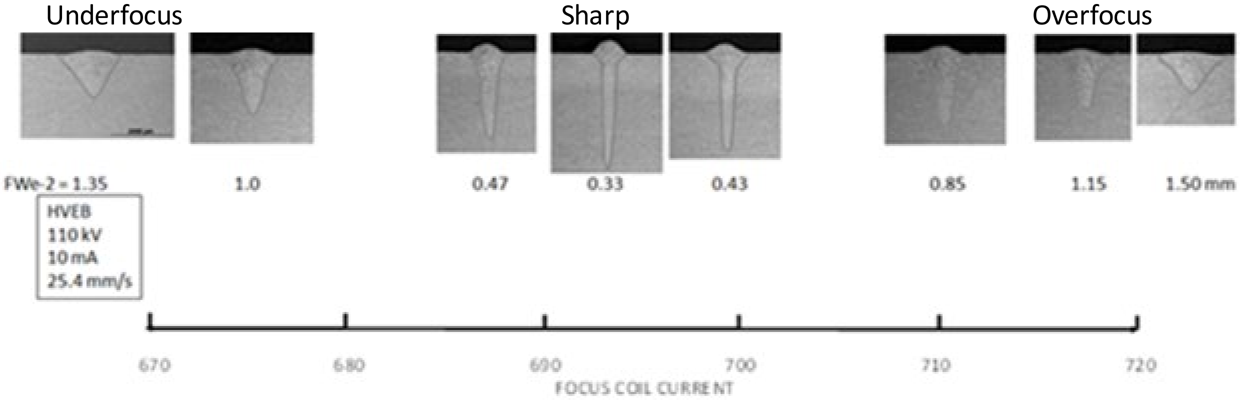
Underfocus
Sharp
Overfocus
FWe-2 = 1.35
1.0
0.47
0.33
0.43
0.85
1.15
1.50 mm
HVEB
110 kV
10 mA
25.4 mm/s
670
680
690
700
710
720
FOCUS COIL CURRENT

Figure 29: Data showing how weld depth of penetration depends on beam diameter (underfocus and overfocus) for EB welds in Type 304 stainless steel. Note: weld penetration at sharp is about 6 mm.

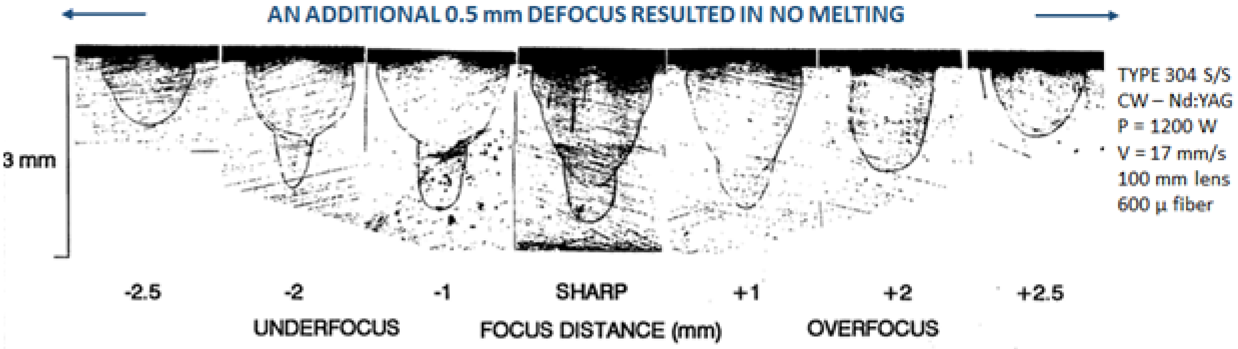

Figure 30: Data showing how weld depth of penetration depends on beam diameter (underfocus and overfocus) for LB welds in Type 304 stainless steel. Notice that penetration rapidly went to zero for small additional defocus in the conduction mode of welding.

Up to this point in the discussion it has been assumed that diameter is a measureable value that is simply defined as its size at the top surface of the metal being welded. Different beam diameters would result from moving the focus point of the focused and converging beam up or down relative to the surface. In that case, beam diameter is simply the value measured at the weld surface for a similar level of defocus. That notion of beam diameter is acceptable at least for fairly small weld penetration. The potential problem with this simple concept is that, since the beam is being focused and is converging/diverging, the most relevant beam diameter is not necessarily that as measured at the top surface.

The comments about the potential ambiguity of beam diameter arise from experience with deep penetration welds with d > 15 mm. The concept to be discussed here is hinted at by the appearance of LB welds, such as in Figure 7-b, and EB welds, such as in Figure 19 at high power. It is clear that the diverging nature of the beam is producing wider fusion zones at the weld root. That behavior suggests that merely measuring beam diameter at the weld top surface isn't entirely describing weld behavior. Perhaps the relevant beam diameter should be referenced to some point other than just the part top surface. In any case, just applying a single value of diameter to the beam is not adequately descriptive. That possibility will be discussed in some detail in the following.

An example of the really relevant consequence of the diverging beam behavior is shown in Figure 31. Notice from Figure 31 that the weld penetration does not decrease smoothly as the focus position moves to underfocus. In fact, the narrowest and deepest welds result from some level of underfocus. Considering data from this source and others found in the literature, it seems that the optimal focus resulting in maximum weld penetration occurs when the sharp focus point is about midway down into the resulting keyhole. Of course the optimal focus conditions are less obvious for the LBW-V welds shown in Figure 30 and probably occurs at somewhat less underfocus than one-half of the penetration, but the basic idea applies. The point made here is that beam diameter is a value that can be measured, but, exactly how the resulting D values should be utilized in weld analysis is a bit complex. From the perspective of common applications with limited weld penetration, the beam diameter referenced to the metal top surface is adequate to predict weld behavior.

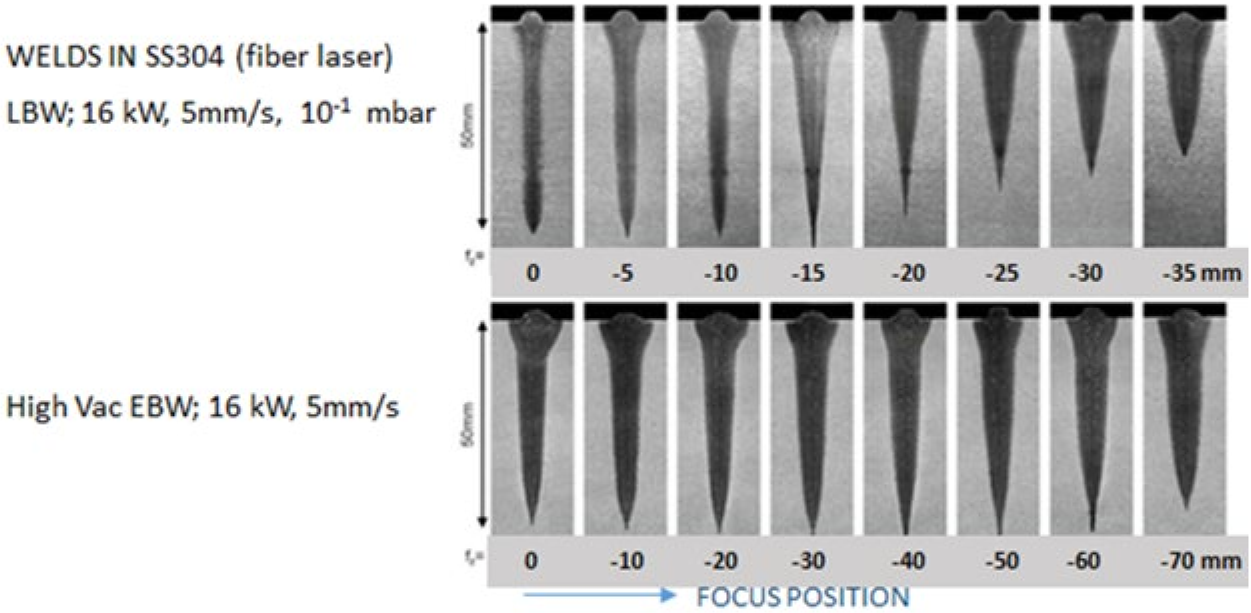
WELDS IN SS304 (fiber laser)
LBW; 16 kW, 5mm/s, 10-1 mbar
50mm
0
-5
-10
-15
-20
-25
-30
-35 mm
High Vac EBW; 16 kW, 5mm/s
50mm
0
-10
-20
-30
-40
-50
-60
-70 mm
FOCUS POSITION

Figure 31: Data showing how weld depth of penetration depends on varying underfocus for EBW and LBW-V in Type 304 stainless steel. Note: weld penetration is about 50 mm in all cases. From: M. Jiang, W. Tao and Y. Chen, "Laser Welding under Vacuum: A Review", J. Appl. Sci., 7, p. 909 (2017).

At this point in this paper some of the fundamental differences between EB and LB machines will be discussed. This is an appropriate place for this discussion since many of the differences between the processes is related to beam focus and the resulting beam diameter.

As has been discussed in some detail, one fundamental difference between the processes is that the weld results for LBW in atmosphere are clearly influenced by the laser plume. Some data again making that point are shown in Figure 32. Notice that the atmospheric pressure LB welds are always considerably shallower and wider than the LBW-V counterparts. That is probably mostly a plume effect. It is important to notice that optimal weld penetration in atmospheric pressure LBW does occur for some level of underfocus and that the presence of the plume did not seem to change that behavior appreciably. Nevertheless, it is clear that plume effects in LBW can make weld behavior different and perhaps more variable than is seen in EBW. The presence of the plume probably further complicates the question of what exactly is the relevant beam diameter and focus location for a particular welding situation? It does appear that LBW-V is more similar to EBW in this regard also.

Another potentially significant difference between EBW and LBW is the typical optics focal length used in these processes. It has been typical of LBW to use fairly short focal length lenses in order to produce the smallest possible beam diameter. In that case, the laser beam is strongly converging/diverging. A way to characterize is this is the Rayleigh length, L_R . This is defined as the distance over which the beam area increases by a factor of two. This is also where the diameter increases to: $D_{LR} = \sqrt{2} \text{ X } D_{sharp}$. The significance of the Rayleigh length is that within that distance from sharp, the converging/diverging beam diameter changes little enough that it affects the resulting weld minimally but, outside that distance, weld penetration changes are fairly large. It is a bit unusual to compute the Rayleigh length for

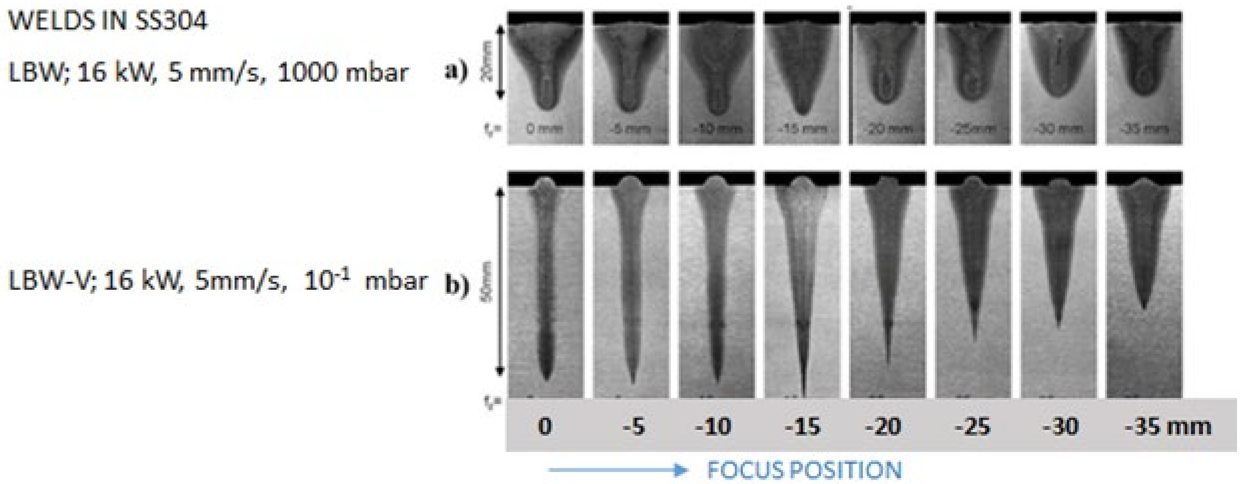

Figure 32: Data showing how weld depth of penetration depends on varying underfocus for LBW and LBW-V in Type 304 stainless steel. Note: weld penetration is about 20 mm for LBW and about 50 mm for LBW-V. From: M. Jiang, et. al., op, cit.

EB but that can be done. Figure 33 shows caustic data for LB with a short focal length lens compared to EB with a typical long work distance. Notice the factor of about 5 difference in the two Rayleigh lengths. The significance is that the LB process would be five times more sensitive to variations in work height and the quality of sharp focus determination and control. Also, exactly how one defines the proper location of sharp relative to weld penetration would be five times more critical for the laser. Do note that the value for EB would be smaller for a shorter work distance and that it would vary depending on the design of the electron optics of any particular machine. Also, it is now possible for the laser process (with small delivery fibers and single-mode behavior) to produce good weld penetration with longer focal length lenses. Thus, the results shown in Figure 33 are not universally applicable but do show that beam focus properties can be substantially different between EB and LB machines. The basic point being that LBW, often made with relatively short focal length optics, would be more sensitive to the location of sharp focus than is normally the case for EBW.

Another important difference between EB and LB beam diameter behaviors is related to the fundamental difference between electrons and light. The beam diameter for a beam of light is controlled by the light source (typically the delivery fiber diameter) and the focus lens but is, at least theoretically, independent of power level for any realistic energy density. The electron beam is different because it is made up of charged particles that interact with each other quite strongly. Manipulating those electrons does lead to fundamental limits on beam size and shape.

From a practical welding perspective it is important to note that the laser beam diameter and sharp focus point can vary a bit with power. Some typical handbook data illustrating this effect are shown in Figure 34. Notice that the beam diameter increases substantially with increasing average beam power. It is likely that the spot diameter change in Figure 34 is a result of heating in the laser elements, which are YAG rods in this example. The resulting change in laser rod dimensions will produce those sorts of changes in beam diameter. It is interesting to note that some more recent laser designs, including disk and slab, are largely intended to provide more effective heat removal from the lasing material. In those machines the spot diameters would be more constant.

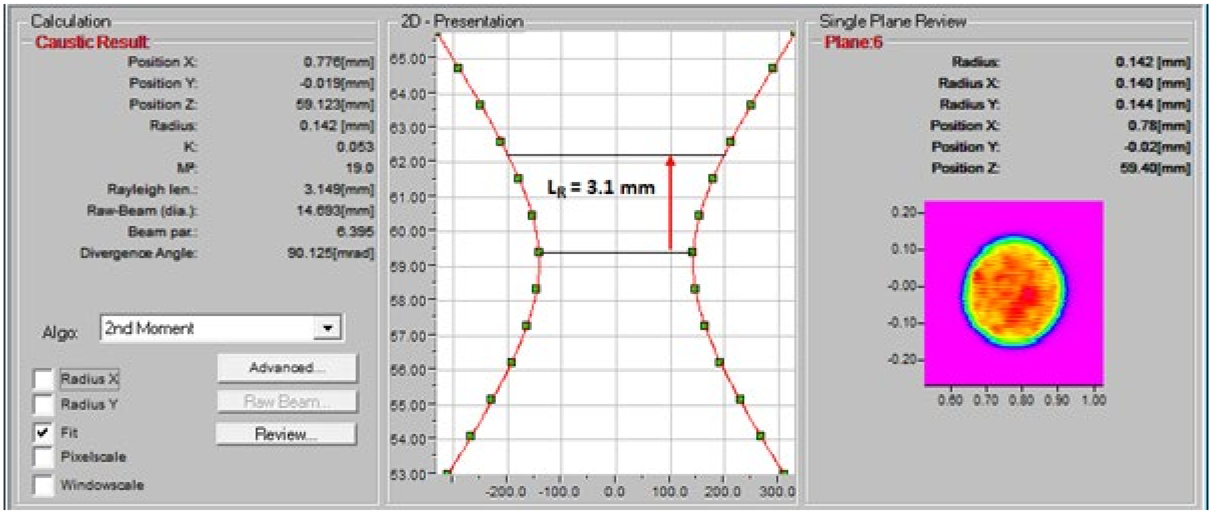
Calculation
Caustic Result
2D - Presentation
65.00
64.00
63.00
62.00
61.00
60.00
59.00
58.00
57.00
56.00
55.00
54.00
53.00
-200.0
-100.0
0.0
100.0
200.0
300.0
L_R = 3.1 mm
Single Plane Review
Plane:6
0.20
0.10
-0.00
-0.10
-0.20
0.60
0.70
0.80
0.90
1.00
Advanced...
Raw Beam...
Review...

Position X: 0.776[mm]
Position Y: -0.019[mm]
Position Z: 59.123[mm]
Radius: 0.142 [mm]
K: 0.053
M^2: 19.0
Rayleigh len.: 3.149[mm]
Raw-Beam (dia.): 14.693[mm]
Beam par.: 6.395
Divergence Angle: 90.125[mrad]

Algo: 2nd Moment

☐ Radius X
☐ Radius Y
☑ Fit
☐ Pixelscale
☐ Windowscale

Radius: 0.142 [mm]
Radius X: 0.140 [mm]
Radius Y: 0.144 [mm]
Position X: 0.78[mm]
Position Y: -0.02[mm]
Position Z: 59.40[mm]

A

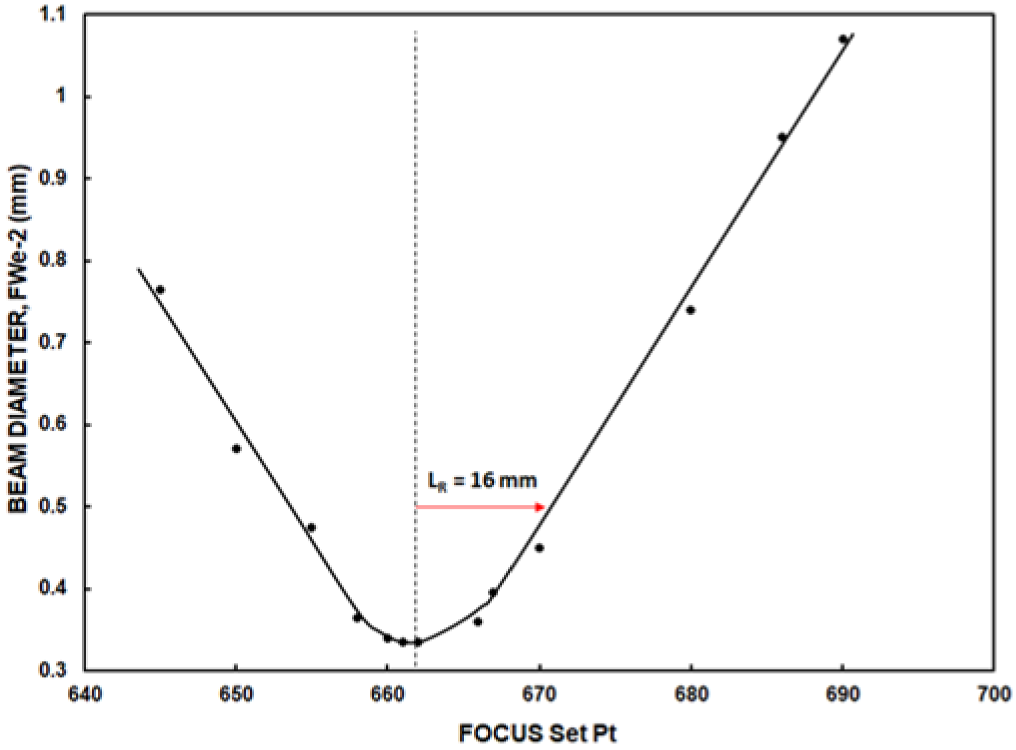

B

Figure 33: Typical caustic diagrams showing the Rayleigh length for: (A) laser; (B) electron beam. The LB data were generated with a 120 mm focus lens and the EB data were generated at a fairly long work distance. Note: LB data from a Primes GmbH Focus Monitor.

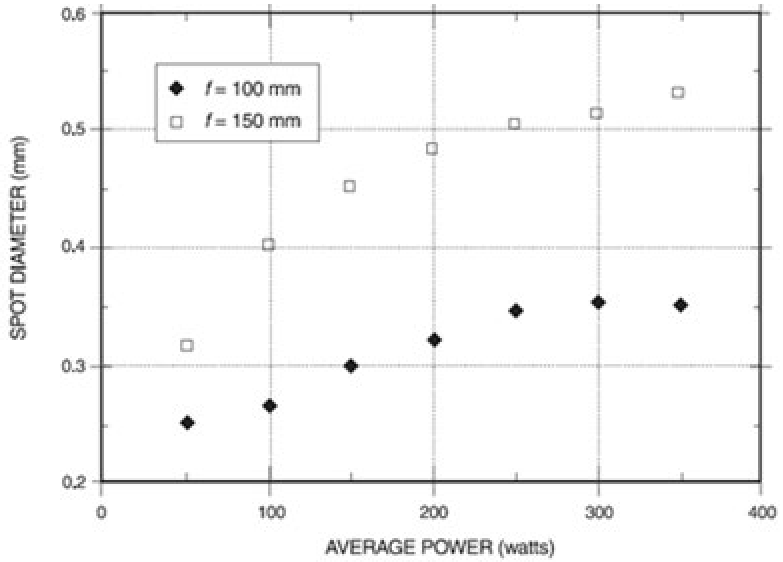

Figure 34: Sample data showing the sensitivity of spot diameter to power level for a pulsed Nd:YAG laser. From: AWS C7.2M:2010LB.

Another recent laser design is the fiber laser. In this case the lasing element is built into an optical fiber as a dopant in the fiber core glass. There are two distinct advantages to this design. First, the lasing element is in a thin fiber roughly 2 meters long. That facilitates heat removal from the laser. The other reason why the fiber laser is efficient is related to the physics of laser action in the particular atoms involved. Solid state lasers typically used Nd atoms ultimately emitting at 1.06 microns while the fiber lasers make use of Yb atoms emitting at about 1.07 microns. Laser action requires that a metastable electron configuration in the atom results in a population inversion. This is accomplished by pumping the lasing atom to an excited state with “white” light and as the atom rapidly attempts to return to its ground state it can end up in a metastable state by creating phonons (heat) in its surrounding matrix. It turns out that this heating effect for the Nb atom is considerably larger than for the Yb atom. Thus, the power effects illustrated in Figure 34 are noticeably less in some recent laser designs utilizing the Yb atom. An example of beam diameter and focus location for a typical fiber laser are shown in Figure 35. Notice that the beam diameter is independent of power level but that some shift in sharp focus location is seen. This focus shift is probably a result of some internal heating in the lenses and dimensional changes as the weld head structure warms up. This illustrates that temperature control (and possibly even cooling water temperature) is a process variable even for the most recent laser designs. Nevertheless, the relative constancy of beam properties over a wide range of process variables is the primary advantage of LBW for production.

In the case of electrons the beam diameter is fairly strongly dependent on the power level. The variations in electron beam size is largely a result of two effects. The first limiting factor is related to the fact that electrons are charged particles. Therefore, their mutual electrostatic repulsion limits the smallest possible spot size; this is often called the space-charge effect. Space-charge beam spreading increases with beam current (electron density) and at lower beam accelerating voltage (the electrons spend more time in the beam when moving slower). The second problem is that the electron source is

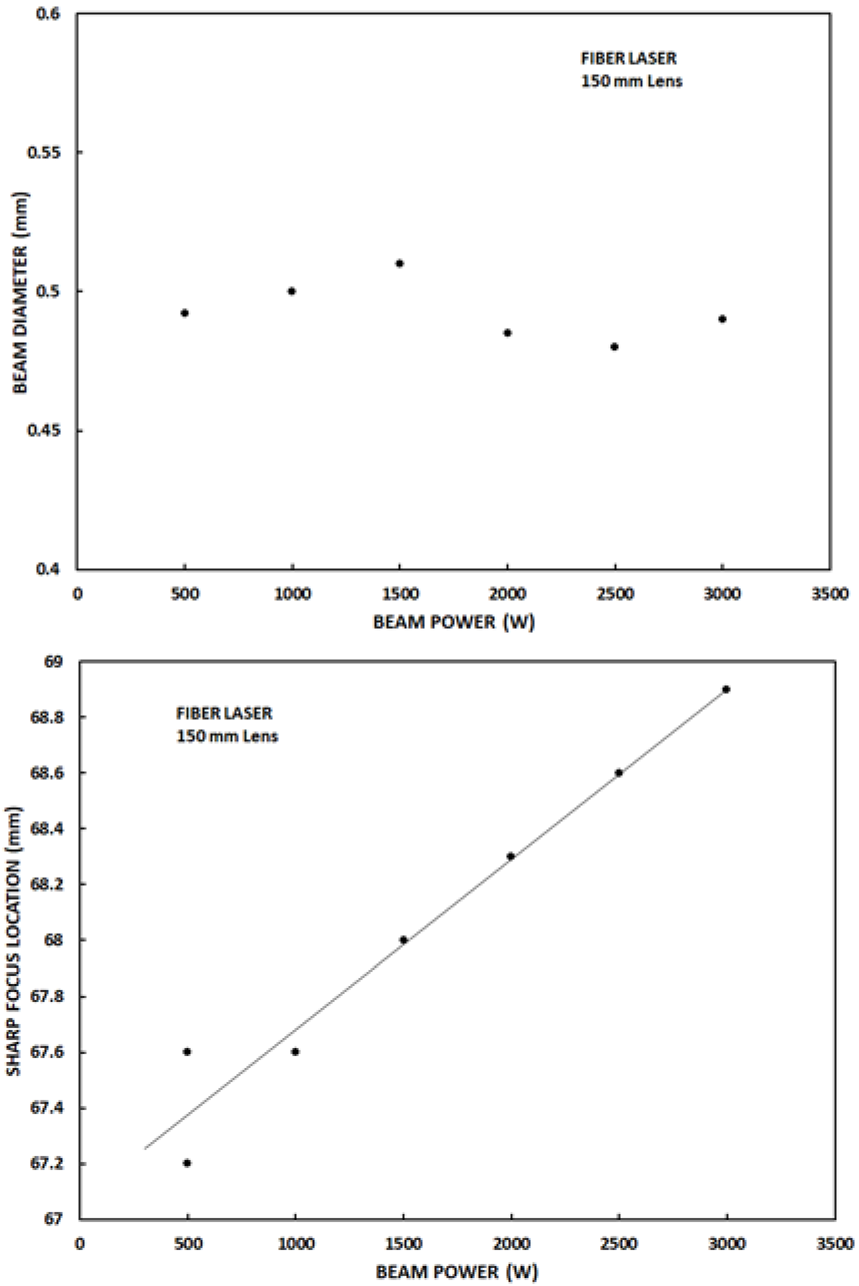

Figure 35: Data for measured beam diameter and sharp focus location versus beam power for a fiber laser.

usually a hot filament giving the electrons at least some amount of random thermal motion, which does cause some beam spreading. More importantly, the beam current is controlled by adjusting the area of the filament where the electrons are allowed to escape. The result is that the originating source size varies with beam current and thereby changes the focused beam diameter. Some data illustrating the beam diameter behavior versus beam current and beam accelerating voltage are shown in Figure 36 for a typical high voltage machine. The important point in Figure 36 is that the sharp focus spot size for EB is significantly dependent on the machine variables. Figure 37 is another example of EB beam diameter data presented to point out that high voltage control is a particularly important variable in EBW.

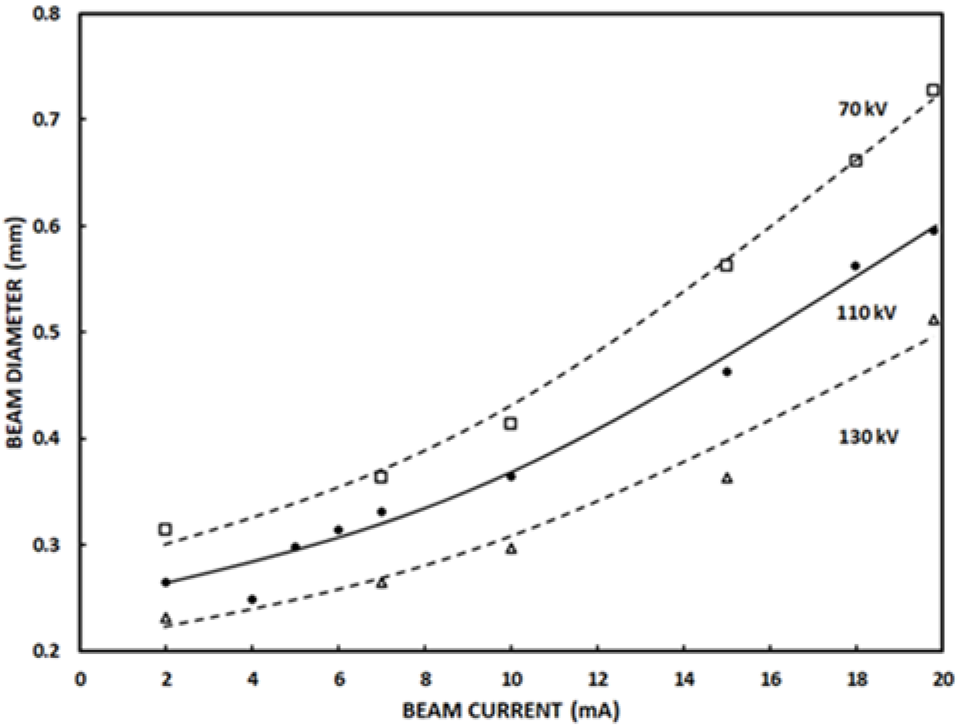

Figure 36: Sharp focus beam diameter values for a particular EB machine versus beam current and accelerating voltage.

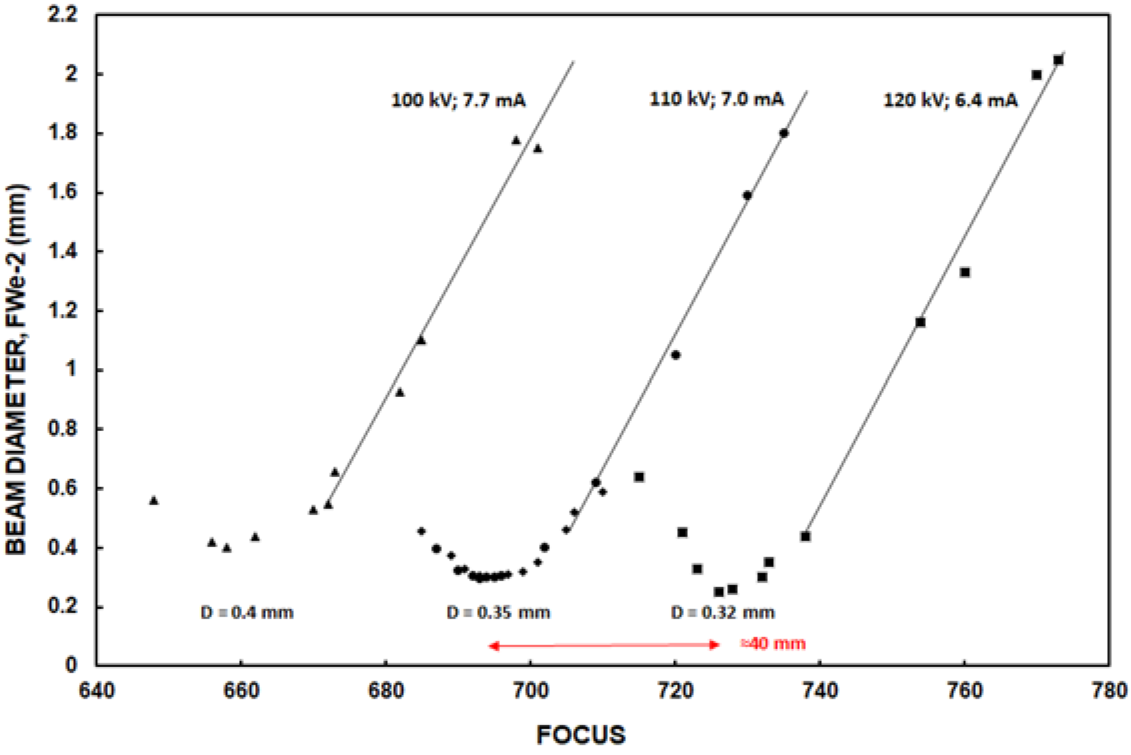

Figure 37: Beam diameter measurements from a particular EB machine versus focus setting for three high voltage values. Notice that the overall beam power is the same in the three examples.

It is also important to note that a number of additional details such as filament size and condition, electron gun assembly, the design of the electron optics and even the vacuum level will also affect the resulting beam diameter. These factors point out the major drawback to EBW in a production environment. Successful EBW requires considerable attention to a variety of machine details and requires operators with considerable training. This also means that different but otherwise similar machines can produce different results. Another important point to notice in Figures 36 and 37 is that a particular beam power can be generated by different combinations of current and voltage, which will yield a bit different weld results due to differences in the beam diameter.

Using the information about EB beam size increase with beam current, it is interesting to apply that to the non-linear power behavior seen in Figure 19. Using the power law dependence of penetration on beam diameter and the determined beam diameter behavior as shown in Figure 36, the measured weld penetration values can be "corrected" for the beam size increase with beam current. It turns out that the corrected penetration values then fall nicely in line with the expected linear behavior, indicating that the non-linear behavior of the data in that figure is mostly a beam diameter effect. Of course, for even deeper weld penetration, the result of the diverging electron beam will eventually become more important and the location of the beam minimum spot relative to the metal surface will influence the results and some amount of underfocus would yield maximum weld penetration.

D. One Approach to Understanding Weld Variable Effects

Another interesting bit of the science of weld variable effects is suggested by the similarity of the power law γ values shown in Figures 23 and 27. It is reasonable to ask if that is a coincidence or does it indicate something more fundamental about the power balance around the weld. In order to address that question, the problem has been analyzed via a traveling line source. There are a number of weaknesses to that model but it does reveal the basics of this question. In those calculations a particular boundary condition was assumed, namely that some temperature, T' (in degrees C), occurs at the beam radius, R = D/2. It turns out that in that calculation, v and R occur together in the analysis as a dimensionless distance: $R^* = (vD/2\alpha)$, where α is metal thermal diffusivity, $\alpha = K/\rho C$. This means that indeed, v and D should be interchangeable on a fundamental level. Another way to make the basic point is that the rate at which heat is used for thermal conduction relative to the rate for heat capacity can be quantified by the Fourier number of the process. The Fourier number, $F = \alpha/vD$ is known to be a fundamental descriptor of the power balance around a moving heat source. Note that F is the mathematical inverse of the parameter, vD/2a, largely used in this discussion. The result of a simple calculation assuming the relevance of R* is the solid line on Figure 38. In Figure 38, the dimensionless weld penetration is: $d^* = \frac{d\,K\,T'}{\eta\,IV}$ where the quantities in that equation are: d = measured weld penetration; K is metal thermal conductivity; T' is a characteristic temperature (essentially the material boiling point); η IV is useful beam power. The slope of that curve is: -0.5 at $vD/2\alpha = 0.03$; -0.6 at $vD/2\alpha = 1$; and about -1 for $vD/2\alpha > 30$. It is important to note that the dependence of weld penetration on beam diameter and travel speed changes significantly for small Fourier number versus large Fourier number. Also note that Figure 38 (and other figures used later in this paper) are logarithmic plots. These are used to conveniently show data over a wide range of variables (at least a factor of 100 for EB welds) and to accentuate the power law type behavior of the data. Figure 38 shows the weld data from Figures 21 and 24 placed onto the 2-D model plot. As can be seen, the data fit very well to the simple heat flow model, which is basically just Equation 4 with $\gamma \approx ½$ for the data with small $vD/2\alpha$. The quality of fit is quite good, however, it turns out that a number of assumptions were made in choosing the various thermal constants used in placing the raw data on the graph. Those assumptions will be the subject of the next section of this paper.

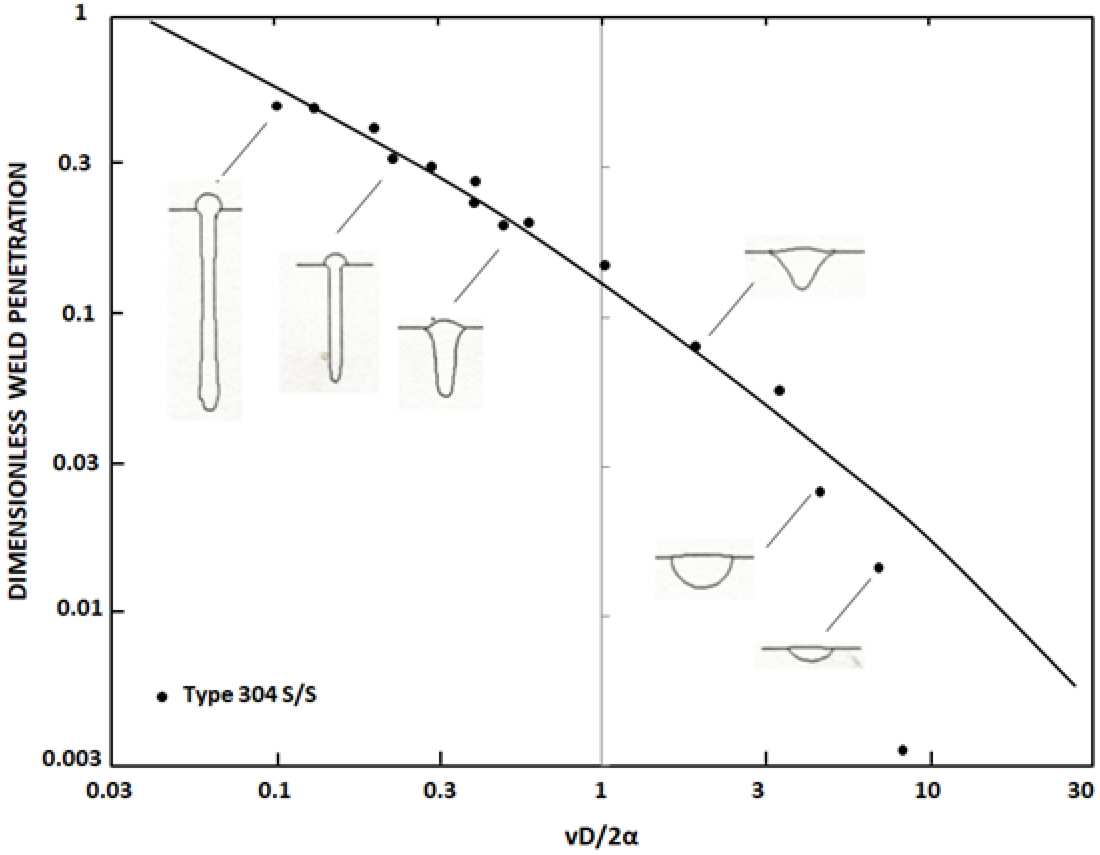

Figure 38: Data for EB welds on Type 304 S/S showing that the data fit the 2-D model fairly well with an appropriate choice of thermal constants. These are the v and D data combined from Figures 21 and 24.

Based on these results it seems that travel speed and beam diameter are completely interchangeable. However, an important comment about the interchangeability of v and D must be made. Changing travel speed and beam focus do produce similar changes in the weld penetration but will result in a bit different weld shapes. Increasing beam diameter decreases weld penetration by making the overall weld wider and shallower. With an appropriate value of travel speed, increasing travel speed decreases weld penetration by making the overall weld shallower with no large difference in weld width. However, at sufficiently slow travel speed the weld will become quite wide due to excessive melting beyond the extent of the keyhole. Weld results illustrating that point are shown in Figure 39. It is important to notice that the weld width was fairly insensitive to travel speed for v > 30 mm/s (70 ipm). Considerable experience with EBW suggests that maintaining a travel speed v > 17 mm/s (40 ipm) will generally produce the desired results.

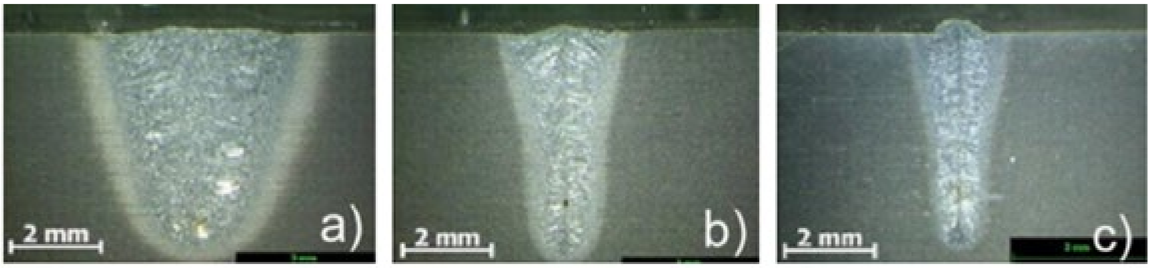

P = 2kW; v = 5mm/s P = 5kw; v = 33mm/s P = 8 kW; v = 84mm/s

Figure 39: Data for LB welds on a mild steel illustrating that similar weld penetration can be achieved by different weld variable combinations but that a particularly slow travel speed would probably not be desirable. These data are from: W.J. Suder and S. Williams, "Power factor model for selection of welding parameters in CW laser welding", Optics & Laser Tech, 56, 223-229 (2014).

In order to make the thermal analysis more useful, we can rearrange the variables to provide a predictive equation for weld penetration, which is as follows:

$$d = C\,\frac{\eta P}{K\,T'}\,\left(\frac{2\alpha}{vD}\right)^{\gamma} \qquad (7)$$

Where: d is the predicted weld penetration and C is a constant, which may be needed to properly match all the units of measurement. Note that Equation 7 is simply Equation 4 with the appropriate thermal constants given explicitly. In order to keep things as simple as possible let us suppose that we are in a regime with Fourier number between 1 and 30 so that $\gamma = 0.5$. In that special case we have:

$$d = C\,\eta P\,\left(\frac{1}{vD}\right)^{\gamma}\,\left[\frac{1}{T'\sqrt{K\,\rho C}}\right] \qquad (8)$$

Equation 8 is formulated in this way to gather the thermal constants into a single term that accentuates the point that weld penetration is limited in materials with high thermal conductivity, large heat capacity, high boiling point or any large product of these values. This equation is expected to have predictive power relative to the effects of different materials on the weld results for a typical range of travel speeds and beam diameters. Notice that the predicted penetration values are relatively insensitive to the particular values chosen for K and ρC and are most sensitive to the value of the keyhole temperature, T'. However, exactly how one chooses appropriate constant values for K, and ρC and T' is really the fundamental difficulty with this simple analysis. That is the basic subject of the next section of this paper.

Notice from Figure 38 that the weld penetration data rapidly fall away from the theoretical curve for $vD/2\alpha > 3$. This behavior happens because at some amount of defocus or sufficiently high travel speed the energy density, E', is simply is too small to form a keyhole and a further decrease in E' will eventually produce no metal melting. In LBW this would happen substantially more precipitously as the beam coupling rapidly decreases when the keyhole is no longer forming.

E. Alternative Approaches to Analyzing Deep Penetration Weld Behavior

A possible criticism of the previous analysis of weld variable effects, and Equation 7, is that it is largely empirical. Perhaps a better understanding of the physics might come from analysis based more directly on thermodynamics. Two specific examples found in the literature will be discussed. Do note that these papers are primarily related to LBW and analyze results over a limited range of beam diameters, which is typical of LBW (limited by LB coupling efficiency) and, therefore, may not be particularly applicable to the larger range of variables possible with EBW. This discussion will start with a publication by: D.B. Hann, J. Iammi and J. Folkes, “A simple methodology for predicting laser weld properties from material and laser parameters”, J. Phys. D: Appl. Physics, 44, 445401 (2011). They start with an essentially exact solution for the heat flow around a Gaussian heat source of characteristic width, σ. They derive an equation for dimensionless weld penetration, which is then related to the enthalpy associated with material heating through a particular phase change, namely the heat of fusion and the heat of vaporization. Doing a bit of algebra to simplify the equation, the result is: $d = C\frac{\eta P}{H\sqrt{\alpha\sigma v}}$ where, all the terms have the same meanings as used previously. This particular equation results from deriving dimensionless variables, which is often quite useful in thermodynamic arguments. Note that this is just Equation 7 with $\gamma = ½$. In this particular formulation of the problem, H is the enthalpy associated with a particular required phase change. The onset of melting requires the metal to be heated to the melting point, Hs, plus the phase change heat of fusion. Keyhole formation requires additional heating to the boiling point plus the heat of vaporization. The only criticism of this thermodynamic approach to HEDW is that Hann et al apparently assume that all material involved in the keyhole must be raised to above the metal boiling point, which clearly is not true. This leads to enthalpy arguments that significantly overestimate the beam power required for keyhole formation.

Finally, Hann et al discuss the enthalpy concept to note that the maximum enthalpy achieved in the metal changes character based on how efficiently the beam energy can heat the metal during the short times associated with the usual high travel speeds used in HEDW. In that case, the maximum enthalpy achieved in the metal is related to the Fourier number for the process: $F = \alpha/2v\sigma$. It is suggested that the maximum enthalpy of the metal decreases a bit proportional to $1/\sqrt{F}$ for $F > 30$. This behavior is related to the fact that an actual heat source does not have uniform coverage of a small circular spot (it may have a Gaussian distribution for example). In that case thermal conduction rapidly carries away beam energy from the low power density portions of the beam such that weld penetration will be lower than that expected by considering total beam power. It is interesting to note that the Hann et al analysis suggests empirical relationships similar to Equation 7 with: $\gamma = ½$ for normal conditions ($F < 10$) and $\gamma < ½$ for large F values. Examples of the smaller γ value for large F will be shown later and this concept was used by Hann et al to properly describe their data for Ta.

Data from the Hann paper illustrating the usefulness of the analysis are shown in Figure 40. The small letters on the figure refer to metallography in the in the original paper that will not be reproduced herein. Notice from Figure 40 that the onset of keyhole requires an enthalpy value of about 10 for these materials. As mentioned above, that is probably significantly overestimating the actual keyhole enthalpy condition. Figure 40 shows that for larger enthalpy the weld penetration is described fairly well by the equation cited above. It is not clear that this approach can entirely describe deep penetration welding for all weld variable combinations (such as EB welds made with a large beam defocus). Nevertheless, it does predict the behavior of LB welds over a fairly wide range of weld variables and materials in which the appropriate enthalpy values are known. The Hann approach does provide a framework for making reasonable choices about weld variable selection for a particular material and desired weld penetration.

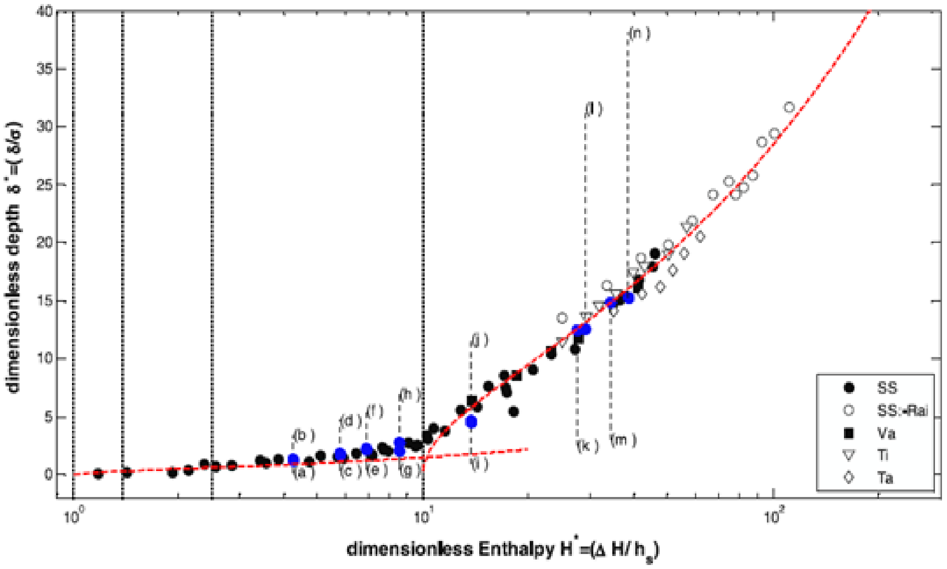

Figure 40: A figure from Hann et al showing that their analysis does describe weld penetration over a range of beam diameters and travel speeds and for several metals.

A bit different approach to weld variable selection in LBW is presented in a series of papers by Suder and Williams. See for example: W. Suder and S. Williams, "Parameter selection in laser welding using the power factor concept", ICALEO 2010 – Conf. Proc., 103 (2010). Their approach to the problem starts with the usual concepts of power density, P', and interaction time, t' (these were defined previously). Since these two variables alone don't fully describe weld behavior, Suder and Williams introduce an additional variable where the energy deposited in the material per unit length of weld is a fundamental process parameter. Therefore, they introduce the notion of power factor, Pf = P/D (units of J/mm). Graphs of LB data using this analysis methodology are copied below in Figure 41. Notice that the data are actually for a limited range of beam diameters. Four beam diameters were generated using different delivery fibers and output optics combinations. In the following discussion of these results, the data for the 2.5ms interaction time were not included because they almost certainly were not keyhole mode welds and would clearly be different than the other results.

The linear behaviors of weld penetration in Figure 41 clearly seem to indicate that interaction time, t', and power factor, Pf, are fundamental process parameters. The left hand graph in Figure 41 is especially interesting because it seems to say that weld penetration actually increases with increasing beam diameter for a particular interaction time, which does seem counter-intuitive. However, any conclusions from these data are complicated because maintaining constant P' or Pf while changing t' and changing D corresponds to corresponding changes in beam power and travel speed. In other words, every data point is actually a different combination of P, v and D. Starting with the constant power density results is particularly revealing. To maintain a constant power density going from the small beam diameter to large actually means that the beam power is increased by roughly a factor of four across the plot. Accepting that the weld penetration, for a particular t' = v/D, increases linearly with D and then doing the algebra it turns out that this simply means that weld penetration is described by: $d = C\frac{P}{\sqrt{vD}}$. Similarly, the data for constant Pf simply show that weld penetration is a weak function of the product

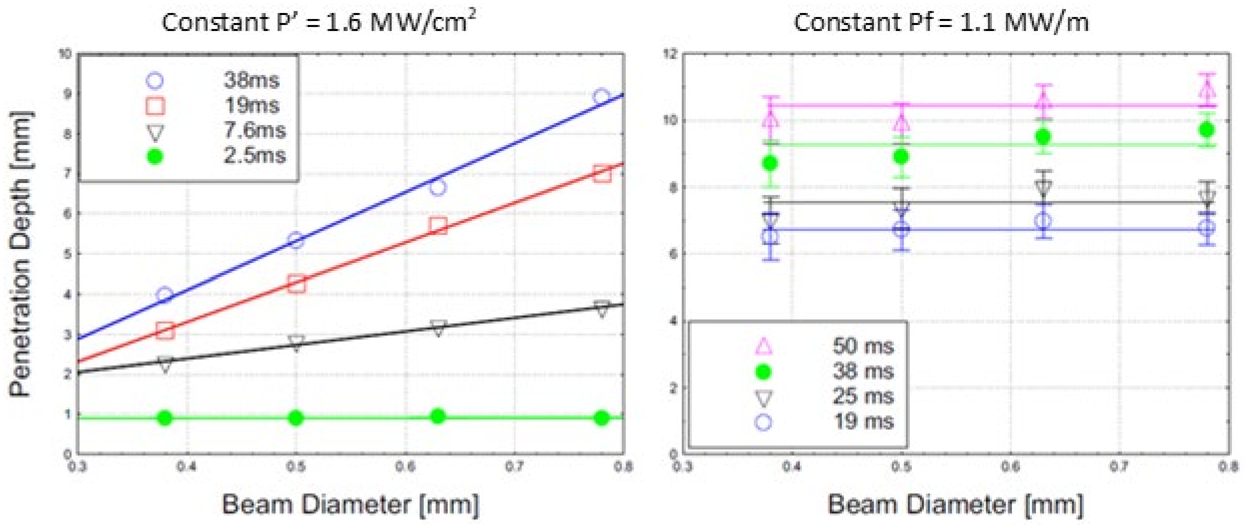

Figure 41: Figures from Suder and Williams (2010) showing LB weld penetration data for conditions of constant power density and constant power factor. The material used here was Type S355 mild steel.

(vD). Reading the actual weld penetration values from the graphs as best as possible and computing the corresponding P and v values results in the graph in Figure 42. A least-squares analysis of all the resulting data points shows that these results are described by Equation 7 with a least-squares fit power law coefficient of $\gamma = 0.47$, which is entirely consistent with expectations such as from Hann op cit.

In a bit later publication, Suder and Williams introduced a different interaction parameter, the specific point energy; see: W.J. Suder and S.W. Williams, “Investigation of the effects of basic laser material interaction parameters on laser welding”, J. of Laser Appl., 24, 32009 (2012). Specific point energy, Esp, is a bit different than their other variables and is representing the total energy deposited in a bit of metal as the beam passes. In actuality, it is an integral of the beam power density over the beam spot dimensions with an integration time of, t’. For a distributed beam, such as a Gaussian, Esp would be calculated by integration using the actual power distribution. This notion is basically equivalent to the beam shape factor introduced by Hann op cit to account for weld behavior for large Fourier number. In the limit of small diameter and/or for uniform power density beams the result is: $Esp = P' \, t' \, D^2$ or, $Esp = P \, D/v$ [units of J]. Assuming that the simple equation for Esp is valid, Suder and Williams analyze their LBW penetration data versus specific point energy. The resulting graph is reproduced in Figure 43. This graph shows weld penetration increasing proportional to Esp suggesting that it is a useful process parameter, at least for the limited range of beam diameters and the one material used in that study.

Analysis of those results showed that the data in Figure 43 are described nicely by: $d = (Esp)^{1/2}$ and that is apparently the curve drawn on that figure. That seems quite significant to understanding the process. However, if one accepts that weld penetration is proportional to $1/(vD)^{1/2}$ and that it is also proportional to $(Esp)^{1/2}$, then following the algebra it turns out that Figure 43 is simply a complicated way to say that the data were collected at a constant value of beam power density. The Suder and Williams data are useful in that they did confirm that weld penetration is given by $d = P/(vD)^{1/2}$ for a particular steel alloy and over a range of weld variables pertinent to LBW.

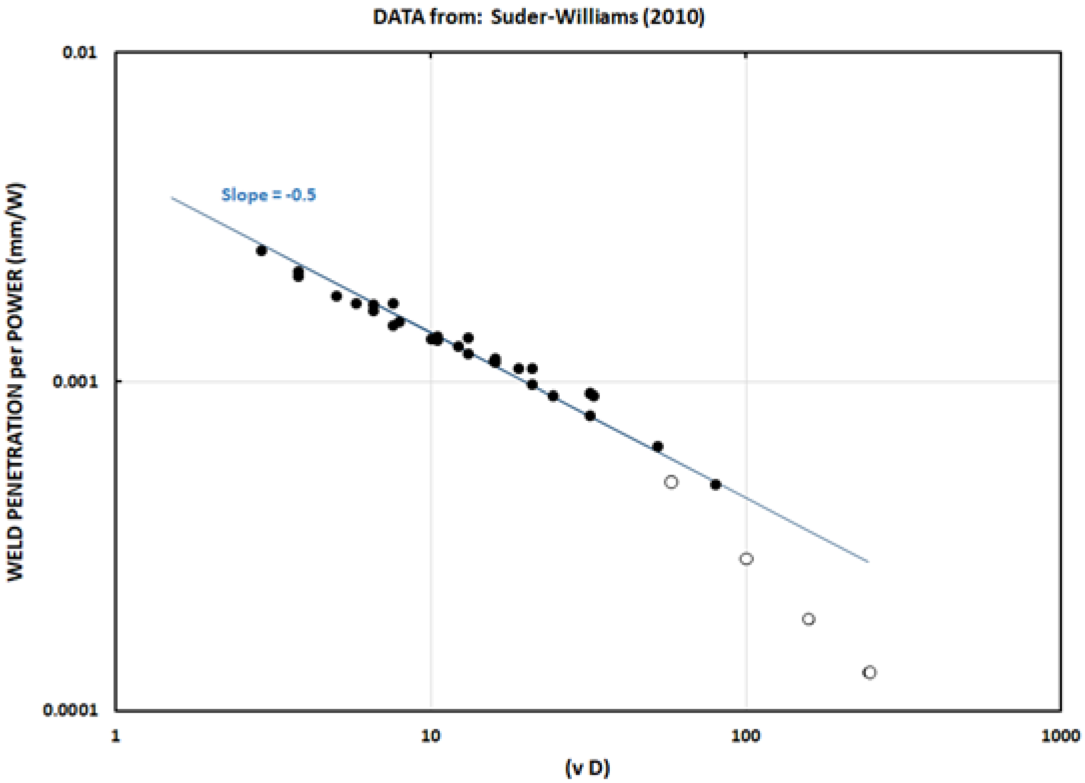

Figure 42: Analysis of data from Suder and Williams (2010) showing LB weld penetration per unit power versus the product of travel speed and beam diameter. The material used here was Type S355 mild steel. The open circles are the four high travel speed data points that are probably not keyhole welds.

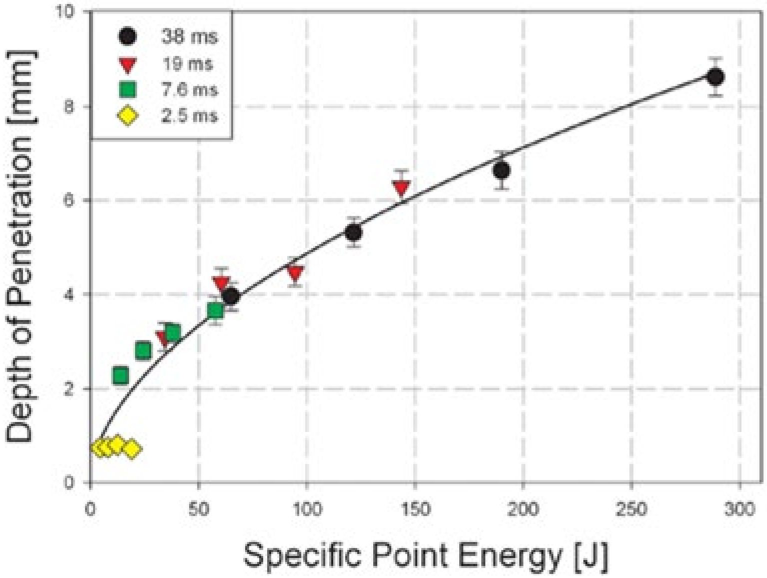

Figure 43: Data from Suder and Williams (2012) showing LB weld penetration versus specific point energy. The data were generated for four LB spot sizes and with a constant P’ = 1.6 MW/cm^2

In fairness to Suder and Williams it should be pointed out that their approach does provide a methodology for choosing appropriate weld variable combinations. Examples of this are shown in Figure 44. Clearly, their approach works quite well to match overall weld behavior. However, it is interesting to note that $P/(vD)^{1/2} = 2100$ for the 9mm penetration data and $P/(vD)^{1/2} = 1350$ for the 6mm data. The ratios being: 9mm/6mm = 1.5 ≈ 2100/1350 (in other words, their result is consistent with Equation 4 with $\gamma = ½$). Another important point about the series of papers by Suder and Williams is that it only dealt with one material, a particular mild steel. How well their approach might work in a variety of materials is not clear. It will be left to the reader to decide if optimizing the combination of P', Pf, t' and Esp is a simpler and more meaningful way to understand and predict LB results rather than using a methodology such as Equation 7 with $\gamma = 0.5$ and with a sensible choice of travel speed. Travel speed would be chosen using interaction time, $t' = D/v$, as a guide with t' generally being no longer than about 100 msec for the usual deep penetration welds.

9 mm penetration with Pf = 10.5 MW/m and t' = 0.040 s

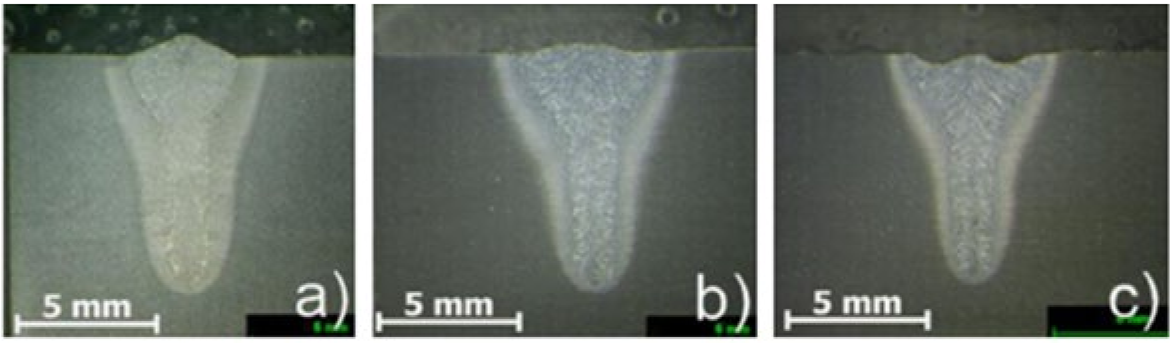

D = 0.38mm; P = 4kW; v = 9.5mm/s   D = 0.5 mm; P = 5.25kW; v = 12.5mm/s   D = 0.75mm; P = 7.9kW; v = 18.7mm/s

6 mm penetration with Pf = 9.5 MW/m and t' = 0.020 s

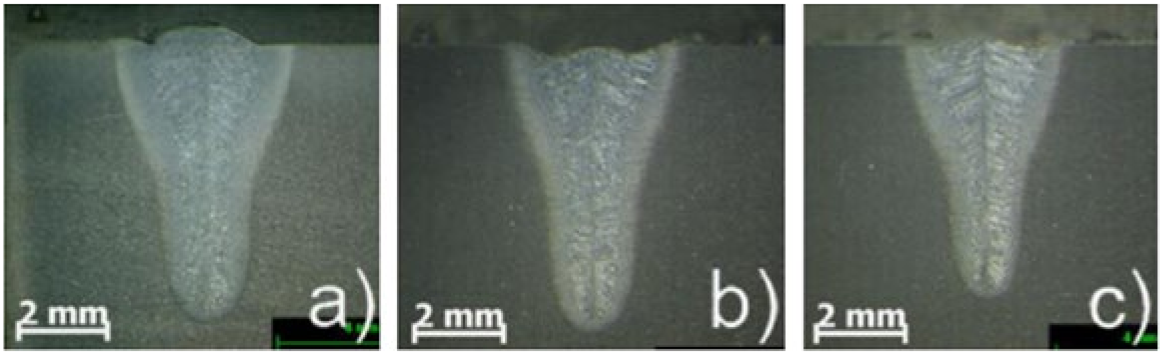

D = 0.38mm; P = 3.6kW; v = 19mm/s   D = 0.5 mm; P = 4.75kW; v = 25mm/s   D = 0.75mm; P = 7.1kW; v = 37.5mm/s

Figure 44: Data from Suder and Williams (2014) showing LB weld penetration for constant combinations of power factor and interaction time. This illustrates the usefulness of their methodology.

PART III: SOME MATERIAL PROPERTY EFFECTS IN HIGH ENERGY DENSITY WELDING

This portion of this document is intended to provide a basic knowledge of how the thermal properties of the welded materials affect high energy density welds. Since much of the previous section discussed results from steel welding, it is important to note that other materials can have much different weld behaviors. The basic goal is to show how the material properties interact with the weld variables (power, focus, travel speed and etc.) to affect the resulting weld depth of penetration.

As a starting point to this discussion recall the simplified equation for predicted weld penetration Equation 8. The predictive power of that equation is illustrated for some handbook data in Figure 45.

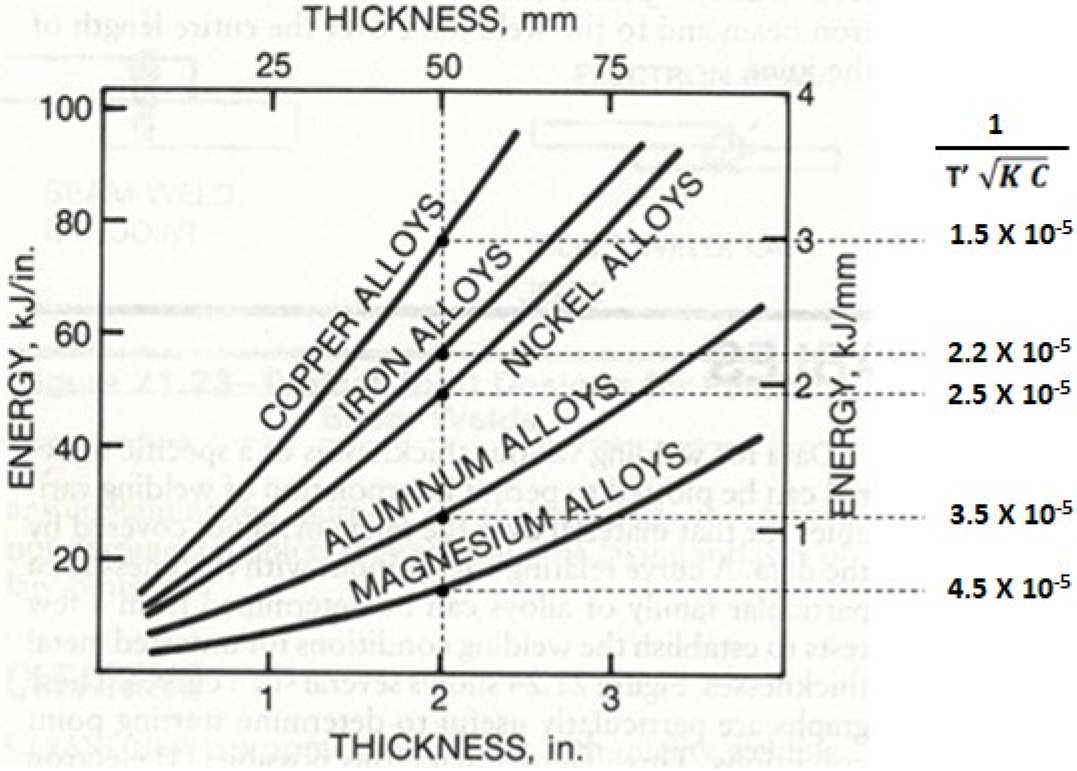

Figure 45: Data showing the electron beam energy per length of weld varies with the desired weld depth of penetration for several different materials. The values to the right are values for the thermal constants used in Equation 8. Data from: "Electron Beam Welding", Welding Handbook Vol. 2, American Welding Society (1991).

The information shown in Figure 45 illustrate that the required power to make a particular weld penetration in EBW is roughly proportional to the simple thermal parameter suggested by Equation 8. Figure 46 shows some additional evidence that the weld penetration in EBW is related to α, ρC and Tb. Another example of the value of Equation 8 is contained in the data in Figures 22 and 25 comparing LB welds in mild steel and stainless steels. Notice that, at the same travel speed of 5 m/min, 3 kw of power produced a bit more penetration in stainless steel than was produced at 4 kW in mild steel (note that only the results for a similar fiber size were considered). These two alloys have similar Tb and ρC but considerably different K with the mild steel value being almost twice that of stainless steel. The ratio of penetration to power in these two examples is about equal to $\sqrt{Kmild/Kss}$. Thus, we can conclude Equation 8 does have some value for predicting weld behavior in different materials.

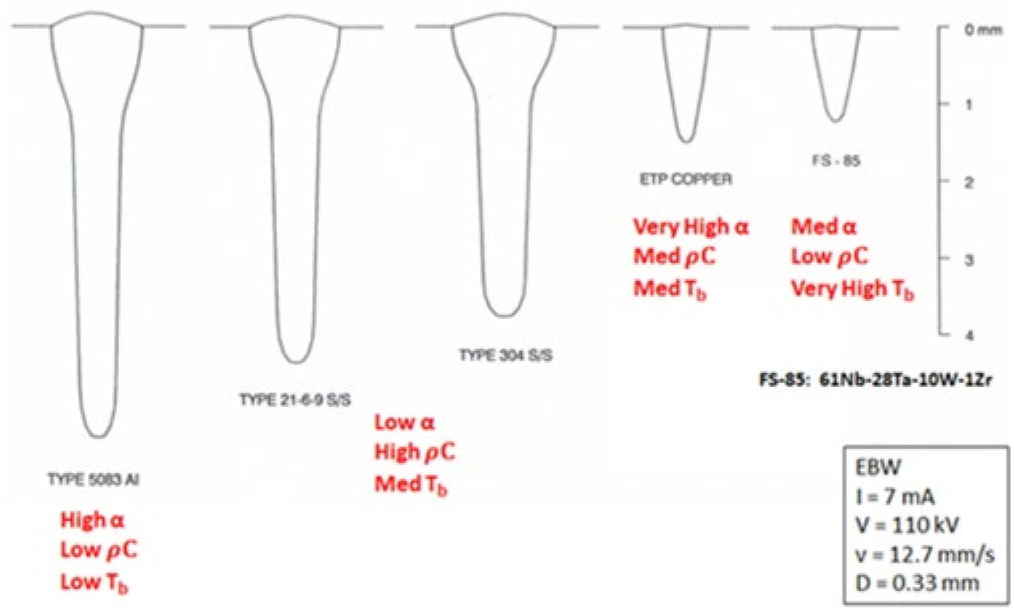

Figure 46: Sketches of EB welds in a variety of materials suggesting that the weld penetration results can be understood by considering boiling point, heat capacity and thermal conductivity.

One fundamental problem with the simple analysis of assuming constant values for K and pC is that these material properties are not just constants and that requires further discussion. Figure 47 shows the thermal conductivity and heat capacity values versus temperature for Type 304 stainless steel. As can be seen, the values are certainly not constant throughout the temperature range relevant to welding. It is the case that the heat capacity, given in the appropriate units of J/mm^3 C, is reasonably similar for most metals and generally doesn't change dramatically with temperature so choosing a single value for heat capacity would not have a large impact on the thermal model. Of course, if a particular metal had an unusual heat of fusion a constant for heat capacity would not be a good approximation. In general, assigning a single value to thermal conductivity is more problematic. It seems that choosing a value for K and ρC midway between room temperature and the melting point is adequately descriptive. Nevertheless, assigning a single value to K and ρC is not correct and could be quite misleading in some materials.

For the purposes of predicting weld behavior in different materials the real question is what value to use for the temperature boundary condition, T'. As was pointed out in Part I of this paper, the keyhole temperature in a vacuum is probably somewhat below the metal boiling point. For example, the Type 304 S/S data shown in Figure 38 were brought to the theoretical curve by assuming T' = 0.9 Tb = 2800 K (note: in this case Tb is the boiling point of iron as given in degrees K). Note that the value T' in this case is similar to the measured value of keyhole wall temperature found in the literature (Schauer et al, op cit). Part of the justification for using that value of T' is that the vapor pressure of most pure metals rises to the necessary level at about that temperature relative to their boiling point. Note that this value for T' makes sense for EBW performed in vacuum and probably applies to LBW-V. However, recall that T' will likely be Tb or even greater in normal LBW due to atmospheric pressure effects. That is one reason why weld penetration in LBW is less than that seen in LBW-V.

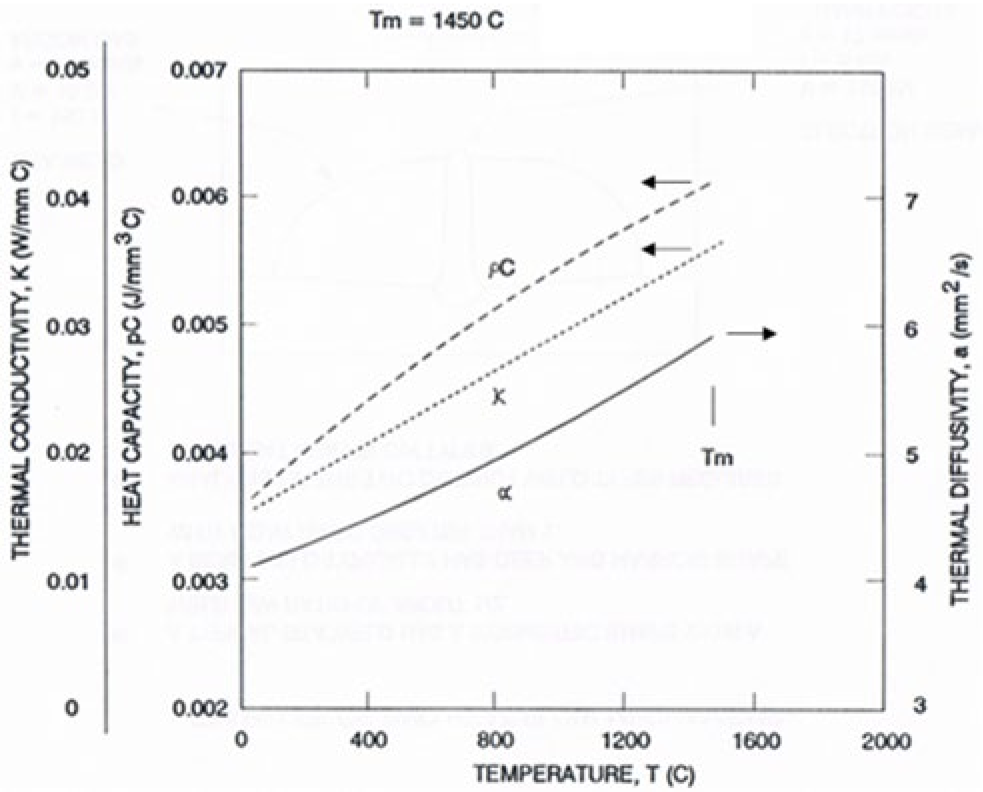

Figure 47: Thermal properties of Type 304 S/S showing that K and pC of this typical alloy are significantly temperature dependent. From: Y.S. Touloukian, R.W. Powell, C.Y. Ho and M.C. Nicoloaou, "Thermophysical Properties of Matter", Vol. 10, Plenum Press, New York, NY (1973).

Another important fact relevant to welding is that realistic values for Tb of many alloys does not appear in the literature. That is so because in many alloys at least one constituent will be evaporating more rapidly than the others. In other words, measuring Tb for an alloy cannot be done easily because its composition is changing as the measurement is being made. However, that experimental difficulty suggests how one might think about T'. One could make the argument that Tb for an alloy should be similar to that of its major constituent, but that may be entirely wrong because T' could be mostly related to the vapor pressure of the most easily volatilized constituent of the alloy. An example of how this may be important is illustrated in Figure 48, where the weld penetration data for a series of EB welds is compared for two stainless steel alloys. Notice that the welds in Type 21-6-9 yielded systematically greater penetration than those made in Type 304 stainless steel. A possible hypothesis for the penetration difference is that the preferential evaporation of the Mn in the Type 21-6-9 alloy allows keyhole formation at about 200K below that seen in Type 304 S/S. In fact, Mn loss in deep penetration welding of Type 21-6-9 alloy has been seen. The important point is that EB and LB welding can be significantly influenced by alloy composition effects on metal vapor pressure especially where some components of the alloy may be easily volatilized. While EBW and LBW-V would probably be similar in these sorts of alloys, it is unclear how to relate this to atmospheric pressure LBW. Whether or not the atmosphere might preferentially suppress the evaporation of some elements and how this may affect the plume is not known. Preferential evaporation of some alloy constituents certainly complicates any understanding of weld behavior in HEDW.

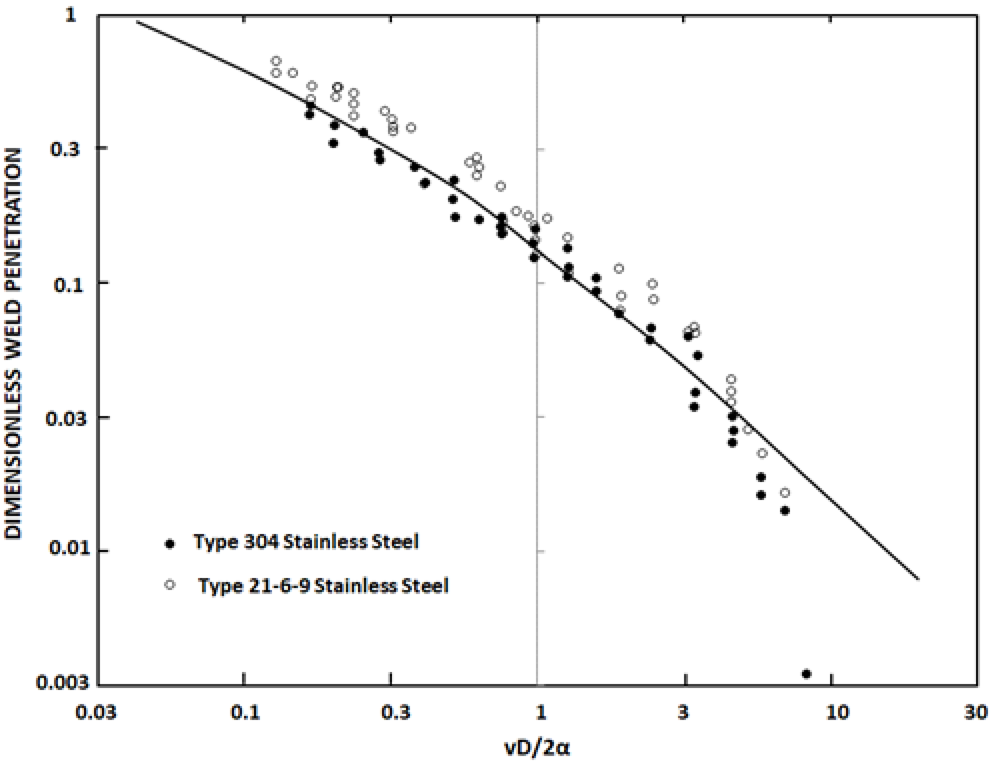

Figure 48: Combined weld penetration data for EBW of Types 304 and 21-6-9 stainless steels. Notice the systematic difference in weld penetration between the two alloys.

Figure 49 shows some additional EB weld data illustrating that assuming K, ρC and α are the "average" values and assuming T' = 0.9Tb does basically describe weld behavior in a variety of metals. It should be noted that the Type 5083 aluminum alloy data were brought onto the theoretical curve by assuming that Tb is the value for Mg, a major constituent of the alloy. A crucial point about Figure 49 must be emphasized. At first glance it seems that the weld penetration of Cu, for example, is significantly larger than for other materials, which is clearly not the case. The important point is that dimensionless penetration, d*, is actually being plotted in Figure 49. The raw penetration values are multiplied by $\frac{K\,T'}{\eta\,IV}$ to place them on this "universal plot". In other words, the Cu penetration values were multiplied by a large number, which is related to its very large thermal conductivity and its fairly high boiling point. In order to perhaps help clarify the actual weld penetration values, Table 1 shows values of the actual weld penetrations achieved in the materials for typical EB weld conditions.

Material	d/P (mm/kW)
Type 5083 Al	7
Type 304 S/S	5.5
ETP Copper	2.1
FS 85 Alloy	1.7

Table 1: Weld penetration per kilowatt beam power for EB welds at sharp focus and v = 17 mm/s showing the considerable difference in weld penetration achieved depending on material. These values are from data shown in Figure 49.

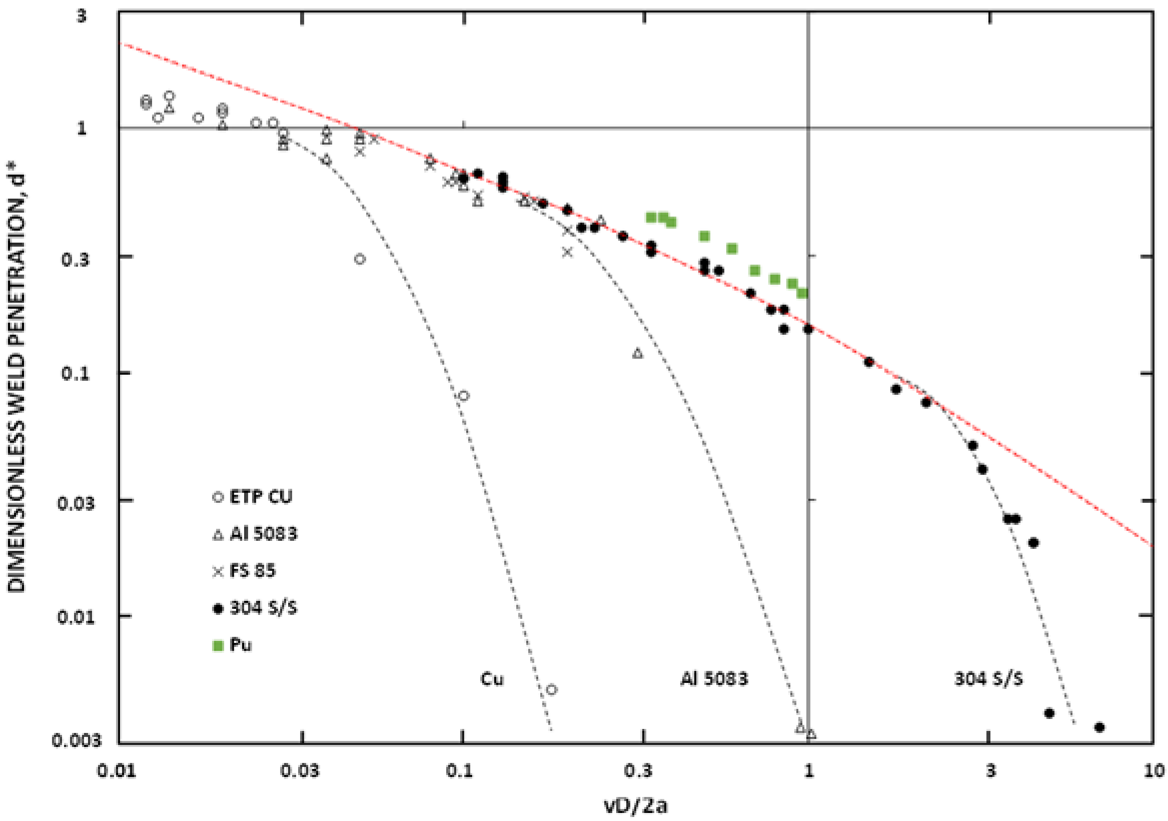

Figure 49: Weld penetration data for keyhole-mode EB welds in several metals. The red dashed line is the expected 2-D heat flow behavior. The weld data are from: P. Burgardt and T.C. Baker, "Relationship Between Beam Shape and Weld Shape in Electron Beam Welding", Rocky Flats Internal Report (1989) and presentation at the annual AWS Welding Society meeting (1990).

Figure 49 shows that the data generally following expectations from 2-D heat flow (with $\gamma \approx 0.5$) for much of the data and for a variety of metals. Since the data can be extended to large beam diameters in EBW, welds were made at fairly large values of vD. In that case, the slope of the curve becomes > 0.5, presumably indicating that the specific heat is becoming more dominant in the process. It is also interesting to note the substantially lower slope of the data achieved in the materials with particularly large thermal diffusivity values (equivalent to Fourier number values, F > 30). The data for Cu and the aluminum alloy are limited but seem adequate to indicate that the power law coefficient is $\gamma \approx 0.4$, which is consistent with thermodynamic considerations presented by Hann op cit. Another aspect of the data in Figure 49 is worth some additional discussion. The data were collected in a way to discern the power level required for the onset of melting in these EB welds. Notice that the energy density required to produce melting is significantly higher for Cu and Al alloys relative to the stainless steel. An equation for the energy density for the onset of melting, E_m', can be written using Equation 3b as a guide and that is given in Equation 9:

$$E_m' = 4.5\,\mathrm{Tm}\sqrt{K\,\rho C} \qquad (9)$$

Equation 9 is certainly not an exact solution of the problem but it does describe the onset of melting at least qualitatively. Of course, because of the intrinsic reflectivity of metals, the constant in Equation 9 would be different for LBW especially in high reflectivity metals such as aluminum and copper alloys.

Another interesting detail of Figure 49 is that a limited data set for plutonium is presented and does not fit onto the "universal" curve. Note that this is presented here because, while Pu welding is clearly not important to common welding interests, it may be of interest to the audience of this document. The plutonium alloy data were analyzed using thermal constants from: Plutonium Handbook, Ed. by O.J. Wick, Amer. Nuc. Soc. Publication (1969). Since Figure 49 is a logarithmic plot, the difference between the data and the expected behavior is larger than it might seem and is nearly a factor of two. Note that the factor of two difference in D* on Figure 49 doesn't actually mean that the Pu penetrations were unusually large (penetrations are roughly comparable to stainless steel) it simply suggests that the assumed values for the thermal constants are somehow in error. The most likely reason for the discrepancy is in the choice of the keyhole temperature boundary condition. In Pu the assumption that T' = 0.9 Tb may be substantially in error. Pu is a highly unusual metal in all regards but from the perspective of heat flow is most unusual because of the large difference between its melting point and boiling point; , Tm = 913K and Tb = 3505K. The weld penetration data would come into agreement with basic heat flow expectations if the keyhole temperature was only about 1900K and much less than the boiling point of the pure metal. The most likely explanation is that the Pu used in these weld tests is actually an alloy. If one assumes a temperature more consistent with the 0.9 times the boiling point of the other alloying element and assume a bit lower thermal conductivity because the material is actually an alloy, the Pu data do fall nicely in line with the other data in Figure 49. This discussion may be a caution for weld development because welds in that material might be highly dependent on minor variations in alloy content of its various constituents. Once again note that atmospheric pressure LBW might be particularly variable in an alloy like this where the suppression of evaporation of its various constituents could be different in that environment. Additionally, experience on the material gained with EBW may not be at all relatable to atmospheric pressure LBW, where the keyhole temperature would undoubtedly be noticeably higher than it is in EBW.

Another important potential ramification of the temperature "problem" noted in Pu is related to stirring of liquid metal in the keyhole-mode welds. Recall that the movement of metal from the front to rear of a traveling weld is largely driven by surface tension, which is proportional to the temperature gradient between those two locations. When welding in vacuum, it appears that the keyhole front wall temperature might be about 1600 C with the rear wall cooling to near the melting point of 640 C. This represents a considerable temperature gradient driving fluid motion. When welding in atmosphere the suppression of vaporization by the atmosphere would probably force the keyhole wall temperature considerably higher. It turns out that the magnitude of the surface tension coefficient (basically the surface free energy, F = G –TS) decreases substantially with higher temperatures. Additionally in the case of atmospheric pressure LBW, the calculations of keyhole wall temperature distribution seem to indicate a small temperature gradient from the front to back in the keyhole in more ordinary materials (from: S. Pang, op cit). The result would be minimal surface tension driven stirring of weld metal in atmosphere LBW. Also, it is plausible to assume that this limited temperature gradient would also limit vapor pressure driven motion of the weld metal in the keyhole. The essential point is that the extent of metal stirring around the weld might be quite limited in atmospheric pressure LBW and any welding variable adjustments trying to improve the stirring will probably be fruitless. Presumably, LBW-V would be more comparable to EBW based on these considerations.

F. Summary

1) The fundamentals of the electron beam (EB) and laser beam (LB) were discussed with the goal of assessing the relative merits of the two processes. It was noted that LBW is limited in versatility largely because of the reflectance of light from a metal surface and plume formation during welding. EBW is more versatile and is clearly the process of choice as long as the facility complications and additional system initial cost attendant to EBW can be accommodated.

2) Additionally, the potential for laser beam welding in vacuum (LBW-V) was discussed. LBW-V generally produces greater weld penetration than atmospheric pressure LBW possibly due to elimination of plume effects. LBW-V does not overcome the problem with laser light reflection from the metal. However, it seems clear that vacuum welding does overcome some LB problems such as void formation and does promise to be a somewhat more stable process than conventional LBW. Also, LBW-V has the major advantage of minimizing or totally eliminating the effects of oxygen, nitrogen and water on the weld metal (especially critical for reactive metals). LBW-V with the best practical vacuum level should at least be given serious consideration for future applications and facilities.

3) Parameter effects on EBW and LBW were discussed and were shown to be related to beam energy density. For both HEDW processes the weld penetration is well-described by:

$$d = \eta \, IV \, \frac{1}{T'\sqrt{K\,\rho C}} \left(\frac{1}{\upsilon D}\right)^{\gamma}$$

With the power law coefficient $\gamma \approx ½$. The significance of the variables is discussed in the text. The primary unknown in this equation, T' = the keyhole wall temperature, is near the metal boiling point.

4) Atmospheric pressure LBW is significantly complicated because of atmospheric pressure effects on the temperature distribution around the weld and by formation of the plume. The parameter effects on LBW are similar to those seen in EBW but are a bit complicated mostly by plume effects. It is likely that LBW-V is more similar to EBW in all regards.

5) Different metals and alloys require different sets of weld variables. The differences were shown to be related to the relative boiling points, thermal conductivities and heat capacities of the metal and are generally related to the parameter: $T'\sqrt{K\,\rho C}$. This means that the energy density required to produce a particular weld result is greater in metals with a high boiling point, large thermal conductivity or heat capacity or a combination of these.

Acknowledgements

I want to thank the staff and management of the Sigma Division for their support over my career. I especially want to thank M.Q. Johnson and P.A. Hochanadel for their friendship and guidance through bad times as well as good. Finally, I especially want to thank A.N. Duffield for being so helpful over the years in generating much of the fundamental weld data that forms the foundation for the results presented herein.

Symbols used in this paper

α = Metal thermal diffusivity = $K/\rho C$
σ = Gaussian width parameter or electrical conductivity, depending on context
γ = Power law coefficient applied to a description of weld variable effects
ρC = Metal volumetric heat capacity
K = Metal thermal conductivity
η = Process efficiency, fraction of beam power entering the metal
A = Light absorptance by a metal surface; in that context, R is surface reflectance = 1-A
d = Weld depth of penetration (usually given in mm)
d/w = Weld aspect ratio; depth to width
d* = Dimensionless weld penetration; $d^* = \frac{d\,K\,T'}{\eta\,IV}$
D = Beam diameter from second-moment calculation = $2\sqrt{2}\sigma$ for a Gaussian beam shape
E’ = Energy density = P/vD
Esp = Specific point energy, energy deposited in a bit of metal = $P'\,t'\,D^2$ for a small uniform beam
F = Process Fourier number, $F = \alpha/vD$
H = Metal heat of melting (or vaporization depending on context)
I = Electron beam current
L_R = Beam Rayleigh length; an indicator of depth-of-focus of the machine optics
P = Beam power setting; = IV for EB
P’ = Power density = $4P/\pi D^2$
Pf = Power factor = P/D (units of J/mm), the energy deposited in a bit of metal by the uniform beam
R = Beam radius = D/2
t’ = Interaction time = D/v
Tm = Melting point of metal
Tb = Boiling point of metal
T’ = Temperature of keyhole inner wall, roughly equal to Tb
v = Travel speed
V = Electron beam accelerating voltage
w = Weld width measured at weld top surface (usually given in mm)
$W_{1/2}$ = Weld width at one-half of penetration; an indicator of keyhole width